University Hospital Ulm, Department of Internal Medicine II
Prof. Dr. Wolfgang Rottbauer

Evaluation of the role of the specific human *DSC2*$^{c.2147G>C}$ mutation

Dissertation to obtain the Doctoral Degree in Medicine of the Medical Faculty of the University of Ulm

Hannah Lena Zuech
born in Merano

2025

Acting Dean: Prof. Dr. rer. nat. Thomas Wirth

1. Rapporteur: Prof. Dr. rer. nat. Steffen Just

2. Rapporteur: Prof. Dr. rer. nat. Susanne Kühl

Promotion Day: 27.02.2026

Dedication

This dissertation is dedicated to all my beloved ones, in particular my family.
To those who were part of it since day one or became part of it along the way.
I am forever grateful for your love and support.

Table of Contents

List of Abbreviations II

1 Introduction 1

1.1 Cardiomyopathies 1

1.2 Desmosomes 6

1.3 *In vivo* and *in vitro* approaches to studying cardiomyopathies: Zebrafish and iPSC-CM 11

1.4 Aim of the thesis 15

2 Material & Methods 17

2.1 Material 17

2.2 Methods 30

3 Results 41

3.1 *In vitro* model revealed arrhythmogenic phenotype of DSC2$^{c.2147G>C}$ mutation 41

3.2 DSC2 knockdown in *Danio rerio* as *in vivo* model confirms *in vitro* data 58

4 Discussion 63

4.1 Clinical and experimental background of known DSC2 mutations in comparison to the novel DSC2$^{c.2147G>C}$ mutation 63

4.2 Patient-derived ventricular DSC2$^{c.2147G>C}$–CM show slight structural impairments 64

4.3 DSC2$^{c.2147G>C}$–CMs show increased arrhythmogenic potential in electrophysiological analyses 65

4.4 DSC2$^{c.2147G>C}$ mutation affects Ca^{2+} handling in ventricular cardiomyocytes .. 66

4.5 DSC2 knockdown in embryonic zebrafish 68

4.6 Drawing a conclusion from the *in vitro* and *in vivo* results 70

5 Summary 71

6 List of References 73

7 Acknowledgements 81

8 Curriculum vitae 82

List of Abbreviations

ACM	Arrhythmogenic cardiomyopathy
AP	Action potential
ARVC	Arrhythmogenic right ventricular cardiomyopathy
bp	Base pair
bpm	Beats per minute
c-Myc	Cellular myelocytomatosis oncogene
cDNA	Complementary deoxyribonucleic acid
CM	Cardiomyocytes
CTRL	Control
Cx43	Connexin 43
DCM	Dilated cardiomyopathy
DES	Desmin
DSC2	Desmocollin-2
DSG2	Desmoglein-2
DSP	Desmoplakin
EAD	Early after depolarization
ECG	Electrocardiography
FP	Field potential
GAPDH	Glyceraldehyde-3-phosphate dehydrogenase
GSK3β	Glycogen synthase kinase 3β
HCM	Hypertrophic cardiomyopathy
hiPSC	Human Induced Pluripotent Stem Cell
hpf	Hours post fertilization
ICD	Implantable cardioverter defibrillator
INJ	Injected
iPSC	Induced Pluripotent Stem Cell
iPSC-CM	Induced Pluripotent Stem Cell-derived Cardiomyocyte
JUP	Plakoglobin
Klf4	Krüppel-Like Factor 4
LATS1/2	Large tumor suppressor homologue 1/2
LBBB	Left bundle branch block

LEAP	Local extracellular action potential
MEA	Multielectrode-array
MEF	Mouse embryonic fibroblasts
MO	Morpholino
MOI	Multiplicity of infection
mRNA	Messenger Ribonucleic acid
MST1/2	Mammalian STE20-like protein kinase
MYH6	Myosin Heavy Chain 6
$Na_v1.5$	Sodium gated voltage channel 1.5
NF2	Neurofibromin-2
Oct4	Octamer-binding transcription factor 4
PAT	Patient
PKP2	Plakophilin-2
PLB	Phospholamban
PPARγ	Peroxisome proliferator-activated receptor-γ
RCM	Restrictive cardiomyopathy
RMSSD	Root Mean Square of Successive Differences
rpm	Rounds per minute
RT-PCR	Reverse transcription polymerase chain reaction
RYR2	Ryanodine receptor 2
SCD	Sudden cardiac death
SCN5A	Sodium voltage-gated channel alpha subunit 5
SERCA2	Sarcoplasmic reticulum Ca^{2+} ATPase 2
SeV	Sendai-virus
Sox2	Sex determining region Y-box 2
SR	Sarcoplasmic reticulum
TCF/LEF	T-cell factor / lymphocyte enhancing factor
TEAD	Transcriptional enhanced associate domain
TTN	Titin
VT	Ventricular Tachycardia
YAP	Yes-associated protein
PAT/DSC2$^{c.2147G>C}$-CMs	Refers to patient-specific iPSC-derived CMs
CTRL-CMs	Refers to control iPSC-derived CMs

Nomenclature of genes and proteins is based on HGNC guidelines [9].

1 Introduction

1.1 Cardiomyopathies

Cardiomyopathies are a heterogeneous group of myocardial pathologies which are predominantly characterized by structural and/or functional changes of the myocardium and can potentially lead to a malfunction of the heart, which often results in progressive heart failure or cardiovascular death [13, 50].

Different types of cardiomyopathies can be distinguished, of which the following are the most relevant ones, depictured in Figure 1: dilated cardiomyopathy (DCM), restrictive cardiomyopathy (RCM), hypertrophic cardiomyopathy (HCM) and arrhythmogenic cardiomyopathy (ACM), of which the most classical form primarily affects the right ventricle (ARVC).

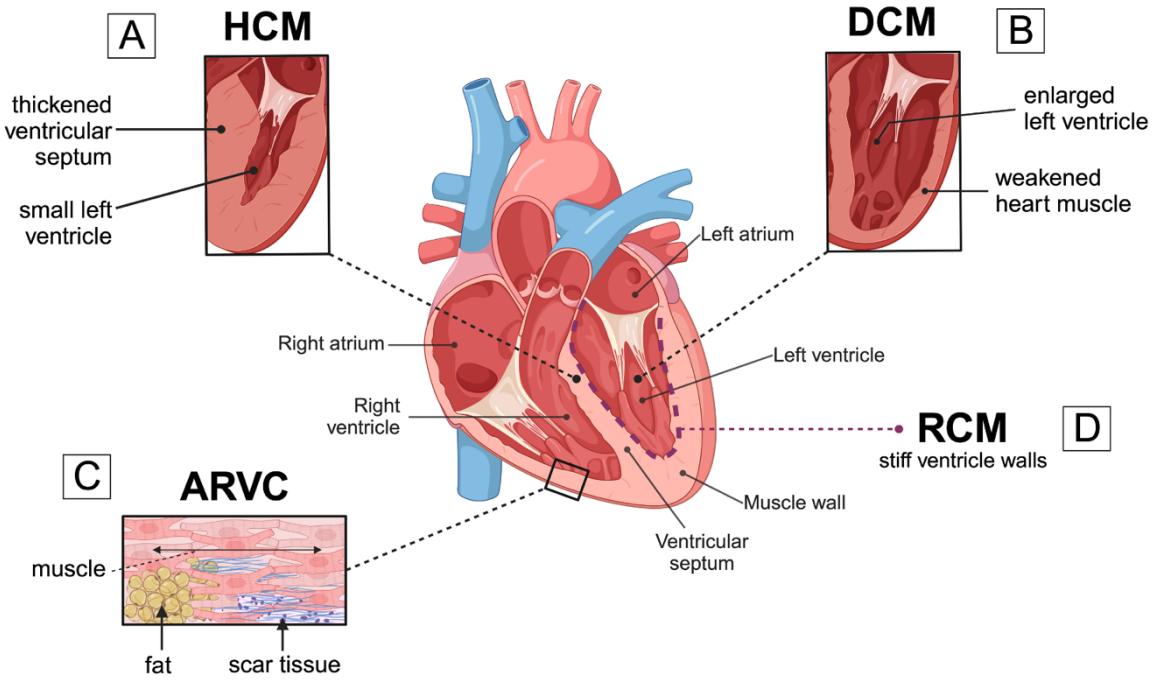

Figure 1: Most relevant cardiomyopathies. **A**: hypertrophic cardiomyopathy; **B**: dilated cardiomyopathy; **C**: arrhythmogenic right ventricular cardiomyopathy; **D**: restrictive cardiomyopathy. Created with BioRender.

I) Dilated cardiomyopathy (DCM), one of the most common causes for heart failure, is characterized by left ventricular dilatation, which consequently leads to contractile dysfunction (Figure 1B) [64, 79].

II) Another heterogeneous group of diseases mainly defined by a restrictive pathophysiology of the left ventricle is described as restrictive cardiomyopathy (RCM) (Figure 1D) [63].
III) Hypertrophic cardiomyopathy (HCM) leads to a thickened ventricular septum and small left ventricle, as shown in Figure 1A. HCM can be caused by mutations in a variety of different genes and therefore is the most common inherited cardiomyopathy [50].
IV) Another disease on a genetic basis is arrhythmogenic cardiomyopathy (ACM). It describes a broad spectrum of disorders and overlaps with other cardiomyopathic phenotypes, however, all are characterized by ventricular arrhythmia and structural myocardial abnormalities [13]. The most classical form of ACM is arrhythmogenic right ventricular cardiomyopathy (ARVC). ARVC is one of the leading causes of ventricular arrhythmias and can potentially lead to sudden cardiac death (SCD) at a young age. The early stage of the disease is defined by a preserved ventricular function and myocardial integrity, despite an increased susceptibility to arrhythmia and SCD. With the progression of the disease the loss of myocardium is accompanied by an inflammatory process and fibrofatty replacement, depictured in Figure 1C [23].

1.1.1 Arrhythmogenic right ventricular cardiomyopathy (ARVC)

In essence, ARVC is an inherited heart muscle disease characterized by the progressive replacement of right ventricular myocardium with fibrofatty tissue, as shown in Figure 2A. The estimated prevalence of this disease is ranging between 1:5000 and 1:2000, although it must be noted that defining a relative prevalence is quite challenging due to overlapping phenotypes, incomplete expression, and highly variable penetrance in carriers of genetic variants causing ARVC. The noticeable variation is most likely caused by the still high rate of under-recognition of the disease, also due to the complex diagnostic criteria [51, 59].

Clinical manifestation usually develops between the second and fourth decade of life and as a progressive disease ARVC can result in right or biventricular heart failure [62].

The disease phenotype of ARVC is highly variable, just as the penetrance of ARVC-related mutations. Increased participation in endurance exercise is related to an increased likelihood of disease penetrance [39].

Diagnostic categories are based on six key points, which in turn are divided into major and minor criteria. The criteria are based on imaging methods (dysfunction and structural alterations of the heart), endomyocardial biopsy (tissue characterization), ECG (de- and repolarization abnormalities and arrhythmias) and genetic background (family history) [19, 59].

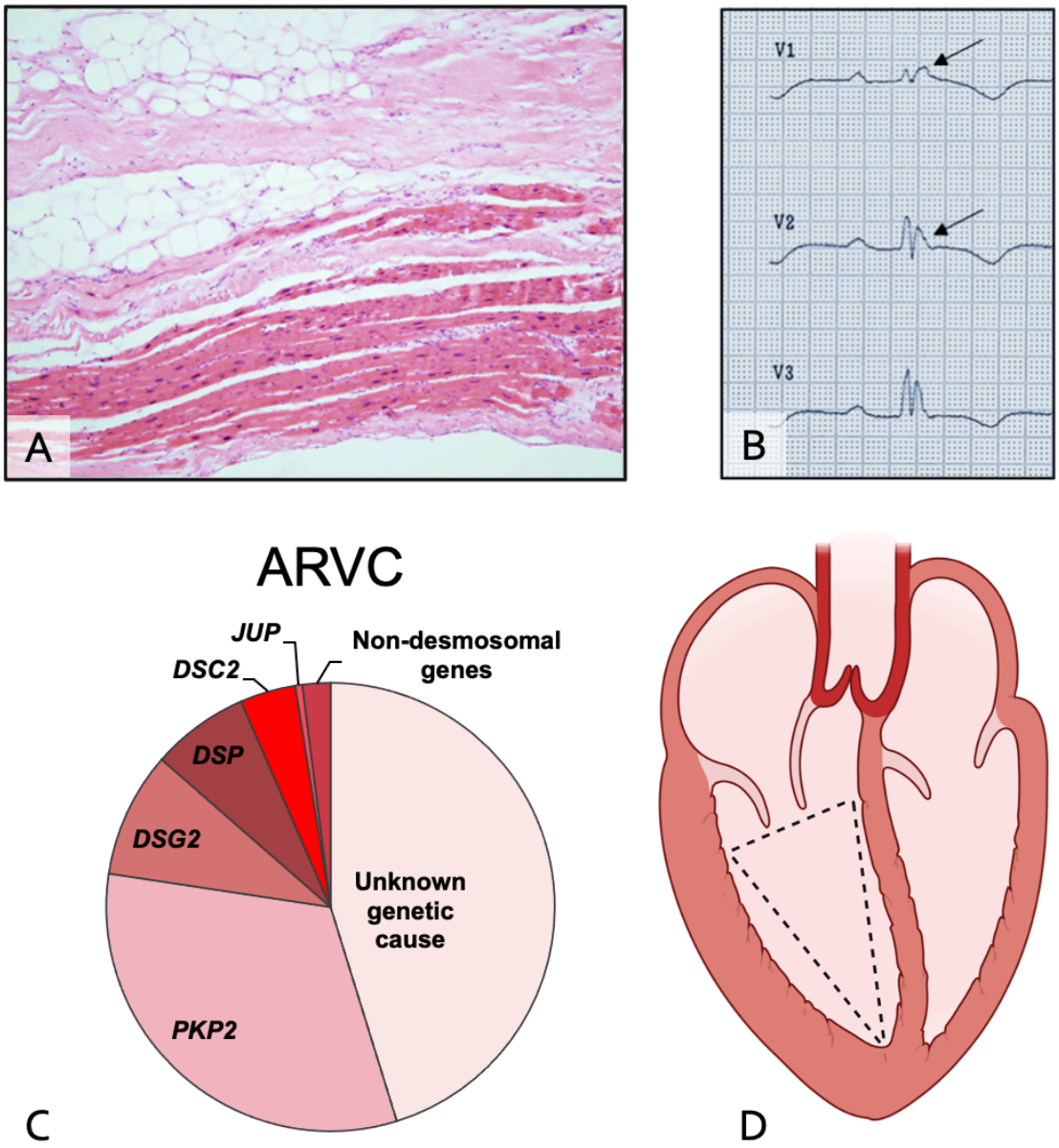

Figure 2: **A**: Histology of right ventricular wall depicturing fibrofatty replacement of myocardium. **B**: Excerpt of 12-lead surface ECG recording of a patient with ARVC, showing inverted T-waves in V1-V3 and positive epsilon potentials marked by arrows. **C**: In 40 % - 50 % of patients with ARVC possible genetic cause remains unknown. The most common mutations known to cause ARVC are in genes coding for desmosomal compounds: plakophilin-2 (*PKP2*), desmoglein-2 (*DSG2*), desmoplakin (*DSP*) and desmocollin-2 (*DSC2*) [30]. **D**: Triangle of dysplasia: most common localization of fibrofatty remodeling. It includes the inflow and outflow tract, and the apex of the right ventricle; created with BioRender. **A**, **B** [59], reproduced with permission from Springer Nature.

Frequently reported symptoms are palpitations, dizziness, paroxysmal tachycardia, which is a form of acute short-lasting tachycardia, or prior syncope [59]. Typical ECG alterations in ARVC patients are inverted T-waves and epsilon waves (Figure 2B), predominantly in right precordial leads, and arrhythmias characterized by a left bundle branch block (LBBB) morphology and thus originating in the right ventricle [21]. Clinical symptoms and signs of primarily right heart failure in ARVC patients seem to mainly occur in later stages of the disease, restricted to patients with a long history of ARVC [22]. Heart failure symptoms were found in 79 % of ARVC patients at an age of 40 ± 14 years [35, 59].

From a pathophysiological point of view, the progressive fibrofatty replacement of myocardium is crucial to the disease development. It initially affects the epicardium and progressively infiltrates the endocardium [48]. The first localization of this pathological process is in the so-called triangle of dysplasia, located in the right ventricle (Figure 2D). The left ventricle can be involved as well [11, 15].

In the disease management of ARVC, the main goal is to prevent SCD. However, therapeutical approaches are limited because the molecular mechanisms causing ARVC are not entirely known. As in most cardiovascular diseases, the first step involves a change of lifestyle. ARVC patients have an increased risk of developing ventricular arrhythmias, especially during high intensity exercises, which is why it is highly recommended to not perform competitive or endurance sport activities [13, 20]. Pharmacological treatment consists of antiarrhythmic drug therapy and mainly focuses on improvement of life quality by preventing symptomatic ventricular arrhythmias [20].

The most effective therapy approach is the implantable cardioverter-defibrillator (ICD). ICD implantation improves the outcome of high-risk patients and interrupts fatal ventricular tachyarrhythmias. It is the only therapeutic strategy focused on the prevention of SCD [16, 17, 80]. The final option in ARVC patients with either severe heart failure or futile ICD therapy is heart transplantation [20].

Figure 2C shows that ARVC has a strong genetic background. However, it is important to state that not all ARVC cases can be attributed to a specific genetic mutation, in such cases the disease is often referred to as idiopathic ARVC: in 40 % - 50 % of patients a positive family history or underlying genetic cause cannot be identified (Figure 2C) [30]. This might be due to the still evolving research in that field, continuously expanding the genetic and phenotypic spectrum of the disease,

or due to a different unknown underlying cause. Nevertheless, ARVC remains predominantly a genetic disease.

Some mutations known to cause ARVC can be found in genes that encode for desmin (*DES*), the sodium voltage-gated channel alpha subunit 5 (*SCN5A*), titin (*TTN*) and many more [21]. However, they account for less than 1 % of mutations identified in ARVC patients [30]. The most frequent mutations known to lead to ARVC are in genes that encode for desmosomal compounds. As depictured in Figure 2C, the most common mutations can be found in the *PKP2* gene, coding for plakophilin-2 (20 % - 45 %). 4 % - 15 % of identified ARVC mutations are in the *DSG2* gene coding for desmoglein-2, 1 % - 13 % in *DSP* coding for desmoplakin, 1 % - 7 % in *DSC2* coding for desmocollin-2 and 1 % in *JUP* which encodes for plakoglobin (Figure 3B) [30].

1.2 Desmosomes

Desmosomes play an important role in cell-cell contacts by helping to resist shearing forces and maintaining tissue integrity. They are found in high concentrations in tissues that undergo strong mechanical stress, such as the epidermis and the heart with its myocardial tissue. Desmosomes are adhesive intercellular junctions that mechanically connect adjacent cells. This works through the interaction of the following components, as shown in Figure 3A: desmoplakin (DSP), desmosomal cadherins desmoglein-2 (DSG2) and desmocollin-2 (DSC2) and cytoplasmic plaque proteins of the armadillo gene family plakoglobin (JUP) and plakophilin-2 (PKP2). DSP provides the link to the intermediate filaments, whereas DSG2 and DSC2 as transmembrane glycoproteins mediate Ca^{2+}-dependent adhesion at desmosomal junctions [53]. Their ectodomains consist of different extracellular cadherin domains, and interactions can be both homophilic and heterophilic (Figure 3A) [72].

JUP and PKP2 work as linker proteins and mediate interactions between the intercellular tails of both transmembrane proteins, DSG2 and DSC2, and DSP.

If any of these components are impaired due to abnormalities in structure or binding, the desmosomes appear to have a predisposition to disrupt over time (Figure 3D(1)). The disruption is reinforced by increased mechanical stress (sports activities e.g.). Parallel to the disruption of the intercellular junctions, multiple pathogenic mechanisms including the Wnt-β-catenin signaling pathway are being activated (Figure 3C-D) [3]. The Wnt-β-catenin signaling pathway plays an important role in cardiac development and cardiomyocyte differentiation and prevents differentiation of precursor cells into adipocytes and fibrocytes. Due to genetic abnormalities, the assembly of desmosomes is impaired, which consequently leads to a translocation of JUP from the sarcolemma to the nucleus (Figure 3D(2)). The internuclear JUP suppresses the Wnt-β-catenin signaling pathway and induces a switch in gene transcription from myogenesis to adipogenesis and fibrogenesis (Figure 3D(3)) [18, 31]. As additional pathogenic mechanism, the Hippo pathway is activated, which leads to an increased pro-apoptotic and adipogenic phenotype (Figure 3D(5)) [4].

These pathomechanisms contribute to the fibrofatty replacement of myocardium and myocardial scarring. Hence, the process of replacement of myocardium by fibrofatty tissue resembles the situation after myocardial infarction.

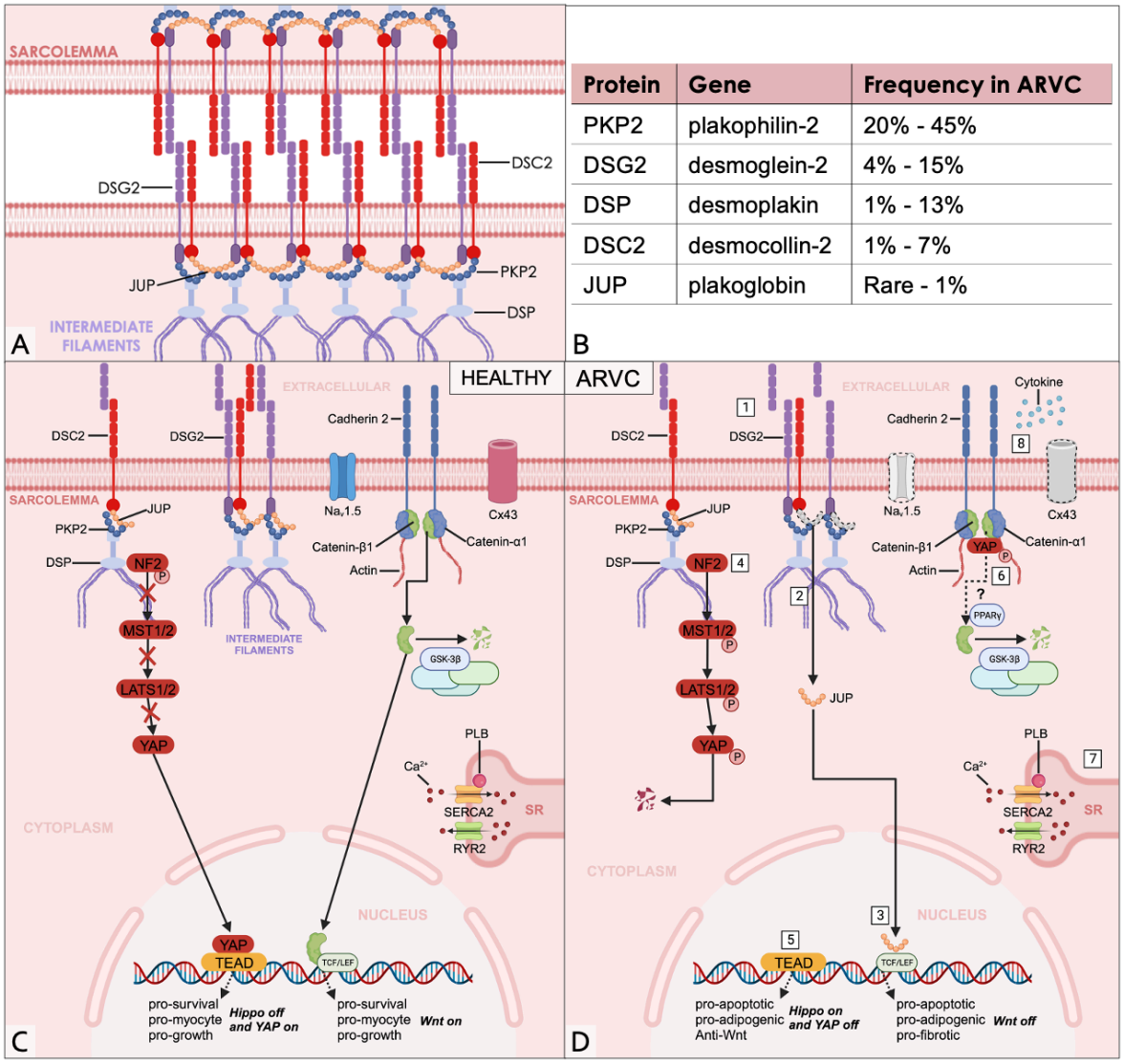

Protein	Gene	Frequency in ARVC
PKP2	plakophilin-2	20% - 45%
DSG2	desmoglein-2	4% - 15%
DSP	desmoplakin	1% - 13%
DSC2	desmocollin-2	1% - 7%
JUP	plakoglobin	Rare - 1%

Figure 3: **A**: Structure of desmosomes in cardiomyocytes. Desmosomes are adhesive intercellular junctions that mechanically connect adjacent cells. DSG2: desmoglein-2, DSC2: desmocollin-2, JUP: plakoglobin, PKP2: plakophilin-2, DSP: desmoplakin. **B**: Desmosomal compounds shown in **A** and their frequency in ARVC, based on Gandjbakhch et al. (2018). **C** and **D** show molecular mechanisms contributing to the pathogenesis of ARVC, based on Austin et al. (2019). Multiple signaling pathways are altered in ARVC. **C** shows regular pathways in healthy individuals. Catenin-β is part of the adherens junctions and plays a role in Wnt signaling. Catenin-β located in the cytoplasm is degraded by a complex which contains GSK3β. In healthy individuals, the Wnt pathway is activated in cardiomyocytes. The Hippo pathway is deactivated, to promote cardiomyocyte survival, function, and growth. Calcium handling is well regulated in the SR. SERCA2, PLB and RYR2 are well functioning. **D** depictures altered pathways in ARVC patients. (1) Desmosomal impairment and disruption leads to increased mechanical stress on cardiomyocytes. (2) JUP can then dissociate from the desmosomes and translocate to the nucleus (3), where it interferes with catenin-β and inhibits the Wnt dependent gene transcription. (4) NF2 is thought to activate the Hippo pathway (5), which leads to increased pro-apoptotic and adipogenic phenotype. (6) Activation of Hippo pathways leads to phosphorylation of YAP, which can interact with JUP and catenin-β, further inhibiting the Wnt pathway. Increased expression of PPARγ can additionally suppress Wnt signaling by potentially directly promoting catenin-β degradation.

Figure 3 continued: (7) An important contribution to arrhythmogenesis is impaired Ca^{2+} handling in the SR. Abnormalities in the functioning of the sodium channel $Na_v1.5$ and Cx43, a component of the gap junctions, potentially contribute to arrhythmogenesis as well. (8) Inflammation due to increased pro-inflammatory and pro-fibrotic cytokine production is thought to have an additional impact on ARVC pathogenesis [4]. NF2: neurofibromin 2; MST1/2: mammalian STE20-like protein kinase; LATS1/2: large tumor suppressor homologue 1/2; YAP: Yes-associated protein; TEAD: transcriptional enhancer factor; TCF/LEF: T-cell factor lymphocyte enhancing factor; PPARγ: peroxisome proliferator-activated receptor-γ; GSK3β: glycogen synthase kinase 3β; PLB: phospholamban; SERCA2: sarcoplasmic reticulum calcium ATPase 2; RYR2: ryanodine receptor 2; $Na_v1.5$: sodium gated voltage channel 1.5 ; Cx43: connexin 43; SR: sarcoplasmic reticulum. Created with BioRender.

The fibrofatty tissue is believed to slow down the intraventricular conduction and contribute to the development of ventricular arrhythmias through a macro-reentry mechanism induced by scarring [18].

However, this is not the only mechanism thought to contribute to arrhythmogenesis and the development of the clinic phenotype of ARVC. PKP2 and the gap junction protein connexin 43 (Cx43) are both part of the intercalated disc structure and have a physical interaction [52]. Mutations in the PKP2 gene can lead to ARVC by causing electric instability. Loss of PKP2 causes Cx43 remodeling, which leads to a reduction of the functionality of $Na_v1.5$, since Cx43 is responsible for the expression and localization of $Na_v1.5$ on the cell membrane (Figure 3D(7)). That results in a reduced Na^+ current and decreased conduction velocity [52].

Another important molecular mechanism likely involved in ARVC arrhythmogenesis is the dysregulation of the Ca^{2+} handling machinery, predisposing or leading to arrhythmia (Figure 3D(7)) [4, 52]. In their adhesive state, desmosomes are Ca^{2+} dependent. Alterations in Ca^{2+} handling or general desmosomal impairment can lead to alterations in the cardiac stromal compartment, which contributes to pathological remodeling found in ARVC patients. Abnormal amplitude and prolongation of Ca^{2+} transients have been noted as well. Cardiomyocytes showed an increased tendency for early and delayed afterdepolarization events.

All these alterations in the Ca^{2+} handling machinery predispose to arrhythmia and contribute to the development of ARVC [4, 74].

1.2.1 DSC2

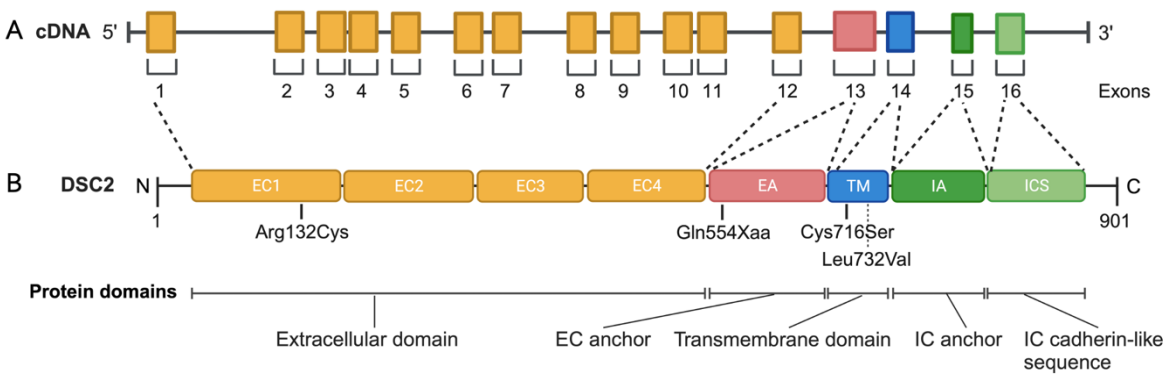

Figure 4: **A**: The *DSC2* gene is located on chromosome 18 and encodes 16 exons. **B**: Desmocollin-2 is a member of the cadherin superfamily and thus has similar organized domains. The DSC2 consists of 901 amino acids and contains four extracellular domains (EC1-4), an extracellular anchor (EA), a transmembrane domain (TM), an intracellular anchor (IA) and an intracellular cadherin-like sequence (ICS). The DSC2$^{p.Cys716Ser}$ (DSC2$^{c.2147G>C}$) mutation is located in the transmembrane domain. Other pathogenic mutations are Arg132Cys [54, 65], Gln554Xaa [34], and Leu732Val [5]. **A, B**: Based on Greenwood et al. (1997) and Kowalczyk and Green (2013). Created with BioRender.

All currently identified mutations in the *DSC2 gene,* a critical component of desmosomes, have been linked to ARVC [30, 69].

Three *DSC* genes can be distinguished in the human genome, all are clustered on chromosome 18. *DSC1* is mainly expressed in the epidermis, *DSC3* in the gastrointestinal tract, and *DSC2* in several organs, including the gastrointestinal tract, the skin, and the heart. Hence, *DSC2* is the only desmocollin gene expressed in cardiac tissue [57]. As members of the cadherin superfamily, DSCs have similar organized domains, as shown in Figure 4B. Binding of DSC to DSG is mediated via their extracellular domains and appears to be Ca^{2+} dependent. The connection to plakoglobin is provided by the intracellular domain (Figure 4B) [75].

As mentioned before, DSC2 is part of the desmosomes, which are complex formations consisting of adhesion molecules, linking molecules and cytoskeletal fibers. The adhesion molecules firmly connect adjacent cells, linking molecules at the cytoplasmic plaque of the desmosomes transmit the mechanical load from the adhesion molecules to the intermediate filament cytoskeleton, and cytoskeletal fibers distribute mechanical forces [44]. DSC2 functions as adhesion molecule. It participates in cell adhesion and signaling pathways within the context of

desmosomes and helps maintain tissue integrity in tissues exposed to increased mechanical stress, such as the heart [72].

Dysregulation of DSC2 can have significant implications for tissue function and can lead to disorders in the heart. Mutations creating structural vulnerabilities adversely affect the desmosomal cadherin function, other mutations compromise Ca^{2+} binding and interfere with mechanisms that are crucial for cell-cell interactions [53]. Figure 4B shows exemplary mutations in DSC2.

All likely-pathogenic or pathogenic *DSC2* mutations found in literature cause ARVC. Moreau et al. (2021) identified the heterozygous missense mutation c.394C>T in exon 3 of the *DSC2* gene (Figure 4A), coding for an amino acid exchange of arginine by cysteine at position 132 (Figure 4B). The patient carrying the Arg132Cys mutation was diagnosed with ARVC at 41 years of age [54]. He survived a SCD after an episode of ventricular tachycardia at age 50 and consequently had an ICD implanted. By 66 years of age, he had to undergo a heart transplantation. The diseased heart of the patient was analyzed and showed fibrofatty remodeling in the enlarged right ventricle. Extensive fibrosis and necrosis were observed as well [54].

Another pathogenic *DSC2* mutation was identified in families of the Alberta Hutterite population [34]. Clinical and genetic evaluation was initiated due to an accumulation of SCDs and severe forms of biventricular cardiomyopathy in that population. Electric and histological features were typical for ARVC. The identified homozygous truncation mutation was located at position 554 of the amino acid sequence (c.1660C>T, p.Gln554Xaa), shown in Figure 4B [34].

Bhuiyan et al. (2009) analyzed several mutations in genes encoding desmosomal compounds in ARVC patients. They found a *DSC2* mutation (p.Leu732Val) closely localized to the mutation of our index patient (p.Cys716Ser, Figure 4B), who was starting point of this thesis. The $DSC2^{p.Leu732Val}$ mutation encodes for an amino acid replacement of leucin by valine at position 732 of the amino acid sequence. The patient carried an additional mutation in the *DSG2* gene found in another patient analyzed in that cohort, which complicated the evaluation of the *DSC2* mutation. However, the patient carrying solely the DSG2 mutation demonstrated a left-dominant arrhythmogenic cardiomyopathy, whereas the patient additionally carrying the $DSC2^{p.Leu732Val}$ mutation had full blown features of ARVC [5].

Despite 40 % - 50 % of ARVC cases having an unknown cause, ARVC is predominantly classified as a genetically determined cardiac disease [30, 52]. The

pathways contributing to arrhythmogenesis are mainly correlated with adipogenesis and electrical dysfunction. Hence, mechanisms which are causative for ARVC might involve defects in the Ca^{2+} handling machinery and alterations leading to pathological remodeling [52].

Although research continues to unveil the mechanisms leading to ARVC, a complete understanding of the pathogenesis is yet lacking.

1.3 *In vivo* and *in vitro* approaches to studying cardiomyopathies: Zebrafish and iPSC-CM

In the last decade models for cardiovascular disease investigation have made significant advances. The main aim in general is to create a disease model which most accurately resembles the human organism. Many approaches have been established over the years. Disease models can be subdivided into *in vivo* and *in vitro* models for disease investigation.

1.3.1 In vivo

Animals as *in vivo* models are frequently used in pharmacological and medical research. Different animal models and their comparability to the human organism have often been subject of discussions in the medical field. The selection of different animals as model organisms should depend on the organs to be studied and the corresponding experiments.

Zebrafish (*Danio rerio*) are frequently used in cardiovascular research and developmental science [41]. They are easy to handle and simple to maintain. Zebrafish have a high fertility and their eggs, of which an adult female can produce approximately 200 per week, are fertilized externally. The embryos develop very quickly, but remain transparent up to five days post fertilization, which facilitates organ observation [61]. Comparison of human and zebrafish genomes showed a conservation of 71 % of human genes in the zebrafish genome [40].

Parameters of the cardiac conduction system of zebrafish resemble the human cardiac conduction system more than other model organisms, like rodents (mice) for instance. Thus, ECG parameters are more comparable (Figure 5D). The average heart rate of zebrafish is approximately 120-180 bpm, the heart rate of humans is around 60-100 bpm, whereas rodents have a heart rate of 300-600 bpm (e.g. mice) [32]. The cardiac conduction system of zebrafish consists of pacemaker cells in the sinoatrial node, the atrioventricular node, and the ventricular conduction system.

Zebrafish have a rather simple circulatory system. The heart is composed of a single atrium and a single ventricle. Pacemaker cells can be found in the sinus venosus and atrium junction [77]. As a contrast to the human heart, zebrafish are missing the His-Purkinje system, but the ventricular trabecular myocardium can be seen as functional equivalent [71]. Both humans and zebrafish generate a similar resting membrane potential and action potential (AP) amplitude in atrial and ventricular cardiomyocytes [55]. The AP upstroke of zebrafish involves Na^+-channels, L-type Ca^{2+}-channels are required for the plateau phase, and I_{Kr}-channels are needed for repolarization [32, 55].

All these attributes and the strong similarity to the human organism support the use of zebrafish as a model to study the function and/or dysfunction of the cardiac conduction system and examine cardiac electrophysiology through ECGs [24, 32] (Figure 5).

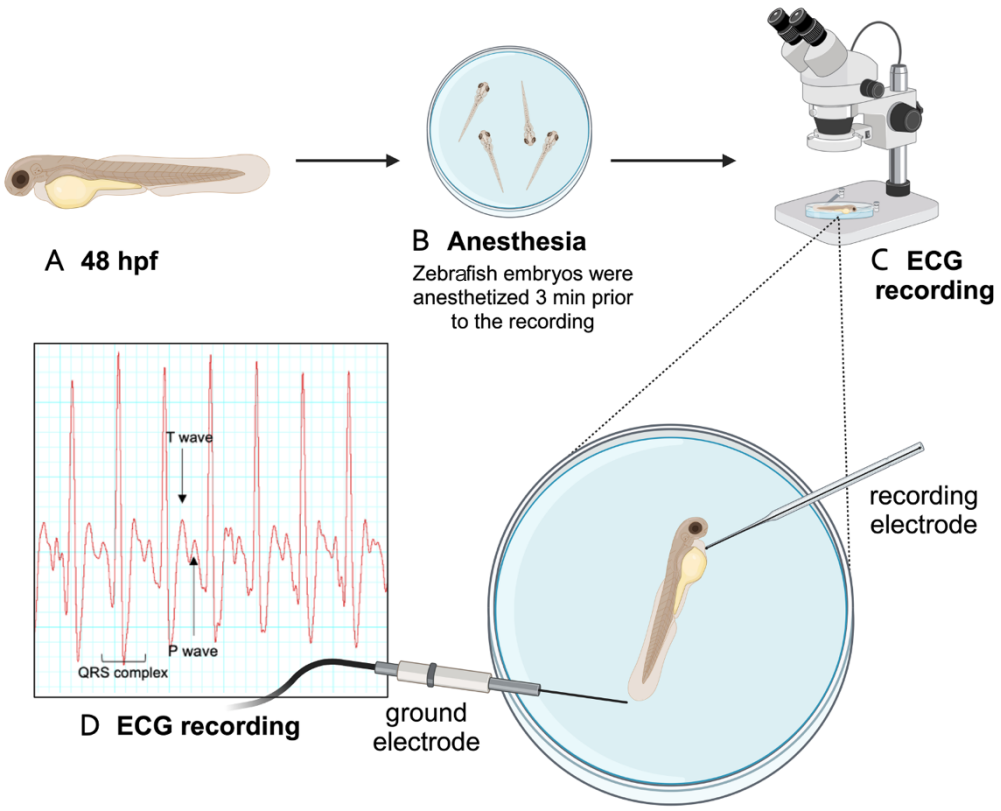

Figure 5: Simplified experimental setup of ECG recording in embryonic zebrafish, 48 hours post fertilization (hpf, **A**). Embryonic zebrafish are anesthetized for 3 min prior to ECG recording (**B**). The setup of the ECG recording consisted of a recording electrode and a ground electrode (**C**). The recorded signal from wild-type embryos at 48 hpf is shown in **D** and resembles a human ECG.

Due to all these characteristics zebrafish models have been an important model organism in research focused on cardiac arrhythmias. Cardiac channelopathies such as long QT syndrome, short QT syndrome, and Brugada syndrome, atrial fibrillation linked to mutations in developmental transcription factors or alterations in cardiac structure, and metabolic dysfunctions in cardiomyocytes have all been studied on zebrafish [32].

An additional advantage is the use of morpholinos to generate gene knockdowns. Morpholinos are directly injected into zebrafish oocytes. They are artificially made and hence not catalyzed by enzymes produced by the zebrafish, which ensures a prolonged effectiveness and more possibilities for analysis. The effect of morpholinos is temporary and thus confines analysis of morpholino-mediated gene knockdowns to the embryonic stages [61]. Morpholinos are synthetic oligonucleotides and have a high binding affinity to the target mRNA. They can either block the start of translation or alter pre-mRNA splicing, by targeting splice junctions or splice regulatory sides [26]. They do not carry a negatively charged backbone, which reduces non-specific interactions with other cell components and thus might make them less noxious [26].

Research suggests that the zebrafish is the most suitable model organism for studying genes associated with cardiac structural formation [41]. Morpholino mediated knockdown of desmosomal compounds in zebrafish has provided further insights into pathogenesis of ARVC. Heuser et al (2006) performed a morpholino mediated knockdown in zebrafish embryos which revealed the requirement of DSC2 in the formation of an adequate myocardial structure and function. DSC2 knockdown showed loss of the extracellular electron-dense midlines of desmosomes and a reduced plaque area, both associated with impaired myocardial contractility [38].

1.3.2 In vitro

In vivo models, despite adequately representing disease phenotypes and allowing many experimental approaches, cannot overcome the difference in genetic background between human and substituted models. Due to that there was a need for a disease model which accurately reflects the patient-specific phenotype and has a patient-specific genetic background [58].

Since the discovery of the reprogramming factors (Figure 6), pluripotent stem cell induction has made significant advances and induced pluripotent stem cell derived cardiomyocytes (iPSC-CM) as *in vitro* models have gained more importance in

cardiovascular research [76, 81]. To date, different integration-free reprogramming strategies for iPSC generation have been developed, using plasmid vectors, adenoviruses, and the Sendai virus [81].

Generating iPSCs by reprogramming patient-derived fibroblasts, which were obtained through a skin biopsy, and further differentiating those patient-derived iPSCs into cardiomyocytes (iPSC-CM), creates a cardiac disease model that fully reflects a patient-specific genetic background (Figure 6).

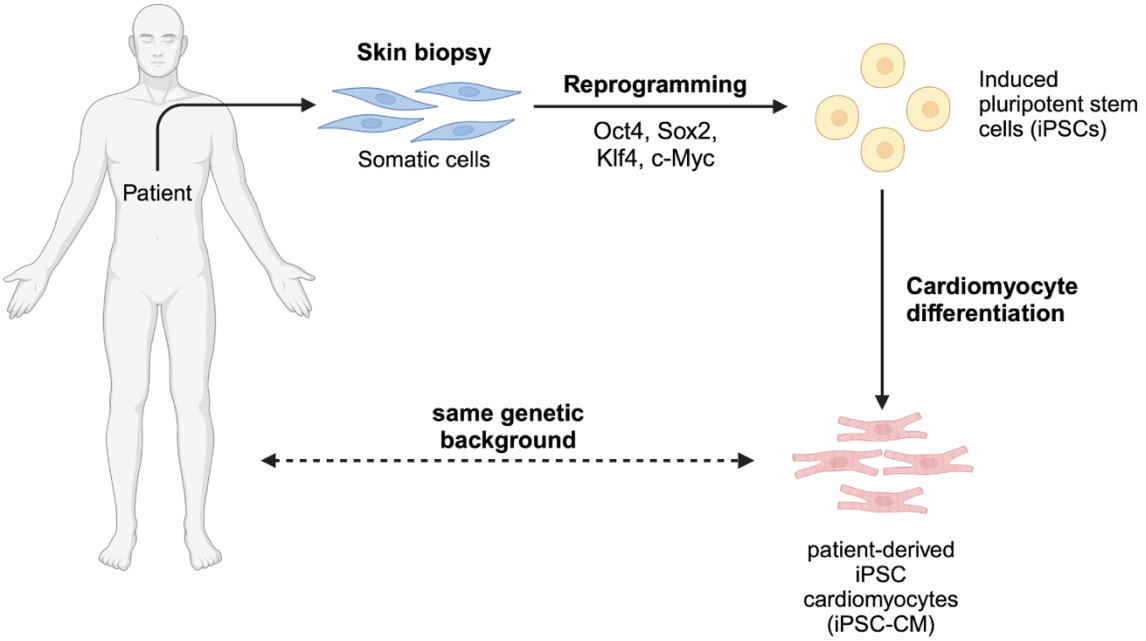

Figure 6: Generation of patient-derived iPSC-CM. Fibroblasts, obtained from the patient, are isolated and reprogrammed to induced pluripotent stem cells (iPSC) with the Yamanaka factors: Oct4, Sox2, Klf4 and c-Myc [76]. Once iPSCs have been tested positive for pluripotency, cardiomyocyte differentiation begins. After 30 days of differentiation, iPSC-cardiomyocytes (iPSC-CM) have reached full maturity. The patient-derived iPSC-CM present the same genetic background as the index patient, which makes them an excellent tool to investigate inherited cardiac disorders [58]. Created with BioRender.

One of the main initial obstacles of iPSC-CM cell culture was the maturation of cardiomyocytes. To mature cardiomyocytes, a long culture period is required, as well as electrical, mechanical, or chemical stimulation [41, 58]. To further avoid undifferentiated cells, specific lineage differentiation has been established.

Beating patient-specific iPSC-CMs express a variety of human genes encoding ion channels, sarcomeric proteins, and cardiac cellular adhesion proteins [10]. This feature makes patient-derived iPSC-CMs an excellent tool to investigate inherited cardiac disorders *in vitro*. As personalized models, they allow patient-specific

screening of potential pharmacological therapies and thus contribute to individualized medical approaches [58].

The first iPSC-CM models in research related to ARVC were established to study mutations in the *PKP2* gene [12, 42, 49]. Ma et al. (2013) initiated the generation of a patient-derived iPSC-CM model to investigate ARVC. They demonstrated that patient-derived iPSC-CMs displayed some of the key features of the disease. iPSC-CMs derived of an ARVC patient with a *PKP2* mutation showed reduced cell surface localization of desmosomal proteins and a more adipogenic phenotype. They therefore stated that these patient-specific cells may be useful to study this complex disease [49].

Another approach evaluated the role of a *DSG2* missense mutation in patient-derived iPSC-CMs [27]. Patient-specific iPSC-CM showed arrhythmogenic events more frequently compared to control and displayed multiple ion channel dysfunctions, abnormal action potential characteristics, and an enhanced sensitivity of ion channel to adrenergic stimulation. All may contribute to the occurrence of arrhythmias in ARVC patients [27].

These studies provide evidence that patient-derived iPSC-CMs are a useful tool for mechanistic and structural investigations of cardiac diseases. They present a platform that enables a better understanding of the pathogenesis and arrhythmogenesis of ARVC to further evaluate new clinical approaches for diagnosis and treatment.

1.4 Aim of the thesis

Previous studies have shown that mutations in the *DSC2* gene can lead to desmosomal impairment, which has an impact on fibrofatty replacement of myocardium and potentially leads to dysfunctions in calcium handling, and thus contributes to the pathogenesis of ARVC, an inherited heart muscle disease associated with life-threatening ventricular arrhythmias and high risk of SCD [7, 28, 38, 54]. Genetic testing of a 26-years-old female patient from the Ulm University Medical Center with suspected ARVC revealed a missense mutation in the *DSC2* gene (c.2147G>C p.Cys716Ser). The aim of this thesis is the evaluation of the role of this specific human DSC2$^{c.2147G>C}$ mutation *in vitro* by generating patient-specific hiPSC-CM, and *in vivo* by performing a morpholino mediated knockdown of DSC2 in a zebrafish model.

To investigate the DSC2$^{c.2147G>C}$ mutation and clarify its pathogenicity *in vitro*, the patient's data is going to be collected, a patient-specific iPS cell-line will be generated using fibroblasts of the index patient and the iPSC-derived cardiomyocytes will be analyzed.

In addition to that, the effects of the mutation *in vivo* are going to be investigated by performing a DSC2 knockdown in zebrafish mediated by morpholino-modified antisense oligonucleotides and analyzing their cardiologic phenotype by performing electrocardiography.

2 Material & Methods

2.1 Material

2.1.1 Consumables

Name	Company
µ-Plate 96-well Black	Ibidi; Gräfeling, Germany
10 µl, 200 µl, 1.000 µl graduated TipOne®	STARLAB GmbH, Hamburg, Germany
12, 6 Well glass bottom plates	Cellvis; Mountain View, USA
Cellculture microplate, 96-well, ps, f-bottom	Greiner bio-one; Kremsmünster, Austria
Corning® 2 mL Internal Threaded Polypropylene Cryogenic Vial	Corning; Corning USA
Costar® Stripette® serologische Pipetten (50 ml)	Merck; Darmstadt, Germany
CytoView MEA 24-well plate	Axion Biosystems; Atlanta, USA
CytoView MEA 6-well plate	Axion Biosystems; Atlanta, USA
Eppendorf Tubes (0.5 ml, 1.5 ml, 2.0 ml)	Eppendorf AG; Hamburg, Germany
Falcon® 15 mL High Clarity PP Centrifuge Tube	Corning; Corning USA
Falcon® 24-well Clear Flat Bottom TC-treated Multiwell Cell Culture Plate	Corning; Corning USA
Falcon® 5 mL Round Bottom Polystyrene Test Tube, with Cell Strainer Snap Cap	Corning; Corning USA
Falcon® Serological Pipet (2 ml, 5 ml, 10 ml, 25 ml)	Corning; Corning USA
Filter 150 ml 0.2 µm PES Membrane sterile	Avantor; Radnor, USA
Filter 500 ml 0.2 µm PES Membran GL45 Gewinde steril	Avantor; Radnor, USA
LUNA™ Cell Counting Slides, 50 Slides	Logos-Biosystems; Villeneuve d'Ascq, France
Multiwell plate for suspension culture, 12-well	Greiner bio-one; Kremsmünster, Austria

Nährmedienflaschen 500 ml PETG, steril, quadratisch	ThermoFisher Scientific; Waltham, USA
SensoPlate™ 96-Well Glass Bottom Microplates	Greiner bio-one; Kremsmünster, Austria
Tissue culture dish, 150 x 20 mm	SARSTEDT AG & Co. KG; Nürnbrecht, Germany
Tube 50 ml, 114 x 28 mm	SARSTEDT AG & Co. KG; Nürnbrecht, Germany
Zellkulturplatte, 6-well, Oberfläche	SARSTEDT AG & Co. KG; Nürnbrecht, Germany
QIAshredder	Qiagen; Stockach, Germany
GeneRuler DNA Ladder Mix	ThermoFisher Scientific; Waltham, USA
Scalpels	B. Braun Melsungen AG; Melsungen, Germany
Silver wire AGW1010	World Precision Instruments, Sarasota, FL, USA
Syringe 1 ml Luer Lock TM Tip	BD; Franklin Lakes, NJ
Matrices for injection ramp	Eppendorf AG; Hamburg, Germany
Microloader	Eppendorf AG; Hamburg, Germany
Glass capillaries TW100F-6	World Precision Instruments; Sarasota, USA
Pasteur pipettes plastic	BRAND, Wertheim, Germany
Petri dishes plastic (fish)	VWR; Radnor, PA, USA
Disposable Reagent Reservoir 25 ml	Thermo Fisher Scientific, Waltham, MA, USA
Alkaline battery 1604AUP, 9 V Plus Ultra	Gold Peak; Hongkong, China
Multimeter VC170 (Voltcraft)	Conrad electronic; Hirschau, Germany
Thin wall glass capillary TW100F-6	World Precision Instruments, Sarasota, FL, USA
Pasteur pipettes plastic	BRAND, Wertheim, Germany

dNTP Mix 25 mM	Thermo Fisher Scientific, Waltham, MA, USA
RNaseOUT™ Recombinant Ribonuclease Inhibitor	Thermo Fisher Scientific, Waltham, MA, USA
Q5 High-Fidelity DNA Polymerase	NEB Biolabs; Ibswich, MA, USA
Cell culture flasks (Cellstar) 250 ml	Greiner Bio one
Cell count slices C-CHIP Disposable Hemocytometer	NanoEntek; Seoul, Korea
Stem Pro Accutase (Gibco)	Thermo Fisher Scientific, Waltham, MA, USA
NuPAGE Tris-Acetate Mini Gels (3-8 %, 1 mm)	Thermo Fisher Scientific, Waltham, MA, USA
Fish Food (dry)	Tetra; Melle, Germany
Fish food Gemma Micro	Skretting; Stavanger, Norway
Nuclease-free-water	QIAGEN; Hilden, Germany
LightCycler®480 SYBR Green	Roche Diagnostics Deutschland GmbH; Mannheim, Germany
Trans-Blot Turbo 0,2µm PVDF membrane	Bio-Rad, Hercules, California, USA

2.1.2 Chemicals

Name	**Company**
Human Albumin, Recombinant	Sigma-Aldrich; St. Louis, MO, USA
Albumin human	Merck KGaA; Darmstadt, Germany
B-27™ Supplement (50X), serum free	ThermoFisher Scientific; Waltham, USA
BenchStable™ DMEM	ThermoFisher Scientific; Waltham, USA
DMEM/F-12	ThermoFisher Scientific; Waltham, USA
DPBS, no calcium, no magnesium	ThermoFisher Scientific; Waltham, USA

Embryonic stem-cell FBS, qualified, US origin	ThermoFisher Scientific; Waltham, USA
Geltrex™ LDEV-Free, hESC-Qualified, Reduced Growth Factor Basement Membrane Matrix	ThermoFisher Scientific; Waltham, USA
Gentamycinsulfat – 10 mg/mL	Genaxxon Bioscience; Ulm, Germany
HEPES (1M)	ThermoFisher Scientific; Waltham, USA
HEPES sodium salt solution	Merck KGaA; Darmstadt, Germany
Insulin-Transferrin-Selenium (ITS -G) (100X)	ThermoFisher Scientific; Waltham, USA
L-Ascorbic acid 2-phosphate sesquimagnesium salt hydrate	Merck KGaA; Darmstadt, Germany
L-Glutamine (200 mM)	ThermoFisher Scientific; Waltham, USA
mFreSR™ Serum-free cryopreservation medium for human ES and iPS cells	Stemcell Technologies; Köln, Germany
mTeSR™1 5X Supplement	Stemcell Technologies; Köln, Germany
mTeSR™1 Basal Medium	Stemcell Technologies; Köln, Germany
Opti-MEM™ I Reduced Serum Medium	ThermoFisher Scientific; Waltham, USA
Penicillin-Streptomycin (10.000 U/ml)	ThermoFisher Scientific; Waltham, USA
PSC Cryomedium	ThermoFisher Scientific; Waltham, USA
RevitaCell™ Supplement (100X)	ThermoFisher Scientific; Waltham, USA
RPMI 1640 Medium, GlutaMAX™ Supplement, HEPES	ThermoFisher Scientific; Waltham, USA

STEMdiff™ Cardiomyocyte Freezing Medium	Stemcell Technologies; Köln, Germany
StemFlex™ Medium	ThermoFisher Scientific; Waltham, USA
StemFlex™ Supplement	ThermoFisher Scientific; Waltham, USA
StemPro™ Accutase™ Cell Dissociation Reagent	ThermoFisher Scientific; Waltham, USA
Trypan Blue Stain, 0.4 %	Logos-Biosystems; Villeneuve d'Ascq, France
TrypLE™ Express Enzym (1x), without Phenolrot	ThermoFisher Scientific; Waltham, USA
Trypsin 0.05 %/EDTA 0.02 % in PBS, w/o: Ca and Mg	PAN-Biotech GmbH; Aidenbach, Germany
Versene Solution	ThermoFisher Scientific; Waltham, USA
Knockout-DMEM (Gibco)	Thermo Fisher Scientific, Waltham, MA, USA
Water, sterile filtered	Sigma-Aldrich; St. Louis, MO, USA
Gelatin Solution 0.5 %	HIMEDIA, Marg, Mumbai - 400 086, India.
RPMI 1640 (without glucose and HEPES) (Gibco)	Thermo Fisher Scientific, Waltham, MA, USA
CHIR 99021 (Merck Millipore)	Merck KGaA; Darmstadt, Germany
IWP-2 (Merck Millipore)	Merck KGaA; Darmstadt, Germany
Retinoic acid	Sigma-Aldrich; St. Louis, MO, USA
Fura-2, AM	Thermo Fisher Scientific, Waltham, MA, USA
Pluronic F-127 (20 % solution in DMSO)	Thermo Fisher Scientific, Waltham, MA, USA

L-ascorbic acid 2-Phosphate	Sigma-Aldrich; St. Louis, MO, USA
Sodium DL-Lactate Solution	Sigma-Aldrich; St. Louis, MO, USA
Thiazovivin	Merck KGaA; Darmstadt, Germany
Potassium chloride solution 3M	Sigma-Aldrich; St. Louis, MO, USA
CellMask™ Deep Red Actin Tracking Stain	ThermoFisher Scientific; Waltham, USA

Buffers and working solutions

Name	**Ingredients**
Blocking buffer (Western Blot)	5 % milk powder in TBST
10x Blotting buffer (1L)	25 mM Tris 192 mM glycine pH 8.3
1x Blotting buffer	150 ml methanol 100 ml 10x Blotting buffer Fill up to 1 L with ddH_2O
E3 buffer	5 mM NaCl 0.17 mM KCl 0.33 mM $CaCl_2$ 0.33 mM $MgSO_4$
6x Loading Dye (agarose)	Purchased from Thermo Fisher #R0611
3x Laemmli-buffer	187.5 mM Tris HCl (pH 6.8) 6 % SDS 30 % glycerol 2 % ß-mercaptoethanol 0.03 % Bromphenol Blue 150 mM DTT
2.5 % Methylcellulose	1.25 g Methylcellulose in 50 ml E3
PBDT	1 % DMSO in PBT

PBSBT	0.1 % Tween 20 0.2 % BSA in PBS
PBT	0.1 % Tween 20 in 1 x PBS
PFA in PBS	4 % Paraformaldehyde in PBS for solving add 0.1M NaCl and heat up to 68 °C
10x SDS Running buffer (1L)	192 mM glycine 25 mM Tris 0.1 % SDS add ddH2O; pH 8.3
10x TBE (1L)	Purchased from Sigma #T4415-10L
TBS 20x (1 L)	2.8M NaCl 500 mM Tris Fill up to 1 L with ddH_2O, pH 7.4
1x TBST	0.05 % Tween 20 in 1x TBS
Washing buffer	110 mM NaCl 3.5 mM KCl 27 mM $CaCl_2$ 10 mM Tris-HCl, pH 8.5
Tyrodes Solution	140 mM NaCl, 5 mM KCl, 5 mM HEPES, 1 mM NaH_2PO_4, 1 mM $MgCl_2$, 1.8 mM $CaCl_2$, 10 mM glucose (pH 7.4) adjusted with NAOH
MESAB	4 mg/ml Ethyl-3-aminobenzoate methane sulfonate salt (MESAB) 1 % Na_2HPO_4 pH 7.0-7.5
Fibroblast culture medium	DMEM, 10 % FBS, 1 x L-glutamine, 1 x sodium pyruvate, 1 x penicillin-streptomycin
KO-DMEM	15 % KnockOut serum replacement, 1 x L-glutamine,

	1 x nonessential amino acids, 1 x penicillin-streptomycin, 0.1 mM ß-Mercaptoethanol, basic fibroblast growth factor (bFGF) 10 ng/ml
Cardio Differentiation medium	RPMI 1640 (with GlutaMAX and HEPES) 0.2 mg/ml L-ascorbic acid 2-phosphate 0.5 mg/ml human recombinant albumin
Cardio Culture medium	RPMI 1640 (with GlutaMAX and HEPES) 1 x B-27 Supplement (50x)
Cardio Recovery medium	Cardio culture medium 20 % Fetal Bovine Serum 2µM Thioazovivin
Cardio Selection medium	RPMI 1640 (without glucose and HEPES) 0.2 mg/ml L-ascorbic acid 2-phosphate 0.5 mg/ml human recombinant albumin 4 mM lactate/HEPES

Primary Antibodies

Name	**Working concentration**	**Company/Catalogue Number**
DSC2 Rabbit pAb	1:1000 for Western Blot	A10211 ABclonal
Desmocollin 2 Polyclonal Antibody	1:2000 for Western Blot; 1:300 for IF	PA5-87712 ThermoFisher
Anti-Desmoglein 2/DSG2 antibody	5 µg/ml for ICC/IF	ab269978 Abcam

Anti-Plakophilin 2/PKP2 antibody	0.25 – 2 µg/ml	ab220840 Abcam
Recombinant Anti-Desmoplakin antibody	1:1000 for Western Blot and IF	ab109445 Abcam
Recombinant Anti-gamma Catenin antibody	1:1000 for Western Blot; 1:250 for IF	ab184919 Abcam
Anti-Plakophilin 2/PKP2 antibody	0.25 – 2 µg/ml for IF	ab223757 Abcam
Anti-α-Actinin antibody (Mouse IgG1)	1:200 for IF	#A7811Sigma Aldrich
GAPDH	1:10000 for Western Blot	ab181602 Abcam

Secondary Antibodies

Name	**Working concentration**	**Company/Catalogue Number**
Anti-mouse IgG HRP linked	1:2000	Cell signaling #7076
Anti-rabbit IgG HRP linked	1:2000	Cell signaling #7074
Goat Anti-rabbit IgG Alexa Fluor 488	1:100	Thermo Fisher #A11034
Goat Anti-mouse IgG1 Alexa Fluor 555	1:100	Invitrogen #A21127

Primers

Name	**Sequence 5'-3'**
DSC2 Exon 11 fwd	CCGAAAATGACTGCACACATCGT
DSC2 Exon 11 rev	CCACAGTTTGGGTTGTGAAGCC
18S (1) fwd	AAATCAGTTATGGTTCCTTTGGTC
18S (1) rev	CCGTCGGCATGTATTAGCTC
GAPDH fwd	CACCCACTCCTCCACCTTTG
GAPDH rev	ACCACCCTGTTGCTGTAGCC
DSC2 (qPCR, 2) fwd	GGAGAGAGACACTGGAAACTTG
DSC2 (qPCR, 2) rev	TCTGGAGTATACCCATCTGGAG

Morpholino

Name (ZFIN ID)	Sequence 5'-3'
ZDB-MRPHLNO-070206-3	CGCACGAGCTATAAACTACAGC

Kits

Name	Ingredients
ISOLATEII PCR and Gel Kit BIO-52060	BioCat, Heidelberg Germany
Human Cardiomyocyte Immunochemistry Kit	Thermo Fisher Scientific, Waltham, MA, USA
Subcellular protein fraction kit	Thermo Fisher Scientific, Waltham, MA, USA
RNeasy Mini Kit	QIAGEN
Pierce™ BCA Protein Assay Kit	Thermo Fisher Scientific, Waltham, MA, USA
Human Tri-Lineage Multiplex PCR-Kit	abm; Vancouver, Canada
Superscript III Reverse Transcriptase	Thermo Fisher Scientific, Waltham, MA, USA
CTS CytoTune-iPS 2.1 Sendai Reprogramming Kit	Thermo Fisher Scientific, Waltham, MA, USA
SuperSignalTM West Femto Trial Kit	Thermo Fisher Scientific, Waltham, MA, USA
Lipid (Oil Red O) staining Kit	BioVision, Inc; Waltham, MA, USA

2.1.3 Technical Equipment

Name	Company
accu-jet® pro	BrandTech® Scientific; Essex, Canada
External light source for fluorescence excitation Leica EL6000	Leica Kamera AG; Solms, Germany
Heraeus HS9	Heraeus; Hanau, Germany
Heraeus HS18	Heraeus; Hanau, Germany
LUNA-II™ Automated Cell Counter	Logos-Biosystems; Villeneuve d'Ascq, France

MediLine refrigerator	Liebherr; Biberach a.d. Riß, Germany
Thermo Scientific™ Precision™ General Purpose Baths	ThermoFisher Scientific; Waltham, USA
Vortex mixer, VV3	Avantor; Radnor, USA
LightCycler® 480 PCR System	Roche Molecular Systems; Pleasanton, USA
Infinite® 200 PRO	Tecan Group; Männedorf, Schweiz

Incubators

Name	**Company**
HeraCell 150 CO2 Inkubator (cells)	Heraeus; Hanau, Germany
Incubator B6200 (fish)	Thermo Fisher Scientific Germany BV & Co KG; Braunschweig, Germany

Scales

Name	**Company**
Scale Sartorius ED124S	Sartorius; Göttingen, Germany
Scale Adventurer AR 5120	Ohaus, Parsippany-Troy Hills, NJ, USA

Centrifuges

Name	**Company**
Biofuge PrimoR	Heraeus; Hanau, Germany
Centrifuge 5418	Eppendorf AG; Hamburg, Germany
Centrifuge 5424R	Eppendorf AG; Hamburg, Germany
CompactStar CS4	VWR; Darmstadt, Germany
Multifuge 3 S-R	Heraeus; Hanau, Germany
Megafuge 1.0R	Heraeus; Hanau, Germany
Centrifuge 5417R	Eppendorf AG; Hamburg, Germany
MiniStar Silverline	VWR; Radnor, PA, USA

Shaking platforms

Name	**Company**
Heidolph Duomax 1030	Heidolph; Schwabach, Germany
IKA Roller 10 basic	IKA; Staufen, Germany

Microscopes

Name	Company
Olympus CKX53	Olympus; Shinjuku Monolith, Japan
Nikon TMS	Nikon; Tokyo, Japan
Leica TCS SP8	Leica microsystems; Wetzlar, Germany
Leica DMIL LED	Leica microsystems; Wetzlar, Germany
Zeiss Axio V.16	Carl Zeiss AG; Oberkochen, Germany
Olympus SZX16	Olympus; Shinjuku Monolith, Japan

Cameras

Name	Company
Leica DFC 400	Leica Kamera AG; Solms, Germany

2.1.4 Software

Name	Application	Company
Leica Application Suite V3.7		Leica Kamera AG; Solms, Germany
ApE	Program for visualization of sequencing	ApE
Finch TV	Tool to visualize chromatograms	Geospiza
Image J	Program to process scientific images	National Institutes of Health
Microsoft office	Writing application	Microsoft
Prism 9	Statistical data analysis	GraphPad
LAS X	Program to acquire and analyze pictures of confocal microscope	Leica Kamera AG; Solms, Germany
Clampfit 11.2	Program to analyze signals	Molecular devices
Labchart 8	Program to record zebrafish ECG	AD Instruments

LightCycler® 480 Software 1.5.0.39	System used to run real-time qPCR	Roche Molecular Systems; Pleasanton, USA
Turbo SM	Calcium Imaging Software	RedShirtImaging™ LLC; Decatur, USA
i-control™	Software for TECAN reader	Tecan Group; Männedorf, Schweiz

2.1.5 Cell lines

Name	**Company**
Thermo IPSC (Gibco Human Episomal A18944)	Thermo Fisher Scientific, Waltham, MA, USA
Patient iPSC DSC2$^{c.2147G>C}$	Reprogrammed from fibroblasts isolated from skin biopsy
CF1 Mouse Embryonic Fibroblasts, MitC-treated	Thermo Fisher Scientific, Waltham, MA, USA
Fibroblasts patient	Extracted from skin biopsy
Fibroblasts control	Extracted from skin biopsy

2.1.6 Fish lines

TÜAB	wild-type line

Sequencing service: Eurofins genomics

Statistics

All graphs and statistical analyses are displayed as means ± standard deviation (SD) and were done by using GraphPad Prism9. Analyses were performed using one-way ANOVA or Mann-Whitney tests. A value of $p<0.05$ was accepted as statistically significant. For each experiment the way of analysis can be found in the corresponding figure legend.

Ethics approval reference number: 394/19

2.2 Methods

2.2.1 Induced pluripotent stem cells (iPS) generation

The index patient underwent a skin biopsy, out of which fibroblasts were isolated and collected. The following steps of iPS generation were performed by following the steps described in the protocol by Li et al [46].

On the day before the transfection, $5.5x10^4$ fibroblast cells were seated out onto each well of a 12-well plate. The fibroblasts were cultured overnight in an incubator (37 °C, 5 % CO_2) to ensure cell adhesion to the plate. The day after the plating, the cells were transfected with a Sendai Virus expressing the Yamanaka factors (Klf4-Oct3/4-Sox2 (KOS), L-Myc and Klf4). The volumes of each virus (one per Yamanaka factor) for $5.5x10^4$ cells were calculated at a multiplicity of infection (MOI) of 4. The culture medium of the fibroblast cells was removed completely and 500 µl of the virus-medium mixture were gently applied to each well. The plates were then put into the incubator overnight. The following day, another 500 µl of fibroblast culture medium was added. Two days after the transfection, the virus-medium mixture was replaced completely by KO-DMEM medium. The incubation was continued for an additional seven days, during which the KO-DMEM medium was changed daily.

Seven days after Sendai transduction, the cell medium was removed, the cells were washed once with PBS and 500 µl of TrypLE Express was added to each well. The plates were incubated at 37 °C for 4 min. The plate was then put out of the incubator and TrypLE express was removed. 2 ml of KO-DMEM medium containing 10 µM ROCK inhibitor was applied to each well, after which the cells were resuspended by gently pipetting up and down. The cells were transferred onto a feeder plate, prepared the day before by inoculating $2x10^5$ Mitomycin-C treated MEF cells on gelatin-coated wells (0.1 %) of a 6-well plate. Cells from one 12-well plate were transferred onto one 6-well plate.

After 24 h of incubation, the medium containing the ROCK inhibitor was replaced by KO-DMEM medium and changed every following day. Colonies started to form during this time. Seven days after passage, the iPS colonies were separated from the fibroblasts and micro dissected into chunks of about 100-150 cells using sterile glass hooks under the microscope. The colony chunks were then transferred onto 12-well plates, which were prepared the day prior to the picking by inoculating $4x10^4$ MEF cells as feeder cells on each well, which has been pre-coated with gelatin

(0.1 %). The plates were put into the incubator, containing the colony chunks and KO-DMEM medium with ROCK inhibitor. The following day, the medium was replaced by KO-DMEM only.

One week after colony transfer the cells were passaged again and kept in culture using conventional methods for iPS cell cultures.

2.2.2 iPS-derived cardiomyocytes differentiation

The subtype-directed differentiation of hiPSCs into atrial and ventricular cardiomyocytes was performed by following the steps described in the protocol by Kleinsorge and Cyganek (2020) [43]. The differentiation was carried out on 12-well plates and the used concentration of CHIR99021 was 0.4 µl/ml. All other steps did not differ from the original protocol.

2.2.3 mRNA extraction from cultured cells

The culture medium was removed, and the cells were washed twice with DPBS. After the washing steps, RLT buffer with β-mercaptoethanol (dissolved 1:100 in the buffer) was added to each well (350 µl in a well of a 12 well plate). With a pipette tip or a cell scratcher, the cells have been scratched from the surface and 700 µl of the cell lysate was transferred to a RNeasy Mini spin column, which was placed in a 2 ml collection tube, and centrifuged for 30 s at 11.000 g. The flow-through was discarded. 700 µl of RW1 Buffer was added and the sample was centrifuged again for 30 s at 11.000 g. The flow through was discarded and 500 µl of RPE Buffer added. After centrifuging for 30 s at 11.000 g, the flow through was discarded and 500 µl of RPE Buffer was added. The sample was centrifuged for 2 min at 11.000 g. The RNeasy spin column was placed into a new 2 ml collection tube and centrifuged at 14.000 g for 1 min to dry the membrane. For the final step, the RNeasy spin column was placed in a new 1,5 ml collection tube and 30 µl nuclease-free water was added directly onto the membrane of the spin column. To elute the RNA, the sample was centrifuged for 1 min at 11.000 g. The extracted mRNA was stored at –80°C until use.

2.2.4 Reverse transcription (cDNA)

For reverse transcription of RNA, following components were added to a 200 µl PCR tube: 1 µl Oligo-dT at a concentration of 50 pmol/µl, 10 pg-5 µg (1-2 µg) RNA, and 1 µl 10 mM dNTP-Mix. The volume was filled up with nuclease-free water to a total of 13 µl. The tube was put into the Thermocycler and the PCR program Sscript III was started. After 7 min, 4 µl of 5x first-strand buffer, 1 µl 0,1 M DTT, 1 µl RNaseOut

recombinant RNase Inhibitor and 1 µl SuperScript III RT was added to the sample. The PCR program was continued after adding the additional components. The synthesized cDNA samples were stored at -20°C until use.

Step	***Temperature***	***Time***
cDNA synthesis	65°C	5 min
	4°C	2 min – pause point
	50°C	60 min
	70°C	15 min
Hold	4°C	unlimited

2.2.5 Polymerase chain reaction (PCR)

PCR was performed to define a gene expression or to amplify a gene of interest using a Taq Polymerase (standard PCR) or a Q5® Hot Start High-Fidelity DNA Polymerase (Gateway PCR) according to the manufacturer's instructions. The thermocycling conditions were as follows:

Step	***Temperature***	***Time***
Denaturation	98°C	30 s
25-35 Cycles	98°C	5-10 s
	50-72°C	10-30 s
	72°C	20-30 s/kb
Extension	72°C	2 min
Hold	4°C	unlimited

2.2.6 Quantitative real-time PCR

Samples and primers were prepared before each experiment. A primer mix was created by diluting forward and reverse primers (50 pmol/l) at a ratio of 1:10 in nuclease free water. cDNA of wild-type and patient-specific cardiomyocytes was diluted at a ratio of 1:15. The quantitative real-time PCR setup consisted of 10 µl SYBR-Green, 2 µl primer mix and 5 µl diluted cDNA. Each experiment has been performed as technical and biological triplicate.

Step	***Temperature***	***Time***
Denaturation	95°C	5 min
Amplification - 45 Cycles	95°C	10 s
	55°C	15 s

	72°C	10 s
Melting Curves	95°C	5 s
	55°C	1 min
Cooling	40°C	10 s

2.2.7 Agarose gel electrophoresis

By taking advantage of the agarose gel electrophoresis, DNA fragments were separated by size. A 1-2 % agarose gel was added to 1xTBE Buffer and boiled until it was completely dissolved. The exact concentration varied depending on the size of the PCR product. After adding Midori Green Advance® at a concentration of 0.04-0.06 µl/ml, the gel was poured into a gel tray of an appropriate size. A well comb, which was chosen based on the PCR volume, was put into the gel tray. After solidification of the gel, 6x Loading Dye® was added to the samples and subsequently the gel was loaded. A GeneRuler DNA Ladder was used as a standard. The gel ran at 200-220 V for 1-2 h, depending on the size of the product. The bands were documented by photograph and cut out of the gel. They were purified for either subsequent cloning or sequencing.

2.2.8 Purification and isolation of DNA after agarose gel electrophoresis

After cutting out the bands from the agarose gel, the DNA was extracted according to the manufacturer's instructions using the Isolate II PCR and Gel Kit. The purified DNA was either sent away for sequencing or used for cloning.

2.2.9 Protein extraction from hiPSc-derived cardiomyocytes

The protein extraction was performed in two different ways, either extracting the protein stepwise from cytoplasmic, membrane, nuclear soluble, chromatin-bound and cytoskeletal extracts, or directly extracting the protein from a cell lysate, without separating the different fractions.

The last mentioned was performed by detaching the cells with force, using a pipette tip or a cell scratcher. The medium with the cell suspension was transferred to a 50 ml falcon and centrifuged at 100 g for 10 min. After removing the supernatant, the cell pellet was resuspended by adding 5 ml of DPBS at room temperature and pipetting carefully. The cell suspension was centrifuged again at 100 g for 10 min. The supernatant was removed, and premixed RIPA buffer with protease inhibitors (diluted 1:25) was added. After resuspending, the suspension was transferred to a 1,5 ml collection tube and put on ice for 15 min. The lysate was centrifuged at

13.200 rpm for 15 min at 4 °C. The supernatant containing the protein extract was transferred to a new collection tube.

The above-mentioned protein extraction of the different cell fractions was performed by using the subcellular protein fractionation kit by Thermofisher scientific. The individual steps were carried out following the manufacturer's instructions.

All protein extracts were stored at -80 °C until use, after measuring the concentration according to the BCA-Assay.

2.2.10 BCA-Assay for measuring protein concentration

The concentration of the protein lysate was measured with the Pierce BCA Protein Assay Kit according to manufacturer's instruction. The measurement itself was carried out with the TECAN Infinite 200 PRO microplate plate reader and the i-control software.

2.2.11 Immunoblotting

A total of 30 µg protein lysate of patient-specific hiPSc-derived cardiomyocytes and Wild-Type cardiomyocytes was used for immunoblotting. The samples were prepared by boiling the protein lysate in 5x Laemmli Buffer at 98 °C for 5 min. The lysate was separated by SDS-PAGE (8-16 % gradient gel; Bio-Rad) and consecutively blotted onto polyvinylidene difluoride (PVDF) membranes. For the blocking of unspecific binding sites 5 % BSA (Bovine Serum Albumin) in TBST was used for one hour at room temperature. The primary antibody was added, and the membranes were incubated at 4 °C overnight. The following morning, the membranes were washed four times for 15 min with TBST and then incubated with the secondary antibody at room temperature for one hour. After the incubation period, the membranes were washed again three times for 10 min with TBST and once with PBS for 5 min. For the development of the signal the Pierce ECL Western Blotting Substrate (Thermo Scientific) and a luminescent image analyzer (Image Quant Las4000 mini) were used.

Analysis was done by using the Gel-Pro Analyzer (Media Cybernetics, Inc.; Rockville, USA).

2.2.12 Immunofluorescence staining

For immunofluorescence staining fully differentiated cardiomyocytes were plated onto 96-well glass plates at a cell density that allowed the cells to adhere as a monolayer. For cell fixation and blocking, the Human Cardiomyocyte

Immunocytochemistry Kit by Thermofisher scientific was used. However, some of the steps differed from the protocol.

First, the cardiomyocyte culture medium was removed, 70 µl of Fixative Solution were added to each well and the plate was incubated for 15 min at room temperature. After that time period, the Fixative Solution was replaced by 70 µl of Permeabilization Solution per well and the plate was incubated for an additional 15 min at room temperature. The solution was removed and 70 µl of Blocking Solution were added to each well. An incubation period of 30 min at room temperature followed. A specific volume of the desired antibody was added directly to the Blocking Solution covering the cells to yield an appropriate concentration. The plate was incubated overnight at 4 °C. The morning after, the solution was removed, and the cells were washed 2-3 times using a Wash Buffer diluted in PBS. The appropriate secondary antibody was added, diluted in the Blocking Solution. An incubation period of 1 hour at room temperature followed, after which the cells were washed another 2-3 times using the above-mentioned Wash Buffer. During the last washing step, 1 drop of NucBlue® Fixed Cell Stain (DAPI) was added to each well and incubated for 5 min.

2.2.13 Lipid Oil-Red-O staining

Oil-Red-O staining was performed by following the manufacturer's instructions of the Lipid (Oil Red O) Staining Kit. Oil Red O Stock solution was prepared by dissolving Oil Red O in 20 ml of 100 % isopropanol. For Oil Red O Working solution, 3 parts of the stock solution were added to 2 parts of dH_2O. It was prepared 15 min before use. The solution was filtered with a 0.2 µm syringe filter.

iPS-derived control and patient-specific cardiomyocytes were fixed by removing the medium and washing each well twice with PBS. Formalin (10 %) was added and an incubation period of 30 min followed. Formalin was removed and cells were washed twice with dH_2O. Isopropanol (60 %) was added, and the plate was incubated for 5 min. After removing isopropanol (60 %), Oil Red O Working Solution was added, evenly covering the cells. The plate was incubated for 15 min whilst rotating. The working solution was removed, and the plate washed 2-5 times with dH_2O. Hematoxylin was added and incubated for 1 min, after which 2-5 washing steps followed.

Staining was now visible under the microscope. For quantification, the cells were additionally washed 3 times for 5 min with isopropanol (60 %) whilst gently rocking.

Oil Red O stain was extracted with 100 % isopropanol for 5 min, 100 % isopropanol was used as background control to subtract background signals. The absorbance was read at 492 nm using the Tecan Infinite® 200 PRO.

2.2.14 Ca^{2+} imaging

For Ca^{2+}-Imaging fully differentiated cardiomyocytes were plated onto 96-well glass plates. The culture medium was removed and 300 µl Cardio Culture medium containing 2 µl/ml Fura-2 were added to each well and incubated for 8 min at room temperature. Prior to adding Fura-2 to the culture medium, it was diluted in 50 µl 2 µM Pluronic acid dissolved in DMSO. Consecutively, the mixture was replaced by 300 µl of Tyrode's solution and the plate was incubated in the dark for 10 min at room temperature. Finally, the Tyrode's solution was removed and 300 µl of Cardio Culture medium were added to each well. After 30 min, the Ca^{2+} sparks were recorded at the Confocal with the Turbo sm software using the following settings:

- exposure time 25 ms (40 frames/s)
- camera gain set at mid low
- number of frames at 1500
- 40x objective

2.2.15 Ca^{2+} imaging analysis

For the analysis of the Ca^{2+}-Imaging recordings the ImageJ software was used. After creating a Z-project and choosing the standard deviation as a projection type, squares were put on each single cell using the ROI-Manager as analysis tool. For each recording, 16 squares and thus 16 single cells were selected for the analysis. The 17th square was set as background. The quantification was obtained by selecting the multi measure tool. The data was then transposed with a template explicitly designed for 1500 frame long recordings to create a curve which was then analyzed with the Clampfit software. Each signal was displayed as one curve. The cursors were positioned at the beginning of the first and the end of the fifth peak of each individual signal. The analyzed part was in between those cursors. Using the Statistics tool of Clampfit, following parameters were analyzed as a mean of each individual signal: time of peak, half-width (Ca^{2+} transient duration 50 %), rise time and decay time. The obtained data was then statistically analyzed.

2.2.16 Multielectrode-Array

For electrophysiological analysis, iPSC-CMs were seeded onto 24-well MEA plates (Axion BioSystems, Atlanta, GA, USA). MEA plates were coated with Geltrex diluted

1:100 in DMEM/F-12. 150,000 cells resuspended in 8 µl of Cardio Recovery medium were plated onto each well. After 1 hour, 1 µl of medium was gently added to the well. iPSC-derived control and patient-specific cardiomyocytes were maintained in culture on the MEA plates for 7 days before starting the experiments. Electrophysiological recordings were done by using the Maestro Edge equipped with the AxIS Navigator software (Axion BioSystems, Atlanta, GA, USA). The temperature of the Maestro Edge was set to 37 °C, the CO_2 concentration to 5 %. For each experiment, the sequence was as follows:

- Spontaneous FP recording for 2 min
- Spontaneous Contractility recording for 2 min
- LEAP induction (10 min)
- LEAP recording for 5 min
- LEAP paced at 1-2 Hz for 5 min

All experiments have been carried out as technical and biological triplicates.

2.2.17 Immunoprecipitation

Dynabeads™ Protein G and Protein A were mixed to obtain a 1:1 solution of Dynabeads™. For each immunoprecipitation a protein amount of 50-100 µg was used. The main steps were carried out as described in the protocol for Immunoprecipitation by Thermofisher scientific. The Dynabeads™ magnetic beads mixture was resuspended, vortexed for >30 s, and transferred to a new tube. For each sample 40 µl Dynabeads™ mixture were used. The tubes were placed on a magnet and the supernatant was removed. The beads were washed twice with PBS containing 0.02 % Tween™ 20. The tubes were then put on a non-magnetic rack and the antibody, diluted 1:40 in 200 µl PBS with 0.02 % Tween™ 20, was added to the Dynabeads™. An incubation period of 10 min at room temperature followed. The tubes were placed on the magnet and the supernatant was removed. After putting the tubes on a non-magnetic rack, the magnetic bead-Ab complex was resuspended in 200 µl PBS with Tween™ 20 and incubated for 1 hour at 4 °C on a tilting rack. The tubes were put on the magnet and the supernatant was removed. 400 µl of each sample containing the antigen were added to the corresponding tube and resuspended after removing the tubes from the magnet. To immunoprecipitate the target antigen, the samples were incubated at 4 °C overnight on a tilting rack. The supernatant was removed again after placing the tubes on the magnet. The magnetic bead-Ab-Ag complex was washed 3 times with 200 µl of PBS containing

0.02 % Tween™ 20. After the last washing step, the magnetic bead-Ab-Ag complex was resuspended in 100 µl washing buffer and transferred to a new tube to avoid co-elution of proteins bound to the tube wall. The tubes were placed on a magnet and the supernatant removed. 40 µl of 2 x Laemmli Buffer were added to each sample. The tubes were removed from the magnet and the solution was resuspended and boiled at 95 °C for 5 min. The tubes were put on the magnet again and the supernatant was transferred to a new tube without the beads. The final solution was then used to run a Western Blot together with the input of the same protein samples used for the immunoprecipitation.

2.2.18 Zebrafish

Care and breeding of zebrafish *Danio rerio* were carried out as described in "The Zebrafish book – A guide for the laboratory use of zebrafish (Danio rerio)" (Rottbauer et al. 2005).

The fish facility was built by Aqua Schwarz Aquarienbau and compromises a total of 10 m^3 of deionized water. The pH is maintained between 7.2–7.4 by adding Na_2CO_3 and the temperature kept at 28 °C constant. The water conductivity is around 200-400 µS/cm. The natural day-night rhythm of zebrafish was maintained by following a 13 h light and 11 h night schedule. The fish were fed twice in the morning with ex-encapsulated Artemia. In the afternoon, the fish were fed with Gemma micro and additionally they got TetraPro dry food once a day. Plastic mating tanks (by Tecniplast) with two movable sieves were used to separate male from female fish, and to separate both from the eggs. The afternoon before collecting the eggs, the zebrafish in the mating tanks are separated by a removable sieve after having been sorted by sex. Those screens are removed the following morning to allow the fish to mate. After 10-15 min, the eggs are removed with a sieve and washed with E3 buffer. They are transferred to a petri dish and at that point an injection with morpholinos or mRNA, for instance, can be performed. The embryonic zebrafish are kept in the incubator at a constant temperature of 28.5 °C for no longer than 5 days.

All zebrafish experiments have been performed at embryonic zebrafish at 48 hours post fertilization.

2.2.19 Microinjection in zebrafish eggs

For injection, the TÜAB wildtype strain was used. Injection ramps are made of 3 % agarose dissolved in E3 medium, which is being poured into a plastic petri dish. A

plastic matrix is placed on top and removed after solidification. The ramps consist out of a total of 6 grooves. Before injection, injection needles are prepared by pulling 0.75 mm glass capillaries with a capillary puller, and afterwards opened using a razor blade. The injection needles are then loaded with the substance to inject (morpholino or mRNA). All injections were performed on zebrafish embryos in the one-cell stage. For morpholino-mediated knockdown, morpholino-modified antisense oligonucleotides by Heuser et al. (2006) were used: 5'-CGCACGAGCTATAAACTACAGC-3'. MO-dsc2 was directed against exon 6 of zebrafish dsc2. Before use, all MOs were dissolved in 0.2 M KCl to a final concentration of 200 µM. The injector was set to an injection pressure between 80 and 350 hPa, which was adapted to assure a constant injection volume. The injection time varied between 0.1 and 0.3 s.

After injection, the eggs were transferred to a petri dish, which contained E3 medium, and finally placed into the incubator. Within the following 48 hours after injection, dead eggs were removed and E3 medium was changed regularly.

2.2.20 Photo and video documentation of zebrafish embryos

Photo and video documentation of zebrafish embryos was made by placing the embryo in a glass microscope slide, which had a small depression. The embryo was put in 2.5 % methylcellulose in E3 medium. The embryos were positioned in such a way that the head was oriented to the left. The images were taken with an Olympus SZX 16 microscope. Video documentation was done on a Leica DM IL LED microscope.

2.2.21 ECG on zebrafish embryos

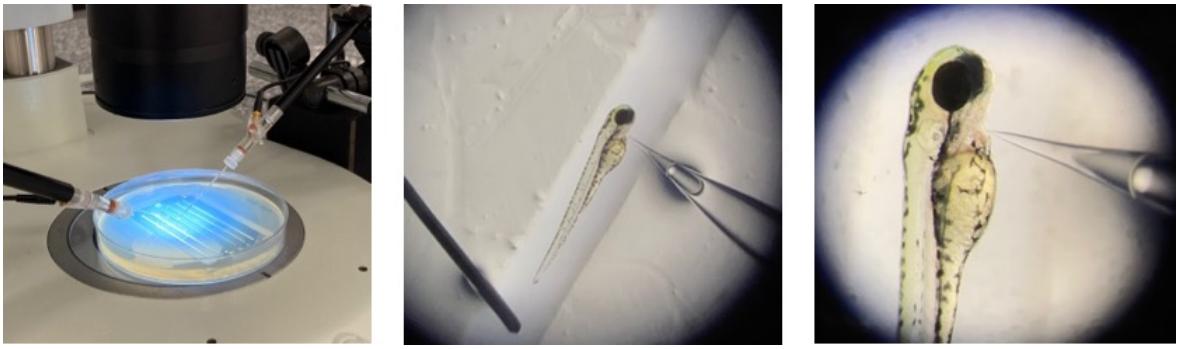

Figure 7: Setup of ECG-recordings on embryonic zebrafish at 48 hpf.

ECG recordings were performed on embryonic zebrafish at 48 hpf (Figure 7). Two conditions were analyzed: wild type control zebrafish and morpholino injected zebrafish (MO-dsc2, 250 µM).

For each ECG experiment, a new recording electrode was prepared. A silver wire was chlorinated and put into a pre-pulled glass capillary, which was filled with a 3 M KCl solution. The silver wire and glass capillary were put into a holder which was fixed on a micro manipulator and connected to the headstage. The ground electrode was connected as well. Embryonic zebrafish were put onto an injection ramp. The recording electrode was positioned in between the atrium and the ventricle of the embryo, only touching the skin surface, whereas the ground electrode was put into the agar plate, not touching the embryo, as displayed in the image. Zebrafish embryos were anesthetized with MESAB (3 mg/ml diluted in E3 medium) for 3 min prior to the recording. The headstage consisted of an EXT-10/2F amplifier connected to the PowerLab 4/35. The amplifier settings were as follows:

- High pass filter: 0.1 Hz
- Low pass filter: 100 Hz
- Gain: 1 k
- OFFSET range: ± 1 V
- OFFSET potentiometer: was adjusted after each new positioning of the electrodes, to assure that analog balance monitor displayed 0
- Balance x10 mV: displayed 0

A filtered output was chosen. The signal was detected with Labchart 8.1.21. The band pass of the digital filter was set at a high cut off frequency of 30 Hz and a low cut off frequency of 4 Hz.

The obtained signal was manually analyzed with the Clampfit software. QT-time and QRS-complex-duration were measured at four different time points. The mean value was formed. QTc-time was calculated using the Bazett-formula. QRS-amplitude was measured as well and the frequency in beats per minute calculated by counting all R-peaks within 15 seconds of each recording, followed by a multiplication by four. For the Root Mean Square of Successive Differences (RMSSD) the RR-interval was measured four times for each recording. RMSSD was calculated using the following formula:

$$\text{RMSSD} = \sqrt{\left(\frac{1}{N-1}\right)\left(\sum_{i=1}^{N-1}((R-R)_{i+1} - (R-R)_i)^2\right)}$$

3 Results

3.1 *In vitro* model revealed arrhythmogenic phenotype of DSC2$^{c.2147G>C}$ mutation

Cardiomyopathic patients from the Ulm University Medical Center are routinely screened for cardiomyopathy candidate genes, as part of a cooperation with the Biobank Cardiomyopathy Ulm (BCMU). Genetic testing of a 26-years-old female patient with suspected ARVC and clustered heart diseases within the family revealed a missense mutation in the *DSC2* gene. Guanin has been exchanged by cytosine in exon 14 of the *DSC2* gene (c.2147G>C), which led to an amino acid exchange of cysteine to serin in position 716 of the amino acid sequence (Cys716Ser).

To investigate the DSC2$^{c.2147G>C}$ mutation and clarify its pathogenicity *in vitro*, the patient's data has been collected, a patient-specific iPS cell-line was generated and the iPSC-derived cardiomyocytes were analyzed. For additional investigation purposes the effects of the mutation *in vivo* were investigated by performing a morpholino-mediated DSC2 knockdown in zebrafish embryos and analyzing their cardiologic phenotype by electrocardiography.

3.1.1 Patient examination led to diagnosis of suspected ARVC

The 26 years old index patient was referred to the cardiology clinic of the Ulm University Medical Center for evaluation because of clustered sudden cardiac deaths within the family and regular occurring, short-lasting heart palpitations. The patient had a syncope once due to a stimulus of the nervus vagus. The father and the sister of the patient survived to a sudden cardiac death (SCD) (Figure 8). The father got an ICD implanted, secondary prophylactic. The mother carries a pacemaker due to an AV-block (III. Grade). The causes that led to the SCDs in both family members are not entirely known. The sister, in her mid-twenties, was diagnosed with permanent atrial fibrillation with normofrequent transition, ventricular bigeminy and mitral valve prolapse with mitral regurgitation. In the context of a long-QT-syndrome she had a SCD, which resulted in hypoxic brain damage and spastic tetraparesis. Due to that a pacemaker was implanted.

Mother and father of the index patient are carriers of mutations in several cardiomyopathy candidate genes. The mother has been tested positive for two mutations in the *TTN* gene and one in the *MYH6*. The father has been tested positive

for mutations in *DSP*, *PKP2* and *DSC2*. Both sisters only inherited the mutation in the *DSC2* gene, whereas genetic analyses of mutations in other mentioned gene loci resulted negative. We therefore assume that this specific *DSC2* mutation is autosomal dominant.

Examinations revealed that the index patient, father, and sister are all carriers of the previously mentioned variation of *DSC2* (*DSC2*$^{c.2147G>C}$), which has been identified as genetic variant of unclear clinical significance.

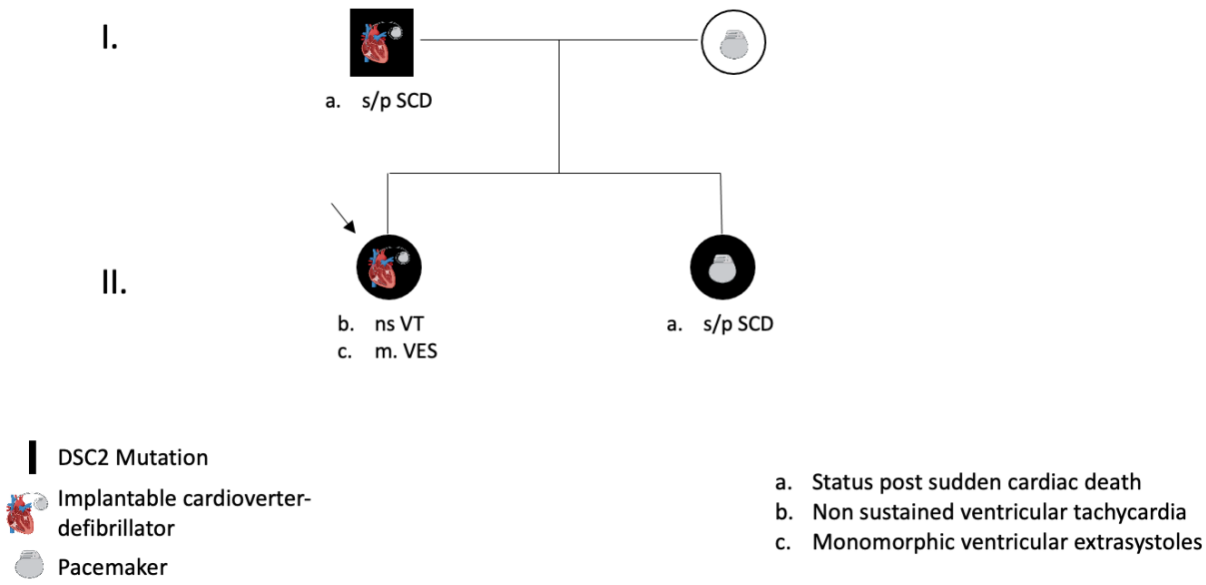

Figure 8: Pedigree of the index patient, marked with an arrow.

Pathogenetic variations in *DSC2* are known to be associated with Arrhythmogenic Right Ventricular Cardiomyopathy (ARVC), which leads to a significantly increased risk for malignant cardiac arrhythmias [59]. Event recorder interrogation of the index patient detected non-sustained polymorphic ventricular tachycardias (VT) over 8 beats and multiple monomorphic ventricular extrasystoles correlating with clinical symptoms, some occurring as single ectopic beats or irregular heartbeats which follow each regular heartbeat, also known as bigeminy. Pharmacological treatment with Bisoprolol 1.25 mg 0-0-1 was initiated. After detailed discussion, the index patient got a subcutaneous ICD implanted for primary prophylaxis.

The final diagnosis was ARVC. Disease progression continued and the index patient is now on the list for heart transplantation.

3.1.2 Mutation is predicted to be probably damaging and to lead to protein instability

DSC2 is a transmembrane protein (Figure 9) and thus consists of an intracellular and extracellular part. The mutation of the index patient (c.2147G>C) led to an amino acid exchange from cysteine to serin at position 716 of the amino acid sequence (Figure 9, 10).

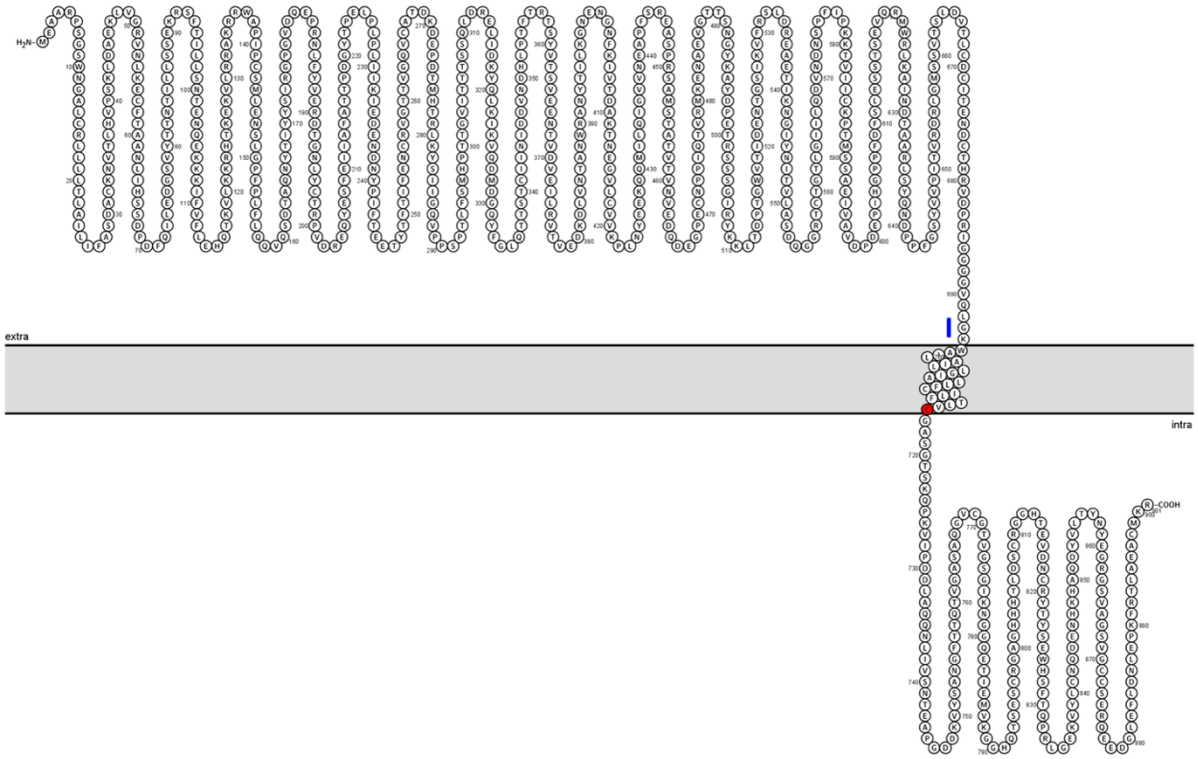

Figure 9: The base pair exchange of guanin by cytosine in position 2147 of the coding sequence, caused by the mutation, led to an amino acid exchange of cysteine by serin in position 716 of the amino acid sequence. The mutation is in the transmembrane part of the protein, which connects the intercellular part to the whole protein structure.

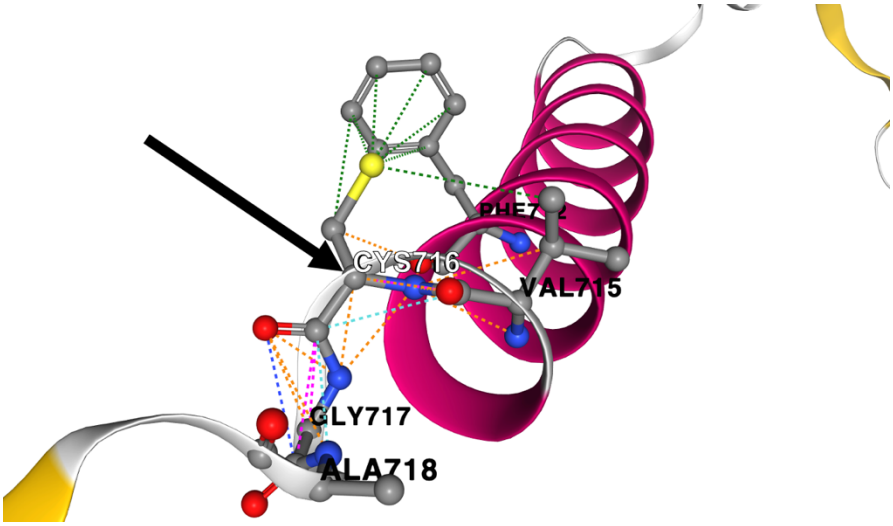

Figure 10: Molecule visualization of DSC2 generated by using mCSM-membrane. Locus of mutation is marked by an arrow (position 716 of amino acid sequence).

As can be seen in Figure 9, the mutation is in the intermembrane part of the protein, which connects the intracellular part to the whole protein structure.

Prediction of the molecular consequences of the mutation using mCSM-membrane has shown a predicted stability change (ΔΔG) of DSC2 by -0.994 Kcal/mol [60]. Hence, according to the prediction the DSC2$^{c.2147G>C}$ mutation has a destabilizing effect. The prediction was reinforced by the evaluation of the potential pathogenicity of the mutation. PolyPhen-2 has shown that the functional effects caused by the mutation are predicted to be probably damaging with a score of 1.0/1.0 (Figure 11) [1].

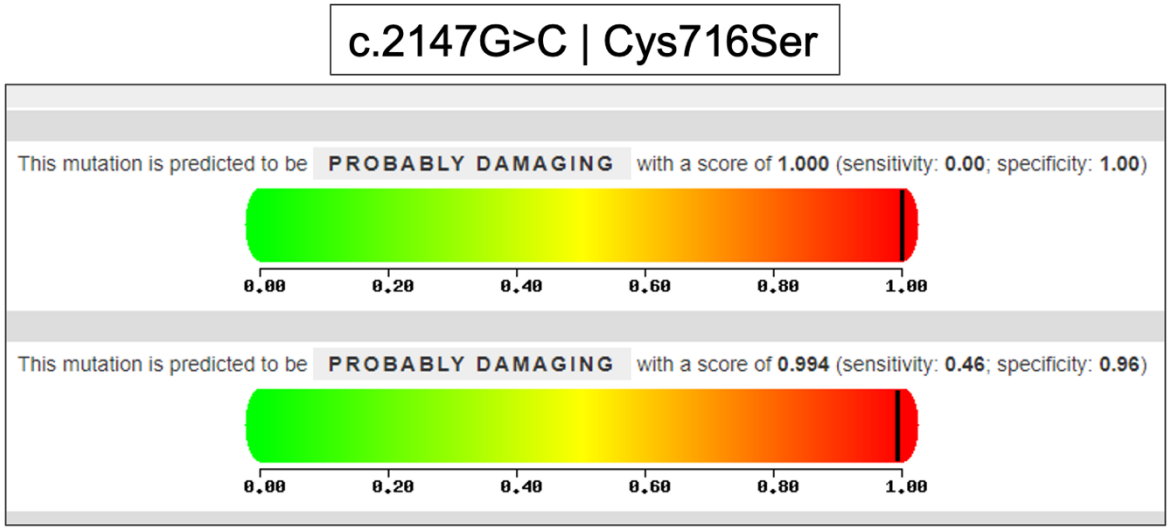

Figure 11: Evaluation of the potential pathogenicity of the DSC2$^{c.2147G>C}$ mutation. According to PolyPhen-2 the functional effects caused by the mutation are predicted to be probably damaging [1].

Due to the clinical features of the index patient and her family members carrying the mutation, and due to the above-mentioned predictions, we generated an iPS cell-line and differentiated those iPSC into patient-specific cardiomyocytes.

3.1.3 Characterization of cell line: Phenotype of patient-specific cardiomyocytes correlates with clinical data of the index patient

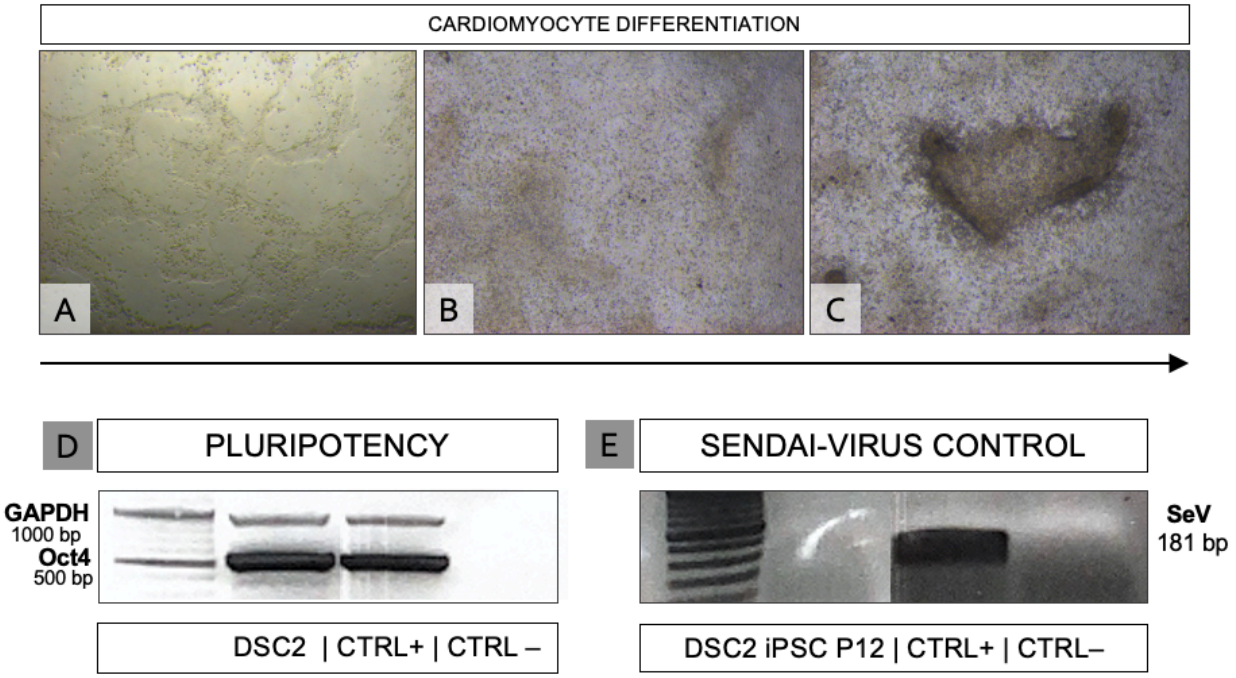

Figure 12: iPSC generation and differentiation of iPSC into ventricular cardiomyocytes. **A** shows iPSC before differentiation. In **B** the cells are at Day 1 of differentiation. **C** shows cells at Day 3 of differentiation, cardiomyocyte clusters start to form. **D** and **E**: Patient specific iPSC were pluripotent (**D**) and they did no longer contain the Sendai-virus (SeV) by passage 12 (**E**).

To evaluate the DSC2$^{c.2147G>C}$ mutation, we generated patient-specific and control iPSC-lines. Both cell-lines were pluripotent and resulted negative after testing for the Sendai-virus used for induction of iPSC generation (Figure 12, D-E). Patient and control iPS cell-lines were differentiated into ventricular cardiomyocytes.

They started to beat approximately around day 12 of differentiation (Figure 13). By day 30, the cells were fully differentiated, as shown by immunofluorescence staining (Figure 14). Performed on mature CMs, the immunofluorescence staining showed that the CMs were negative for NKX2-5, which is expressed in early cardiac mesoderm and therefore an indicator of embryonic cell-lines [47]. Immunofluorescence staining showed a positive result for cardiac muscle troponin T (cTNT) with a well-organized sarcomeric structure. The results proved that mature human cardiac cell-lines were successfully generated.

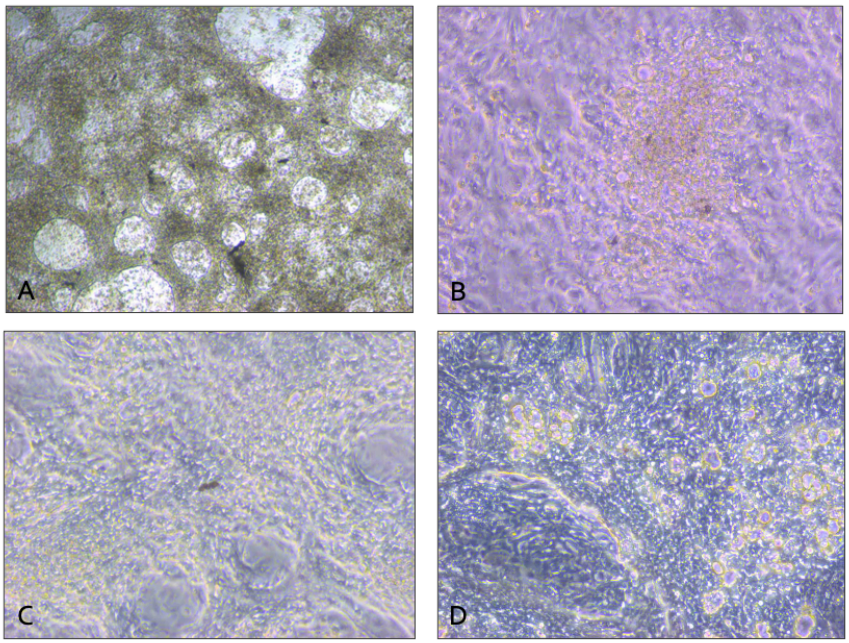

Figure 13: Patient-specific and control iPSC-derived cardiomyocytes (M=40x): **A**: patient DSC2 ventricular cardiomyocytes, day 14; **B**: control ventricular cardiomyocytes, day 24; **C**: patient DSC2 ventricular cardiomyocytes, day 34; **D**: patient DSC2 atrial cardiomyocytes.

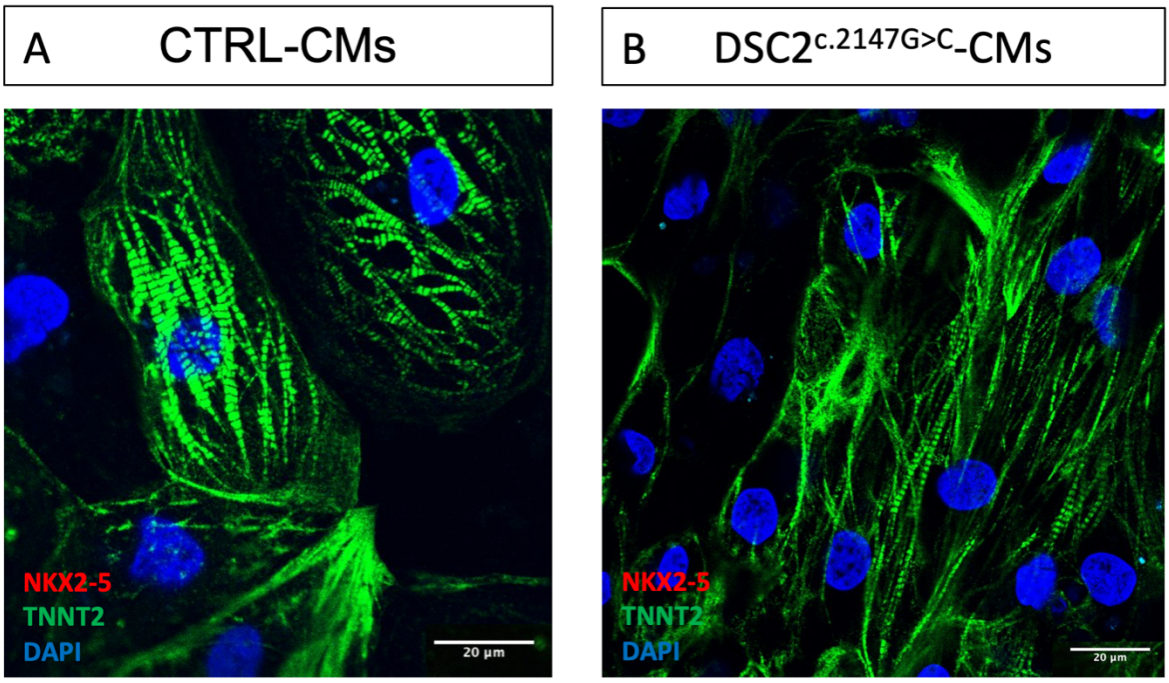

Figure 14: Immunofluorescence staining targeting NKX2-5 (red) and TNNT2 (green) of CTRL- and DSC2$^{c.2147G>C}$-CMs by day 30 of differentiation (M=40x). By day 30, the cells were fully differentiated, shown by the non-expression of NKX2-5, a marker for early cardiac mesoderm. Nuclei are stained with DAPI (blue).

To assure that an adequate model for disease investigation was developed, the cardiomyocyte cell-lines were sequenced. The sequencing confirmed that the

DSC2$^{c.2147G>C}$–CMs were heterozygous for the c.2147G>C mutation in the *DSC2* gene (Figure 15).

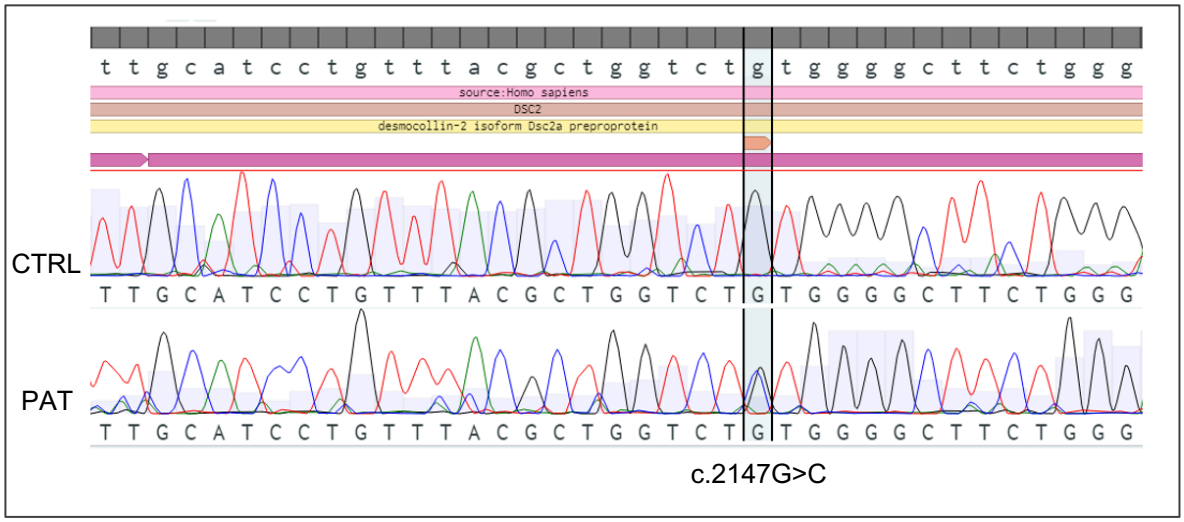

Figure 15: Sequencing of CTRL- and DSC2$^{c.2147G>C}$–CMs (PAT referring to DSC2$^{c.2147G>C}$–CMs).

Since studies revealed a correlation between desmosomal structural abnormalities and predisposition to accumulation of triglycerides, we performed an Oil-Red-O staining on DSC2$^{c.2147G>C}$– and CTRL–CMs (Figure 16A-B) [29]. The staining solution stains neutral fat or polyethylene granula red. Semi-quantification resulted in a non-significant difference but revealed a tendency of increased accumulation in DSC2$^{c.2147G>C}$–CMs (0.1730 ± 0.0476) compared to control (0.1496 ± 0.0172) (N=2, mean ± S.D., P=0.3333 determined using Mann-Whitney test) (Figure 16, C).

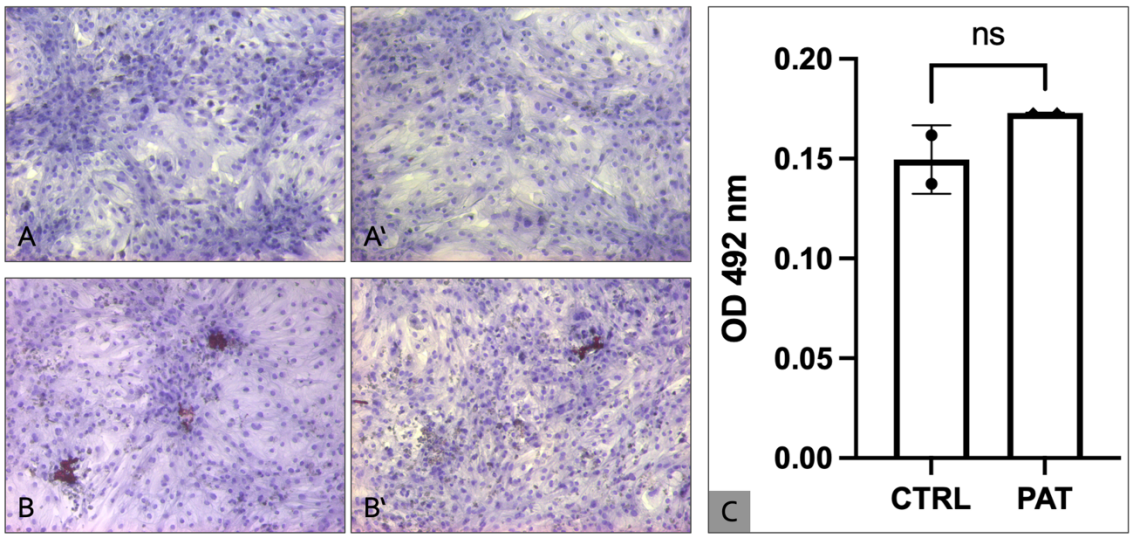

Figure 16: Oil-Red-O staining of CTRL– (**A**, **A'**) and patient-specific DSC2$^{c.2147G>C}$–CMs (**B**, **B'**). **C** shows semi-quantification. Semi-quantification resulted in a non-significant difference but revealed a tendency of increased accumulation in patient cells (0.1730 ± 0.0476) compared to control (0.1496 ± 0.0172) (N=2, mean ± S.D., P=0.3333 determined using Mann-Whitney test) (PAT referring to DSC2$^{c.2147G>C}$–CMs).

To gain further insights into the phenotype of DSC2$^{c.2147G>C}$ –CMs, the relative *DSC2* mRNA expression and the protein level of DSC2 compared to CTRL–CMs were analyzed. The analysis of the relative *DSC2* mRNA expression showed no significant difference between patient (1.330 ± 0.5206) and control cells (1.000 ± 0.000) (N=6, mean ± S.D., P=0.3636 determined using Mann-Whitney test) (Figure 17).

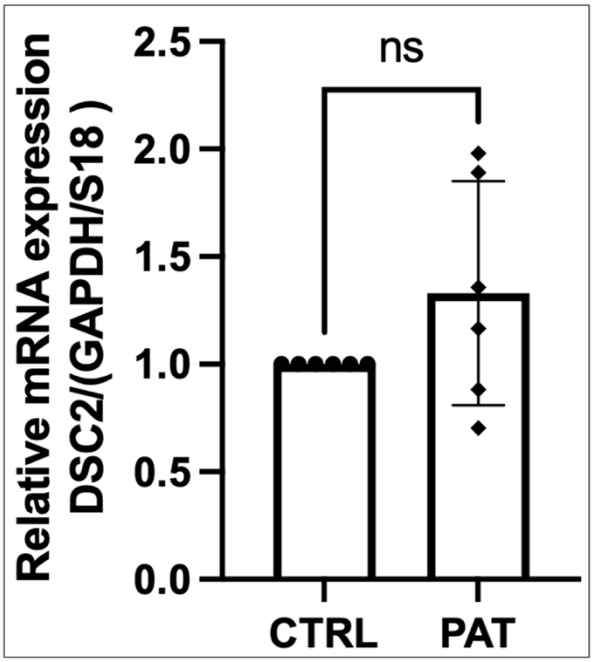

Figure 17: Analysis of relative mRNA expression of DSC2 (standardized to GAPDH/S18) showed no significant difference between patient-specific cardiomyocytes and control cardiomyocytes (PAT referring to DSC2$^{c.2147G>C}$–CMs) (CTRL: 1.000 ± 0.000, PAT: 1.330 ± 0.5206, N=6, mean ± S.D., P=0.3636 determined using Mann-Whitney test).

In contrast to the *DSC2* mRNA expression, relative protein expression analyzed through Western Blot showed reduced DSC2 protein levels in DSC2$^{c.2147G>C}$–CMs. Standardized to GAPDH, the average relative expression of DSC2 in patient cardiomyocytes was reduced (0.7103 ± 0.1075) when compared to control (1.000 ± 0.000) (N=7, mean ± S.D., ***P=0.0006 determined using Mann-Whitney test) (Figure 18).

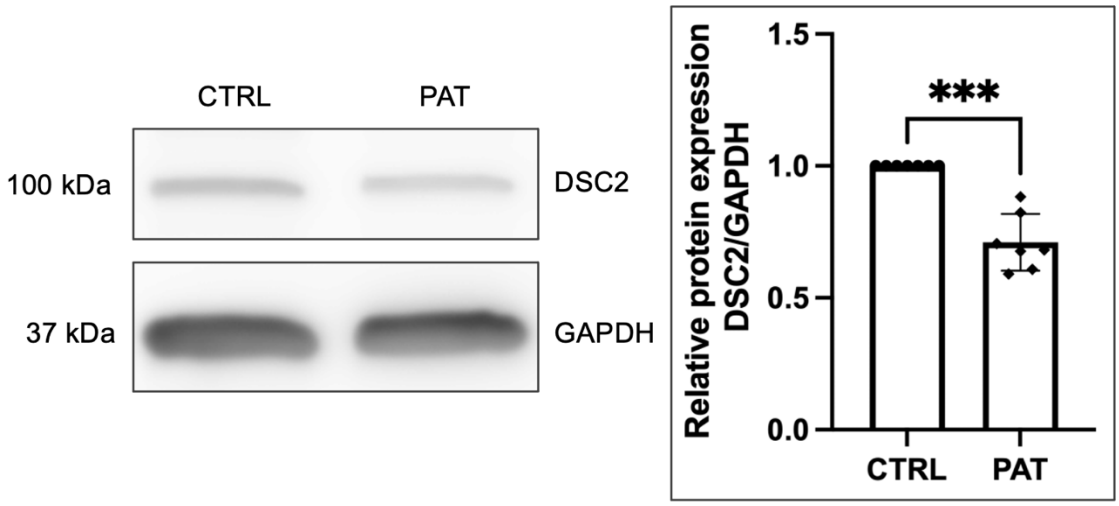

Figure 18: Relative protein expression of DSC2 was reduced in patient cells (0.7103 ± 0.1075) when compared to control and standardized to GAPDH (PAT referring to DSC2$^{c.2147G>C}$–CMs) (N=7, mean ± S.D., ***P=0.0006 determined using Mann-Whitney test).

mRNA and protein expression analyses provide insights into DSC2 levels. However, they do not capture the structural organization of desmosomes. To assess whether desmosomal integrity is preserved, we performed immunofluorescence staining to visualize the localization and distribution of desmosomal proteins in DSC2$^{c.2147G>C}$–CMs compared to CTRL–CMs.

In performed immunofluorescence stainings, binding of DSC2 antibodies showed sufficient specificity. In comparison to the control cardiac cell-lines a perinuclear accumulation of the antibody has been noticed in DSC2$^{c.2147G>C}$–CMs (Figure 19).

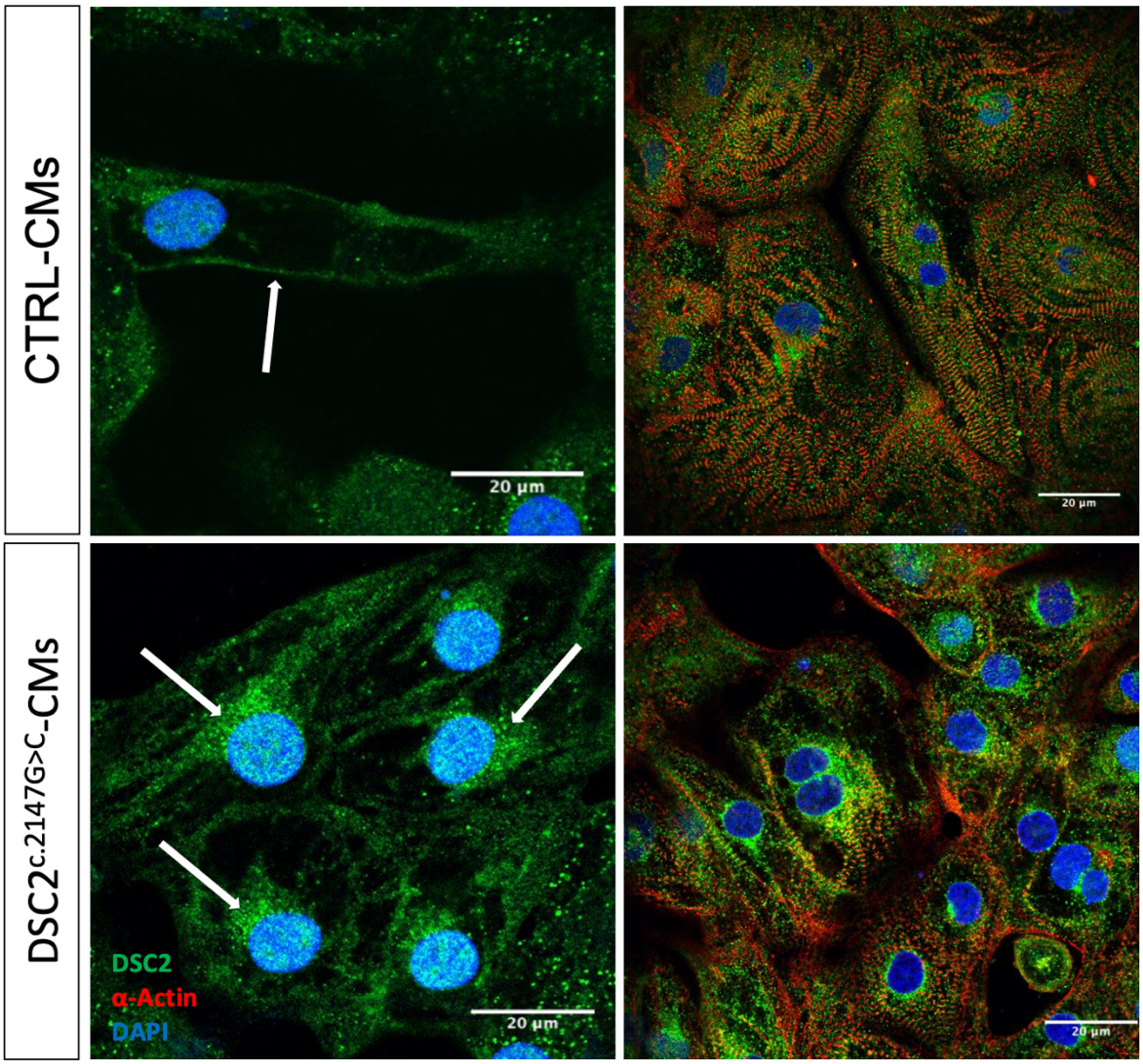

Figure 19: Immunofluorescence staining targeting DSC2 (green), α-Actin (red) and DAPI (blue). By comparing the patient-specific cardiomyocytes to control cardiac cell-lines, an increased perinuclear accumulation of the antibody has been noticed in patient-specific cardiomyocytes. Arrows indicate localization on membrane of DSC2 in CTRL–CMs and increased perinuclear accumulation in DSC2$^{c.2147G>C}$–CMs.

Immunofluorescence staining of desmoplakin-2 showed regular localization at the cell membrane in CTRL-CMs. In DSC2$^{c.2147G>C}$–CMs, localization of desmoplakin-2 appeared to be abnormally increased in the perinuclear fraction of the cell (Figure 20).

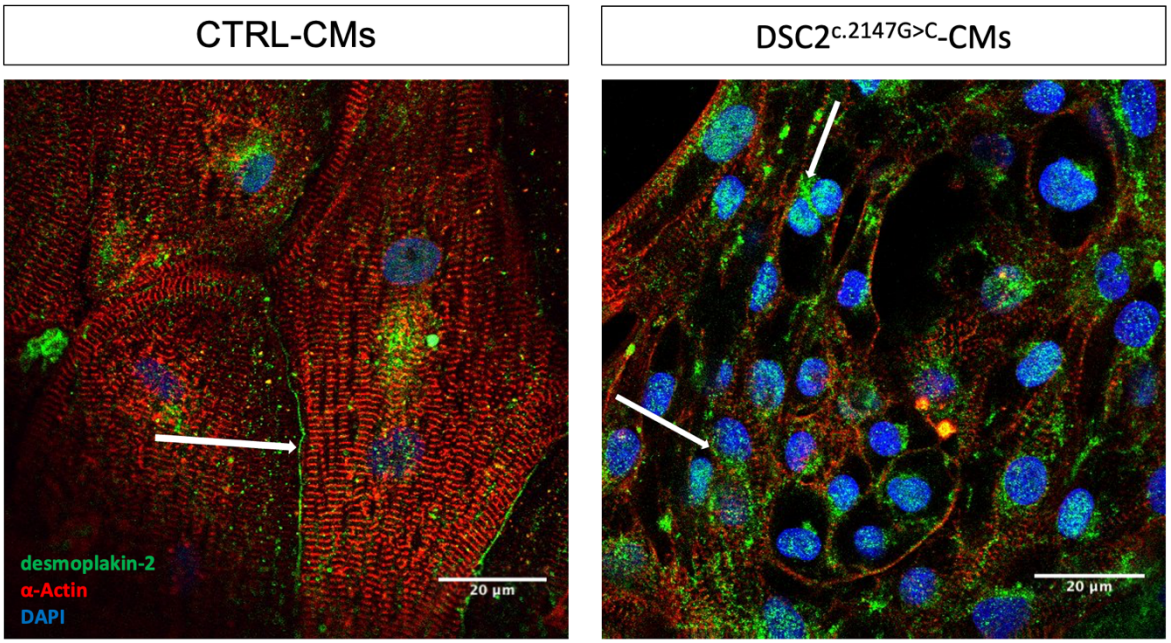

Figure 20: Immunofluorescence staining of desmoplakin-2 (green), α-Actin (red) and DAPI (blue). White arrows show regular localization of desmoplakin-2 on cell-membrane in control cardiomyocytes and perinuclear accumulation in patient-specific cardiomyocytes.

Staining of plakoglobin-2 showed similar results in both conditions (Figure 21). Overall, integrity of desmosomal structures seemed to be altered in DSC2$^{c.2147G>C}$–CMs.

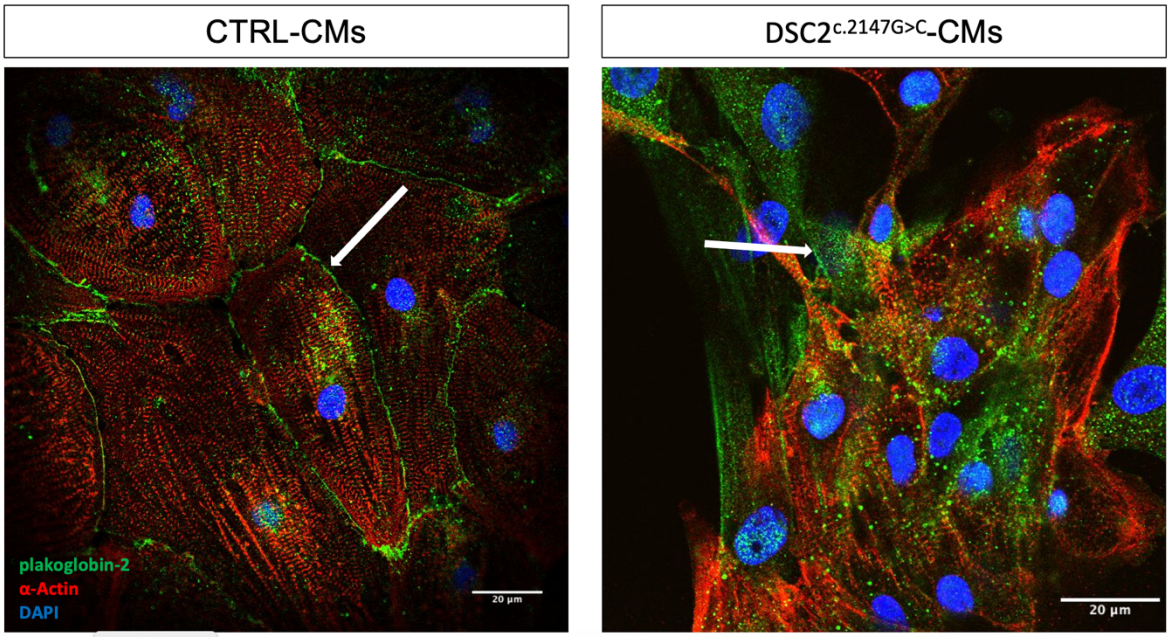

Figure 21: Immunofluorescence staining targeting plakoglobin-2 (green), α-Actin (red) and DAPI (blue). White arrows show localization of plakoglobin-2 on cell membrane in control cells and delocalization in patient-specific cardiomyocytes.

Additionally, during immunofluorescence staining experiments in which α-Actin was stained, structure of α-Actin in DSC2$^{c.2147G>C}$–CMs was noted to be impaired. To ensure impaired actin-structure was not caused by fixation of cardiomyocytes, an *in vivo* staining on living cardiomyocytes for both DSC2$^{c.2147G>C}$– and CTRL–CMs was performed using an immunofluorescent stain that targets actin and is capable of penetrating living cells. No alterations of the actin-structure were observed in CTRL–CMs, whereas it was impaired in DSC2$^{c.2147G>C}$–CMs (Figure 22).

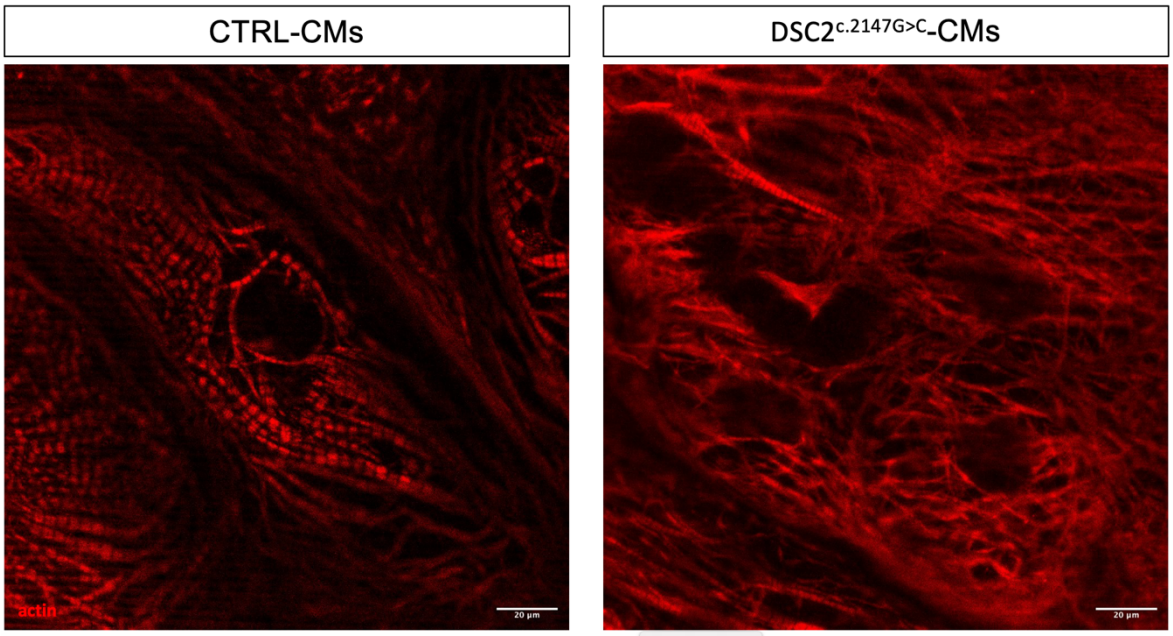

Figure 22: *In vivo* staining of actin (red) in CTRL– and DSC2$^{c.2147G>C}$–CMs. Actin structure was not altered in CTRL–CMs, whereas in DSC2$^{c.2147G>C}$–CMs an impaired actin structure was observed.

3.1.4 Multielectrode-array (MEA) analysis confirms arrhythmogenic phenotype in DSC2$^{c.2147G>C}$–CMs

Since carriers of the *DSC2*$^{c.2147G>C}$ mutation showed an arrhythmogenic phenotype, electrophysiological analyses were performed on patient-derived DSC2$^{c.2147G>C}$–CMs. Multielectrode-array analyses were carried out with the main aim of gaining further insights into the spontaneous electrophysiological behavior of DSC2$^{c.2147G>C}$–CMs.

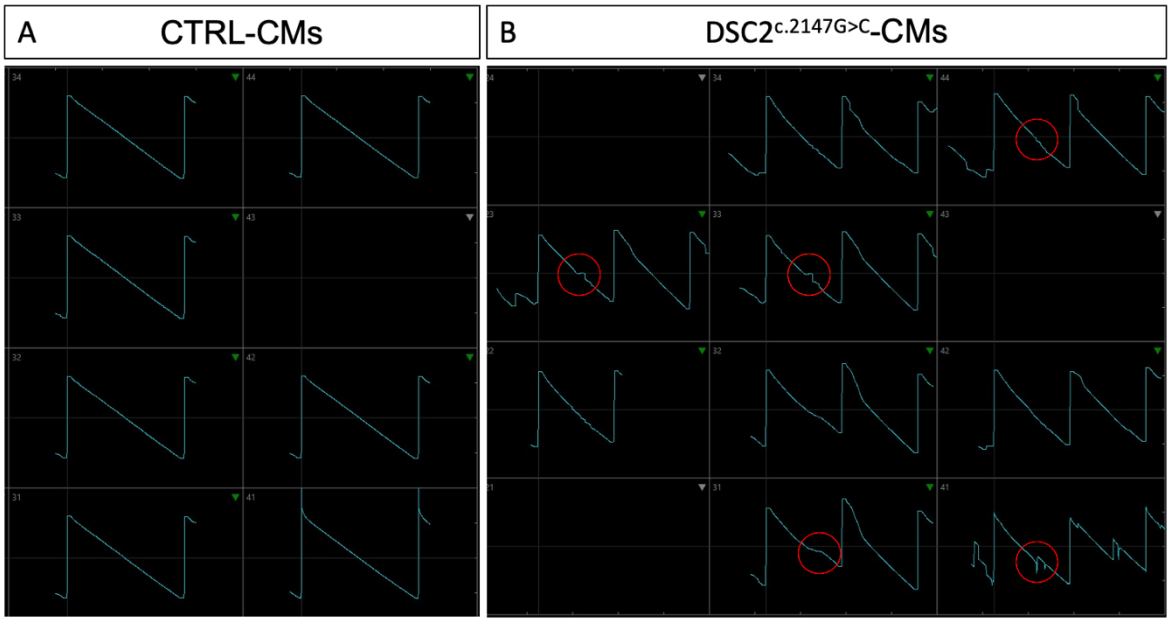

Figure 23: LEAP of CTRL-CMs (**A**) and DSC2$^{c.2147G>C}$–CMs (**B**) paced at 1 Hz. Recording of DSC2$^{c.2147G>C}$–CMs revealed additional spikes within the repolarization phase of the action potential like waveform. These peaks, marked by red circles, have been identified as EADs.

Recordings have shown irregular electrophysiological behavior within DSC2$^{c.2147G>C}$–CMs. Figure 23 shows additional spikes within the repolarization phase of the action potential like waveforms of DSC2$^{c.2147G>C}$–CMs. These additional spikes have been identified as so called early after depolarizations, EADs. They appeared on recordings of spontaneously beating DSC2$^{c.2147G>C}$–CMs and did increase when the cells have been put under stress, by pacing them for instance. CTRL-CMs did not develop such EADs.

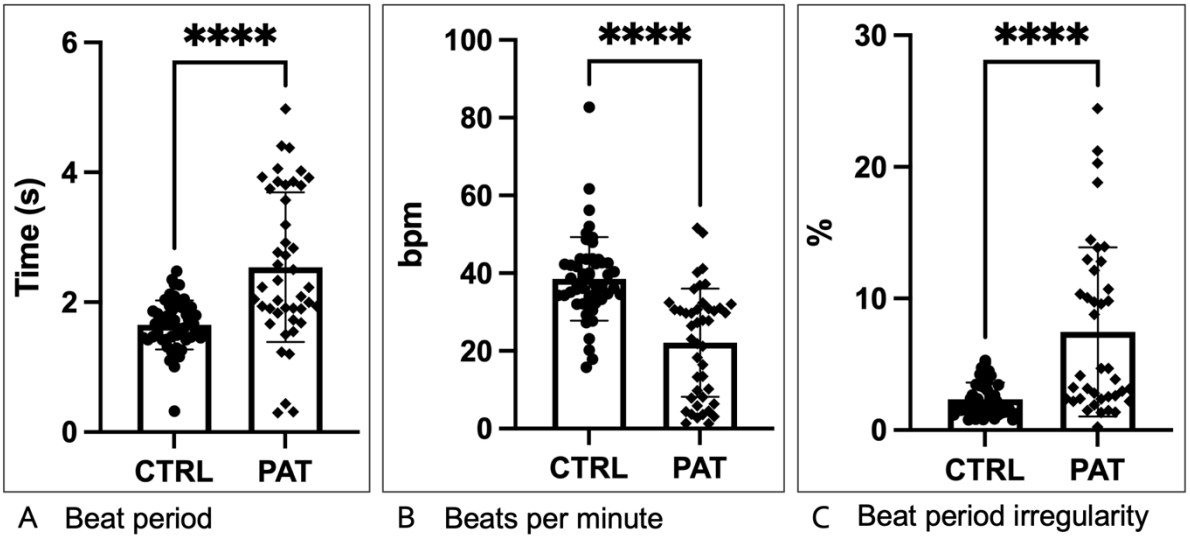

Figure 24: Field Potential recordings of multielectrode-array. **A** shows beat period (s), **B** the calculated beats per minute, and **C** shows relative beat period irregularity (%). All experiments have been performed as biological quadruplicate (PAT referring to DSC2$^{c.2147G>C}$–CMs) (A: CTRL 1.650 ± 0.3781 s, PAT 2.539 ± 1.154 s, n=13/11, N=4, mean ± S.D., ****P<0.0001 determined using Mann-Whitney test) (B: CTRL 38.54 ± 10.75 bpm, PAT 22.13 ± 13.93 bpm, n=13/11, N=4, mean ± S.D., ****P<0.0001 determined using Mann-Whitey test) (C: CTRL 2.328 ± 1.273 %, PAT 7.466 ± 6.430 %, n=11, N=4, ****P<0.0001 determined using Mann-Whitey test).

The results obtained with the multielectrode-array were further quantified. Field Potential recordings showed increased beat period duration in DSC2$^{c.2147G>C}$–CMs (2.539 ± 1.154 s, n=11) compared to CTRL–CMs (1.650 ± 0.3781 s, n=13, N=4, mean ± S.D., ****P<0.0001 determined using Mann-Whitney test) (Figure 24A). As can be seen in figure 24B, CTRL–CMs had an average of 40 beats per minute (38.54 ± 10.75 bpm). The average beats per minute in DSC2$^{c.2147G>C}$–CMs was reduced by half (22.13 ± 13.93 bpm) (n=13/11, N=4, mean ± S.D., ****P<0.0001 determined using Mann-Whitney test). Analysis of beat period and of the calculated beats per minute revealed a bradycardic phenotype in DSC2$^{c.2147G>C}$–CMs. Beat period irregularity in DSC2$^{c.2147G>C}$–CMs was significantly increased as well (CTRL 2.328 ± 1.273 %, PAT 7.466 ± 6.430 %, n=11, N=4, ****P<0.0001 determined using Mann-Whitey test) (Figure 24C).

Additional Field Potential recordings showed a significantly increased spike amplitude in DSC2$^{c.2147G>C}$–CMs (CTRL 1.083 ± 0.5577 mV, PAT 1.603 ± 0.7832 mV, n=12/10, N=4, mean ± S.D., **P=0.0018 determined using Mann-Whitney test) (Figure 25A).

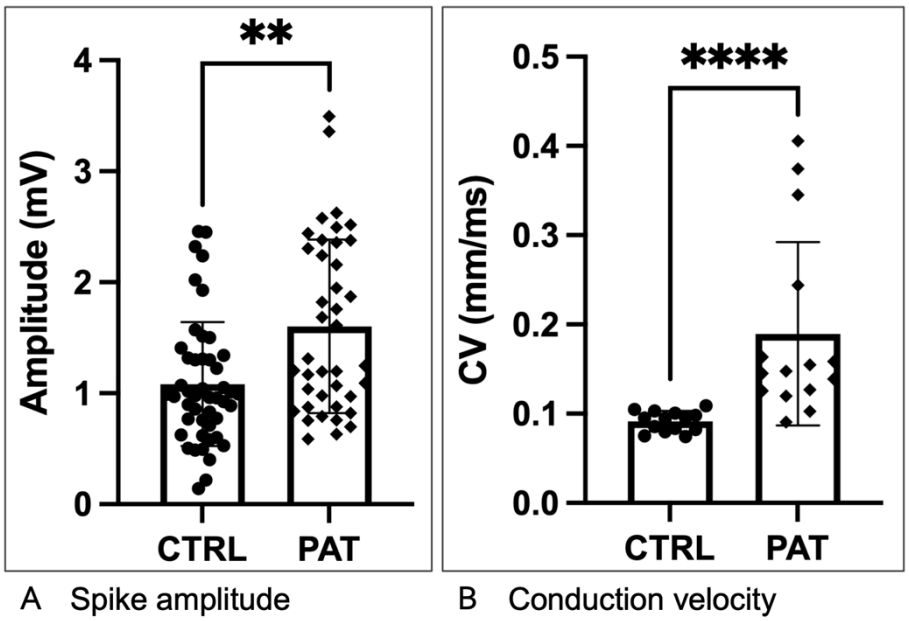

Figure 25: Field Potential recording of spike amplitude (mV) shown in **A**. **B** shows conduction velocity (mm/ms) as result of further calculations using the MEA cardiac metrics tool (PAT referring to DSC2$^{c.2147G>C}$–CMs) (A: CTRL 1.083 ± 0.5577 mV, PAT 1.603 ± 0.7832 mV, n=12/10, N=4, mean ± S.D., **P=0.0018 determined using Mann-Whitney test) (B: CTRL 0.09162 ± 0.01137 mm/ms, PAT 0.1895 ± 0.1026 mm/ms, n=5, N=3, mean ± S.D., ****P<0.0001 determined using Mann-Whitney test).

The conduction velocity appeared to be increased in DSC2$^{c.2147G>C}$–CMs (0.1895 ± 0.1026 mm/ms) compared to control (0.09162 ± 0.01137 mm/ms, n=5, N=3, mean ± S.D., ****P<0.0001 determined using Mann-Whitney test) (Figure 25B).

In summary, EADs in recordings of DSC2$^{c.2147G>C}$–CMs have been frequently observed. DSC2$^{c.2147G>C}$–CMs showed a bradycardic phenotype, indicated by the prolonged beat period. The increased irregularity of the beat period indicates instability or variability in the rhythm, which is an indicator for arrhythmias. Spike amplitude and conduction velocity were also altered compared to CTRL–CMs.
All these results indicate an increased arrhythmogenic potential in DSC2$^{c.2147G>C}$–CMs, suggesting alterations at a level that affect the electrophysiological properties.

3.1.5 Ca^{2+} imaging measurements show abnormal electrophysiological behavior in $DSC2^{c.2147G>C}$–CMs

Arrhythmogenic potential in cardiomyocytes can be increased by changes in calcium handling, among other aspects. For this reason, Ca^{2+} homeostasis of $DSC2^{c.2147G>C}$–CMs and CTRL-CMs was investigated by Ca^{2+} imaging experiments. Figure 26 shows average Ca^{2+} transients of CTRL-CMs compared to $DSC2^{c.2147G>C}$–CMs. Double spikes appeared regularly in recordings of $DSC2^{c.2147G>C}$–CMs and the frequency of Ca^{2+} sparks was reduced. As shown in Figure 26C, rise time was significantly prolonged in $DSC2^{c.2147G>C}$–CMs (261.1 ± 211.3 ms) compared to control (202.9 ± 160.0 ms) (n=208 cells, N=3, mean ± S.D., ****P<0.0001 determined using unpaired t-test), potentially caused by the double spikes, whereas the decay time in $DSC2^{c.2147G>C}$–CMs was reduced (Figure 26D, CTRL 1102 ± 608.8 ms, PAT 938.4 ± 642.3 ms, n=208 cells, N=3, mean ± S.D., ****P<0.0001 determined using unpaired t-test).

As shown in figure 27A, the peak amplitude in $DSC2^{c.2147G>C}$–CMs was decreased (CTRL 365.9 ± 223.8 mV, PAT 333.6 ± 235.8 mV, n=208 cells, N=3, mean ± S.D., *P=0.0160 determined using unpaired t-test). $DSC2^{c.2147G>C}$–CMs took longer to reach the peak of the Ca^{2+} transient compared to CTRL-CMs (Figure 27B, CTRL 3798 ± 2332 ms, PAT 5230 ± 3590 ms, n=208 cells, N=3, mean ± S.D., ****P<0.0001 determined using unpaired t-test). And half-width was reduced as well in $DSC2^{c.2147G>C}$–CMs (Figure 27C, CTRL 853.8 ± 467.6 ms, PAT 756.8 ± 498.7 ms, n=208 cells, N=3, mean ± S.D., ***P=0.0006 determined using unpaired t-test).

Overall, our findings show that the DSC2c.2147G>C mutation affects the Ca^{2+} handling in ventricular cardiomyocytes. Although providing insights in cellular electrophysiology, iPSC-CMs do not fully recapitulate the complexity of the intact heart. To investigate cardiac function in a whole-organism context, *in vivo* experiments in zebrafish were performed.

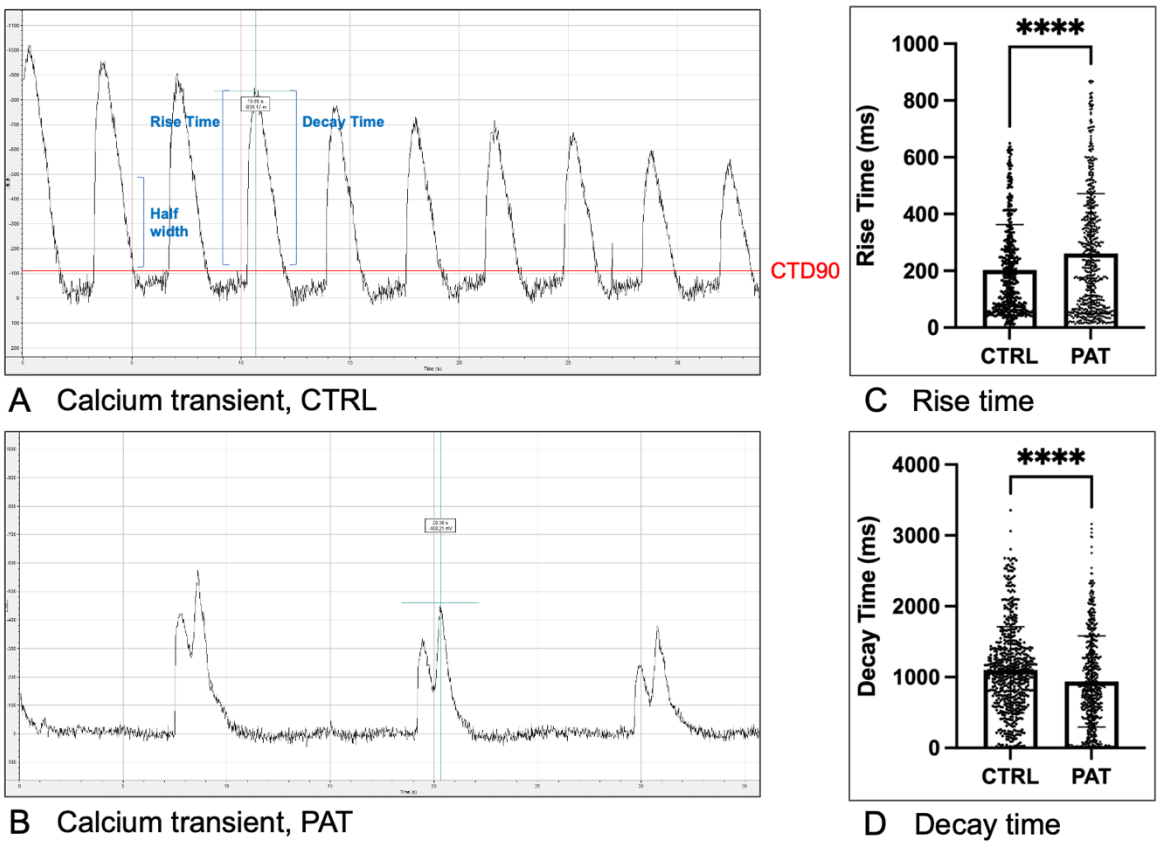

Figure 26: **A**, **B**: Calcium transient of CTRL– and DSC2$^{c.2147G>C}$–CMs. **A** shows analyzed parameters. **C**, **D**: Quantification of rise time and decay time (PAT referring to DSC2$^{c.2147G>C}$–CMs) (C: CTRL 202.9 ± 160.0 ms, PAT 261.1 ± 211.3 ms, n=208 cells, N=3, mean ± S.D., ****P<0.0001 determined using unpaired t-test) (D: CTRL 1102 ± 608.8 ms, PAT 938.4 ± 642.3 ms, n=208 cells, N=3, mean ± S.D., ****P<0.0001 determined using unpaired t-test).

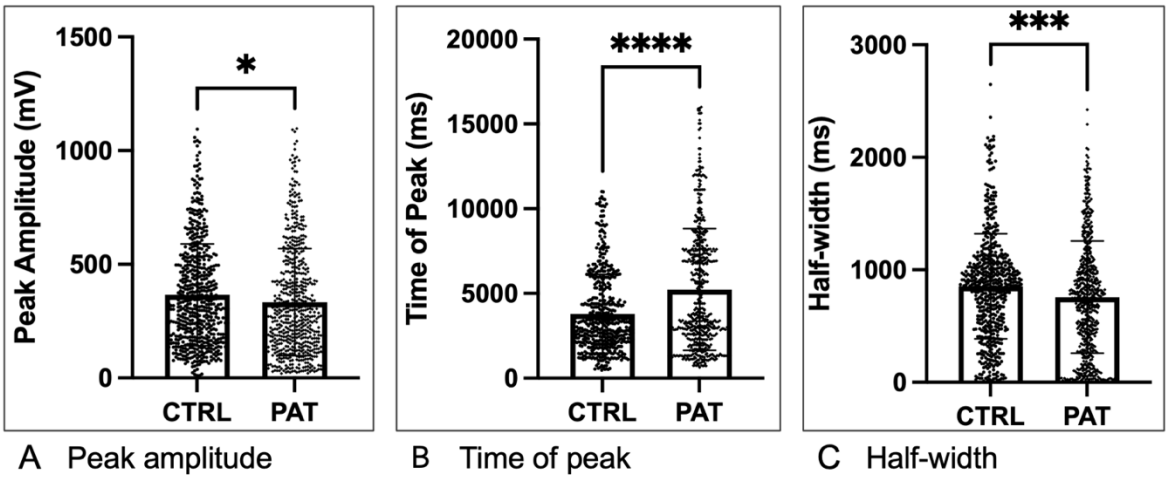

Figure 27: Analysis of calcium imaging experiments showed a decreased peak amplitude in DSC2$^{c.2147G>C}$–CMs (**A**), an increased time of peak (**B**), and a reduced half-width (**C**, calcium-transient-duration 50) (PAT referring to DSC2$^{c.2147G>C}$–CMs) (A: CTRL 365.9 ± 223.8 mV, PAT 333.6 ± 235.8 mV, n=208 cells, N=3, mean ± S.D., *P=0.0160 determined using unpaired t-test) (B: CTRL 3798 ± 2332 ms, PAT 5230 ± 3590 ms, n=208 cells, N=3, mean ± S.D., ****P<0.0001 determined using unpaired t-test) (C: CTRL 853.8 ± 467.6 ms, PAT 756.8 ± 498.7 ms, n=208 cells, N=3, mean ± S.D., ***P=0.0006 determined using unpaired t-test).

3.2 DSC2 knockdown in *Danio rerio* as *in vivo* model confirms *in vitro* data

In vitro analyses revealed electrophysiological alterations in DSC2$^{c.2147G>C}$–CMs. To investigate that, we mimicked a DSC2 knockdown in a living organism. As *in vivo* model the *Danio rerio*, zebrafish, was chosen. The *DSC2* gene of *Danio rerio* and human is similar, and especially the transmembrane region of the DSC2 protein is highly conserved. Position 716 of the DSC2 aminoacidic sequence, where the amino acid exchange has occurred in the index patient, consists of cysteine in both species (Figure 28) [14].



Figure 28: Alignment of amino acid sequence of human DSC2 and Danio rerio DSC2. Similarities are highlighted in blue. Position 716 consists of cysteine in both species (red rectangle).

We performed a morpholino (MO) mediated DSC2 knockdown. For that a splice morpholino targeting exon 6 of zebrafish *DSC2* was chosen.

3.2.1 MO-mediated DSC2 knockdown in zebrafish resembles ARVC phenotype

The phenotype of morphant zebrafish embryos was most pronounced by 48 hpf. Morphant embryos developed a mild cardiac edema and were bradycardic compared to control embryos (Figure 29). A slightly slower development was noted within morphant embryos (Figure 30).

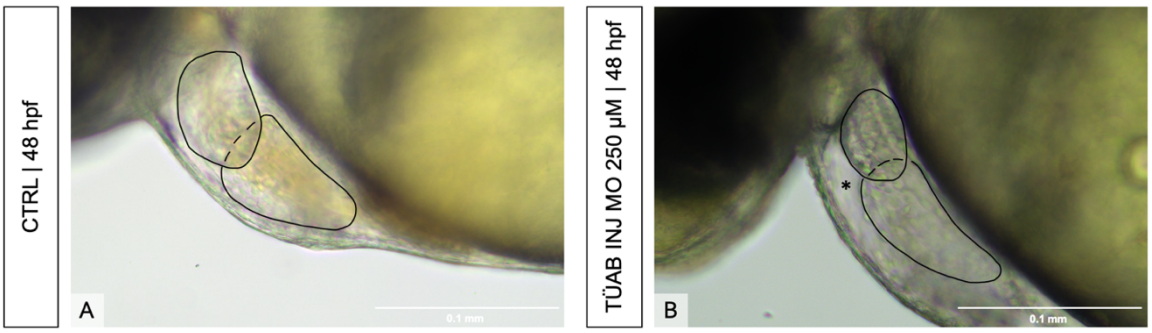

Figure 29: Phenotype of zebrafish embryos at 48 hpf. Morphant embryos (**B**) developed a mild cardiac edema (marked by an asterisk) and a bradycardic phenotype. Morpholino concentration at injection was 250 µM.

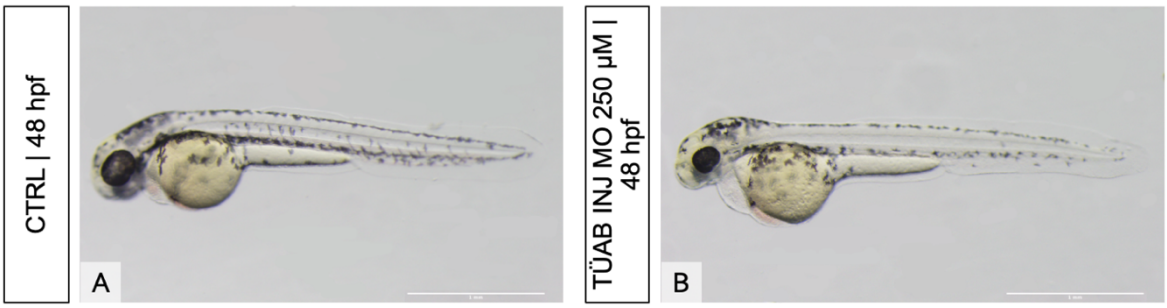

Figure 30: Phenotype of zebrafish embryos at 48 hpf (**A** – control, **B** – morphant embryo). Slightly slower development was observed within morphant embryos. Morpholino concentration at injection was 250 µM.

3.2.2 ECG analyses of transient DSC2 knockdown *in vivo* matches arrhythmogenic disease of index patient

Since an arrhythmogenic disease possibly linked to a DSC2 mutation is being investigated, electrophysiological analyses on morphant zebrafish embryos compared to control have been performed by electrocardiography (ECG) (Figure 31A-B). The methodology of ECG recordings is described in detail in the Methods section.

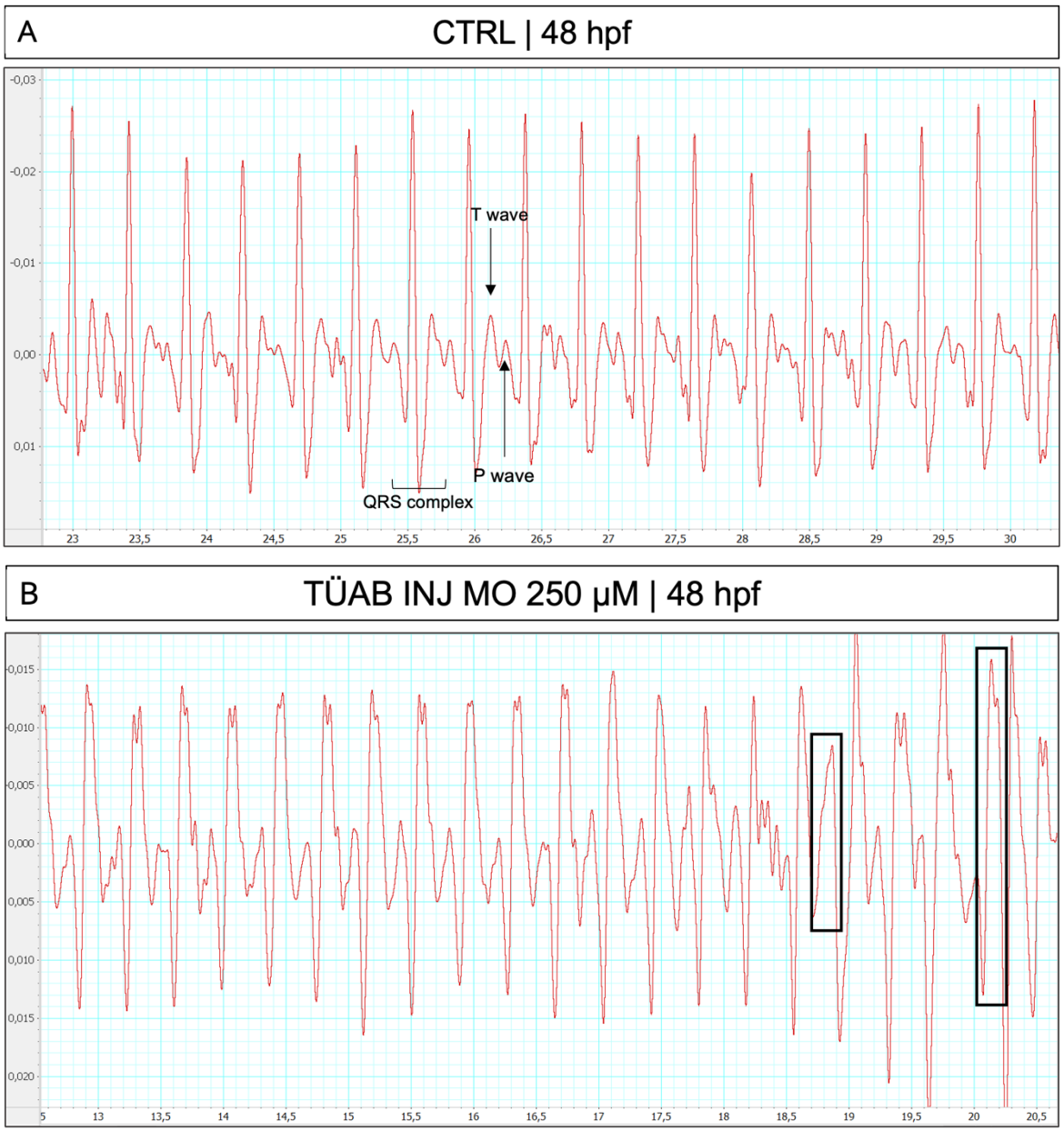

Figure 31: ECG recording of control zebrafish embryo (**A**) and morphant zebrafish embryo (**B**) at 48 hpf. ECG recording of control embryo depictures regular frequency and distinguishable P and T waves (**A**), whereas ECG recording of morphant embryo (**B**, DSC2-morpholino concentration=250 µM) depictures irregular frequency and extrasystoles were noted (black rectangles).

The bradycardic phenotype, which was already evident upon visual observation, was confirmed by ECG: The morphant embryos revealed a significantly reduced frequency (Figure 32A, CTRL 156.4 ± 21.87 bpm, INJ MO 138.1 ± 22.04 bpm, n=4-4-8-5/5-5-6-5, N=4, mean ± S.D., **P=0.0037 determined using Mann-Whitney test). Hence, the beats per minute were reduced. For further analysis the RR-time, QTc-time, QRS-complex duration, QRS-amplitude and the RMSSD were assessed as well.

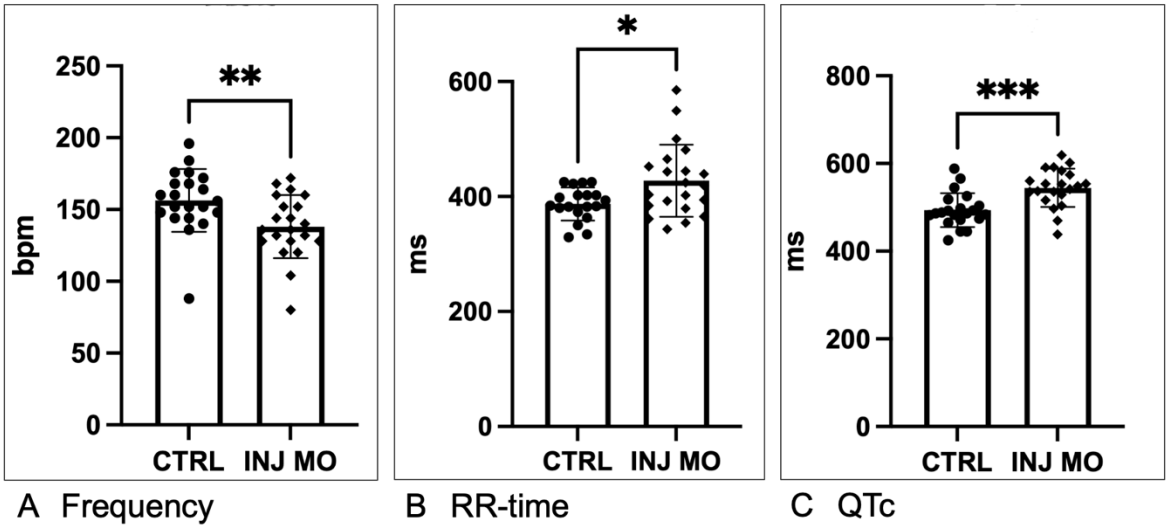

Figure 32: Heart frequency of morphant zebrafish embryos (INJ MO) was reduced compared to control. RR-time and QTc-time were both significantly prolonged (A: CTRL 156.4 ± 21.87 bpm, INJ MO 138.1 ± 22.04 bpm, n=4-4-8-5/5-5-6-5, N=4, mean ± S.D., **P=0.0037 determined using Mann-Whitney test) (B: CTRL 387.0 ± 28.63 ms, INJ MO 427.5 ± 62.92 ms, n=5, N=4, mean ± S.D., *P=0.0317 determined using Mann-Whitney test) (C: CTRL 493.7 ± 38.81 ms, INJ MO 544.4 ± 43.66 ms, n=5, N=4, mean ± S.D., ***P=0.0003 determined using Mann-Whitney test).

RR-time measures the time between two R-peaks. QTc-time is being calculated based on the Bazett-formula by measuring the time between Q- and T-waves. QRS-complex duration describes the time between beginning and end of the QRS-complex. RR-time and QTc-time were both significantly prolonged in morphant embryos (Figure 32B, CTRL 387.0 ± 28.63 ms, MO INJ 427.5 ± 62.92 ms, n=5, N=4, mean ± S.D., *P=0.0317 determined using Mann-Whitney test) (Figure 32C, CTRL 493.7 ± 38.81 ms, MO INJ 544.4 ± 43.66 ms, n=5, N=4, mean ± S.D., ***P=0.0003 determined using Mann-Whitney test). The prolonged RR-time (beat period duration) fits to the reduced frequency. The QRS-complex duration was shorter in morphant embryos compared to control (Figure 33A, CTRL 140.7 ± 27.54 ms, MO INJ 128.0 ± 35.62 ms, n=5, N=4, mean ± S.D., *P=0.0483 determined using Mann-

Whitney test), and the QRS-amplitude was significantly reduced (Figure 33B, CTRL 50.99 ± 24.80 mV, MO INJ 32.73 ± 20.61 mV, n=5, N=4, mean ± S.D., *P=0.0149 determined using Mann-Whitney test).

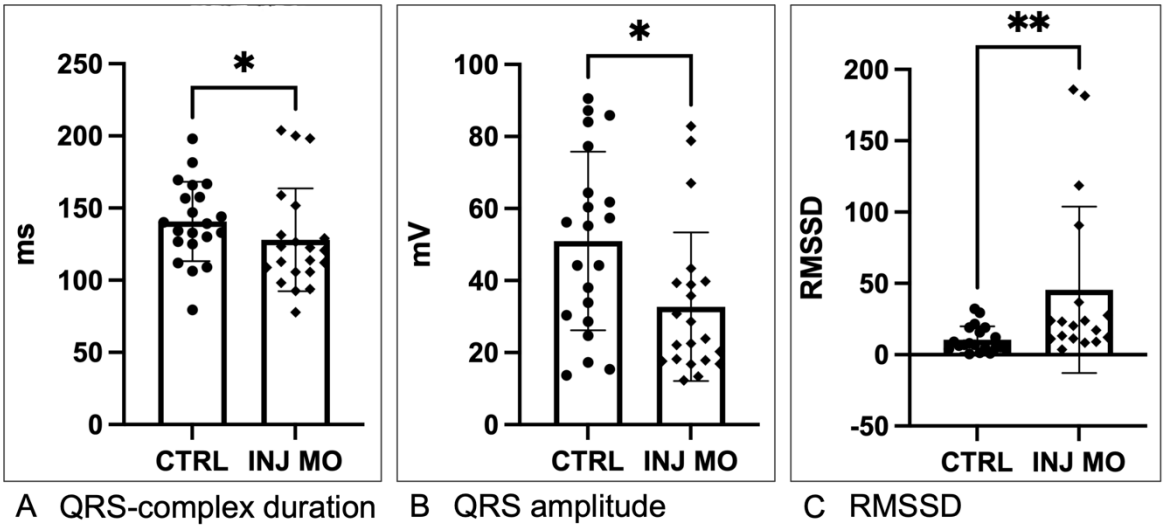

Figure 33: QRS-complex duration was shorter in morphant embryos compared to control, and the QRS-amplitude was significantly reduced. RMSSD presented a much greater heart rate variability in morphant embryos compared to control (A: CTRL 140.7 ± 27.54 ms, INJ MO 128.0 ± 35.62 ms, n=5, N=4, mean ± S.D., *P=0.0483 determined using Mann-Whitney test) (B: CTRL 50.99 ± 24.80 mV, INJ MO 32.73 ± 20.61 mV, n=5, N=4, mean ± S.D., *P=0.0149 determined using Mann-Whitney test) (C: CTRL 10.58 ± 9.249, INJ MO 45.48 ± 58.34, n=5, N=4, mean ± S.D., **P=0.0014 determined using Mann-Whitney test).

To assess heart rate variability on a shorter time frame, since ECG recordings lasted for approximately 3 min, the root mean square of successive differences (RMSSD) was calculated. The RMSSD presented a much greater variability in morphant embryos compared to control: it was significantly increased (Figure 33C, CTRL 10.58 ± 9.249, MO INJ 45.48 ± 58.34, n=5, N=4, mean ± S.D., **P=0.0014 determined using Mann-Whitney test).

In summary, knockdown of DSC2 in zebrafish embryos indicate an electrophysiological cardiac impairment. Particularly noteworthy are the frequently recorded extrasystoles in DSC2 knockdown embryos, as marked in Figure 31, which were observed in multielectrode-array analyses of DSC2$^{c.2147G>C}$–CMs as well. Taken together, our results demonstrate that the *in vitro* findings align with the *in vivo* data, indicating a clear correlation.

4 Discussion

4.1 Clinical and experimental background of known DSC2 mutations in comparison to the novel DSC2$^{c.2147G>C}$ mutation

ARVC can be caused by various mutations in desmosomal compounds [21]. Notably, all likely pathogenic or pathogenic *DSC2* mutations reported in literature appear to be exclusively associated with ARVC [69]. One such mutation, *DSC2*$^{c.394C>T}$, was studied by Moreau et al. (2021) in a 41-year-old ARVC patient. This patient survived a sudden cardiac death (SCD) at age 50, after which an ICD was implanted, and by the age of 66 a heart transplant was necessary [54]. The pathogenicity of this *DSC2* variant was further supported using both a zebrafish model and hiPSC-CM cell lines. Similarly, Gerull et al. (2013) identified the *DSC2*$^{c.1660C>T}$ mutation in families within the Alberta Hutterite population [34]. Genetic testing was initiated due to an increased accumulation of SCDs. Electric and histological features in individuals carrying the *DSC2*$^{c.1660C>T}$ mutation presented typical ARVC characteristics.

Building on these findings, the starting point of this thesis was the genetic analysis of a 26-year-old ARVC patient with a positive family history. Testing revealed a previously undescribed *DSC2* mutation. Specifically, the patient presented an alteration on one allele of the *DSC2* gene encoding for the *DSC2*$^{c.2147G>C}$ mutation, resulting in an amino acid exchange from cysteine (Cys) to serin (Ser) at position 716 of the amino acid sequence (p.Cys716Ser), located within the transmembrane domain. Pedigree analysis revealed an autosomal dominant inheritance pattern.

Clinically, the index patient exhibited features consistent with ARVC, confirming the diagnosis. Given the combination of clustered SCDs in the family, the patient's clinical presentation, and the positive genetic testing, the index patient got a subcutaneous ICD implanted. Despite that preventative measure, the disease continued to progress, and the patient is currently on the list for a heart transplant. These cases highlight the importance of ongoing research into novel ARVC-associated mutations. Characterizing such mutations enhances our understanding of ARVC pathogenesis and may provide a foundation for translating genetic findings into clinical practice.

4.2 Patient-derived ventricular DSC2$^{c.2147G>C}$–CM show slight structural impairments

The reprogramming process of fibroblasts into hiPSC and differentiation into cardiomyocytes was not affected by the DSC2$^{c.2147G>C}$ mutation. The DSC2$^{c.2147G>C}$–CMs did not show any differences in cell culturing, cell adhesion, or macroscopic beating behavior when compared to control.

Analysis of *DSC2* gene expression in control and DSC2$^{c.2147G>C}$–CMs showed no significant difference. In contrast, protein expression analysis revealed a reduced DSC2 protein level in DSC2$^{c.2147G>C}$–CMs when compared to control. Contrary to our findings, Moreau et al. (2021) observed a down-regulation of DSC2 mRNA in DSC2$^{c.394C>T}$–CMs [54]. Other analyses of an explanted myocardial tissue of an ARVC patient with the homozygous deletion variant DSC2$^{c.1913_1916delAGAA}$ showed similar results to Moreau et al. (2013) [8, 54]: a reduced DSC2 level at the mRNA and the protein level was detected, indicating that the truncated DSC2 is not processed to the intercalated disc [8]. This was not consistent with our results, as will be discussed in more detail below.

Desmosomal structural abnormalities and predisposition to accumulation of triglycerides are known to correlate with each other [12, 29]. To analyze lipid accumulation in DSC2$^{c.2147G>C}$–CMs, an Oil-Red-O staining was performed, which showed the tendency of increased accumulation in DSC2$^{c.2147G>C}$–CMs. Our findings were consistent with previous Oil-Red-O stainings performed on ARVC-iPSC-derived cardiomyocytes [49]. Ma et al. (2013) observed dense positive staining of lipid droplets on ARVC-iPSC-CMs, whereas control iPSC-CMs showed only sparse positive staining. Quantification of the Oil-Red-O staining showed significantly greater intensity in ARVC-iPSC-CMs [49]. The lower number of cells analyzed may have affected the quantification of our Oil-Red-O staining.

Immunofluorescence staining of DSC2$^{c.2147G>C}$–CMs showed perinuclear accumulation of DSC2 and impaired actin structure. Similar results were observed with DSP2 and JUP in DSC2$^{c.2147G>C}$–CMs (Figures 19-22).

Moreau et al. (2021) detected reduced DSC2 labeling in immunostainings of DSC2$^{c.394C>T}$–CMs, with an additional loss of DSC2 membrane enrichment when compared with CTRL-CMs [54]. Interestingly, the perinuclear accumulation of DSC2 we observed in our DSC2$^{c.2147G>C}$–CMs was consistent with their findings [54]. Identical results regarding the perinuclear accumulation were described by

Hawthorne et al. (2021) performing an immunofluorescence staining targeting DSG2 on DSG2$^{c.2358del}$–CMs [37]. The perinuclear accumulation and loss of membrane enrichment regarding DSC2 suggests defects in trafficking of the protein in mutated cardiomyocytes, as reported in zebrafish models investigating mutations of desmosomal compounds leading to ARVC [2, 37].

To summarize our findings, the heterozygous DSC2$^{c.2147G>C}$ mutation leads to slight structural impairments, which did not affect cell-culture handling, cell adhesion or macroscopic beating behavior when compared to control.

DSC2 showed a reduced protein level and was delocalized in DSC2$^{c.2147G>C}$–CMs in the context of loss of membrane enrichment, suggesting defects in trafficking of DSC2. Consequently, no absolute absence of DSC2 in heterozygous DSC2$^{c.2147G>C}$–CMs was detected.

At this point, it would be interesting to investigate the DSC2$^{c.2147G>C}$ mutation in homozygous conditions. It could be assumed that in iPSC-CMs that are heterozygous for the DSC2$^{c.2147G>C}$ mutation, the healthy allele that still encodes the wild-type protein compensates for the impairments of the mutant allele. iPSC-CMs in a homozygous DSC2$^{c.2147G>C}$ condition may show new structural or functional changes because of the absence of a wild-type allele still able to maintain the physiological function of the protein.

Hence, based on our results in context of previous literature, we do not primarily assume a structural but rather a molecular pathomechanism leading to ARVC.

4.3 DSC2$^{c.2147G>C}$–CMs show increased arrhythmogenic potential in electrophysiological analyses

In individuals carrying the DSC2$^{c.2147G>C}$ mutation, an arrhythmogenic phenotype is evident, with electrophysiological alterations meeting the diagnostic criteria for ARVC. To better understand the spontaneous electrophysiological behavior of DSC2$^{c.2147G>C}$–CMs, we conducted analyses using a multielectrode-array (MEA), a technique increasingly valued in cardiovascular research for studying the electrophysiological properties of cardiomyocytes. Our laboratory was the first to investigate the DSC2$^{c.2147G>C}$ mutation using MEA.

Recordings of DSC2$^{c.2147G>C}$–CMs showed early afterdepolarizations (EADs) in all recordings, which were not observed in recordings of CTRL-CMs. Analyses of spontaneous field potential recording showed prolonged beat period in

DSC2$^{c.2147G>C}$–CMs (CTRL 40/min, PAT 20/min), representing a bradycardic phenotype. Measured beat period irregularity was significantly increased in DSC2$^{c.2147G>C}$–CMs, suggesting instability or variability in the rhythm, which is an indicator for arrhythmias. The spike amplitude and conduction velocity were significantly increased as well. Abnormal patterns in conduction velocity can potentially contribute to arrhythmogenesis by leading to altered pathways for electrical signals [36].

All these results indicate an increased arrhythmogenic potential in DSC2$^{c.2147G>C}$–CMs and hence suggest alterations at a level that affect the electrophysiological properties. In fact, studies have shown that mutations in desmosomal compounds can disrupt conduction of excitation in cardiomyocytes [33, 70]. Conversely, maintaining desmosome function requires effective excitation conduction, which depends on adequate SR Ca^{2+} ATPase (SERCA) activity with proper regulation of Ca^{2+} flux [70].

4.4 DSC2$^{c.2147G>C}$ mutation affects Ca^{2+} handling in ventricular cardiomyocytes

Studies with ARVC-iPSC-CMs support the theory of direct involvement of cardiomyocytes in arrhythmogenesis. The idea is that arrhythmias would not only result from structural and morphological remodeling such as fibrofatty replacement but would also directly arise from a modification of the cell's electrical profile. Due to that cardiomyocytes would become more susceptible to the development of arrhythmias [66].

To analyze the Ca^{2+} current and Ca^{2+} homeostasis of DSC2$^{c.2147G>C}$–CMs, Ca^{2+} imaging experiments have been performed, in which Ca^{2+} dynamics have been made visible through Fura-2AM. The analyzed parameters included rise time, decay time, peak amplitude, and half-width of Ca^{2+} transients.

The rise time indicates the function or misfunction of ion channels such as ryanodine (RyR) and sarcolemmal ion channels. Alterations of the decay time are related to the removal of Ca^{2+} through the sarcolemmal sodium Ca^{2+} exchanger (NCX) and SERCA [73]. Double spikes appeared regularly in recordings of DSC2$^{c.2147G>C}$–CMs and overall frequency of Ca^{2+} sparks was reduced. Rise time was significantly prolonged in DSC2$^{c.2147G>C}$–CMs compared to control, indicating an alteration of the function of the RyR or sarcolemmal ion channels. Interestingly, the decay time in DSC2$^{c.2147G>C}$–CMs was reduced, which suggests an impaired Ca^{2+} removal

through NCX and SERCA. The peak amplitude in DSC2$^{c.2147G>C}$–CMs was decreased, and DSC2$^{c.2147G>C}$–CMs took longer to reach the peak of the Ca^{2+} transient compared to control. This was supported by the fact that the half-width was reduced as well in DSC2$^{c.2147G>C}$–CMs.

Our findings show that the DSC2$^{c.2147G>C}$ mutation affects the Ca^{2+} handling in ventricular cardiomyocytes. The impaired Ca^{2+} transient may be a result of alterations of the function of SERCA, NCX and/or RyR. Abnormalities of Ca^{2+}-handling and enhanced pro-arrhythmogenic irregular or ectopic Ca^{2+}-events are known to increase cellular excitability [45, 67]. By increasing cellular excitability, an increased occurrence of EADs is triggered as well [67, 68]. This is consistent with our multielectrode-array analyses. Hence, alteration of the cell's electrical profile would make cardiomyocytes more susceptible to the development of arrhythmias [66]. A study with HL1 cells with homozygous knockouts of *PKP2*, *DSG2*, and *DSC2* supports this thesis [78]. Knockouts of each desmosomal compound resulted in alterations of Ca^{2+} handling. Specific knockout of *DSC2* led to a prolonged rise time and decay time in Ca^{2+} imaging, and reduced half-width, comparable with our results. The longer half-width duration compared to wild type indicates a slower Ca^{2+} removal [78]. Prolonged rise time and decay time both indicate a slower Ca^{2+} release and re-uptake in HL1 cells [78]. Furthermore, Kim et al. (2013) demonstrated that a *PKP2* mutation in iPSC-CMs leads to Ca^{2+} handling deficits [42]. Ca^{2+} imaging demonstrated that mutant iPSC-CMs had a prolonged Ca^{2+} relaxation phase. Consequently, qRT-PCR analyses were performed, resulting in downregulated expression levels of SERCA and NCX1. Kim et al. (2013) suggested that the impaired Ca^{2+} relaxation phase in *PKP2* mutated iPSC-CMs may be altered due to abnormal Ca^{2+} handling capability [42]. Ca^{2+} imaging of hiPSC-CMs expressing a *DSC2* mutation determined an increased Ca^{2+} transient frequency and decreased decay time [65]. Additionally, an increased number of pro-arrhythmogenic abnormal spontaneous Ca^{2+} sparks during diastole was observed. This suggests a Ca^{2+} leak from the sarcoplasmic reticulum through the RyR [65].

In conclusion, our electrophysiological results in the context of literature indicate that mutated cardiomyocytes not only undergo slight morphological and structural remodeling. DSC2$^{c.2147G>C}$–CMs may primarily undergo an electrophysiological remodeling which contributes to the development of ARVC by increasing the cardiomyocytes susceptibility to the development of arrhythmias.

A detailed investigation of ion channels of cardiomyocytes taking part in Ca^{2+} handling would provide more information. Further, additional electrophysiological experiments such as patch clamp would allow to make more differentiated observations and give more specific ideas of altered function of ion channels and how it is affecting the genesis of arrhythmias.

4.5 DSC2 knockdown in embryonic zebrafish

Since parameters of the cardiac conduction system of zebrafish resemble the human conduction system more than other model organisms, we modeled a DSC2 knockdown in zebrafish embryos to gain further insight of the pathophysiology *in vivo* [32]. Main aim was to assess the effects of a DSC2 knockdown on whole heart electrophysiology, which is why we performed electrocardiography (ECG) on knockdown DSC2 zebrafish embryos and compared them to wildtype.

4.5.1 Phenotype of DSC2 knockdown embryonic zebrafish is consistent with previous findings

The phenotype of morphant embryos was most pronounced by 48 hpf and resulted in mild cardiac edema. DSC2 knockdown embryos revealed a bradycardic phenotype. Our findings are consistent with what has been described previously. Heuser et al. (2006) as well as Moreau et al. (2021) both noted a reduced ventricular contraction and a cardiac edema in embryos after DSC2 knockdown [38, 54]. Knockdown of DSC2 in zebrafish embryos resulted in bradycardia, chamber dilatation and abnormal cardiac contractility [38]. A rescue experiment was attempted by injecting full-length human DSC2 mRNA into morphants [38, 54]. Injection of wildtype human DSC2 mRNA succeeded in rescuing the stroke volume and ventricle defects observed in morphants. The experiment was repeated with human mRNA encoding a $DSC2^{c.394C>T}$ mutation, which failed to rescue the described cardiovascular phenotype, suggesting that the DSC2 mutation impairs DSC2 function *in vivo* [54]. Repeating this rescue experiment with the $DSC2^{c.2147G>C}$ mutation would additionally prove its pathogenicity.

4.5.2 DSC2 knockdown in embryonic zebrafish leads to impairment of electrophysiological conduction of the heart

ECGs on zebrafish embryos were recorded at 48 hours post fertilization (hpf) for 3 min each. RR-time and thus the beat period were prolonged in DSC2 knockdown embryos. Interestingly, a prolonged beat period was observed in $DSC2^{c.2147G>C}$–

CMs as well. Average heart frequency of zebrafish embryos at 48 hpf typically ranges around 180 bpm [25]. That was the case for CTRL embryos, whereas knockdown DSC2 embryos showed a reduced heart frequency in correspondence to a bradycardic phenotype.

In DSC2 knockdown embryos a prolonged QTc-time was observed. In comparison, a prolonged QTc-time in the human ECG indicates changes in the depolarization or repolarization of the ventricles, whereby depolarization disorders typically lead to a prolonged QRS-complex duration [6, 56]. This was not the case for DSC2 knockdown embryos, which showed a reduced QRS-complex duration compared to control. Prolongation of the repolarization, however, can trigger the occurrence of EADs, which in turn increases occurrence of extrasystoles and the risk of developing arrhythmias [6]. In this context, it is a noteworthy finding that in contrast to wildtype embryos, extrasystoles were regularly observed in DSC2 knockdown embryos. This result aligns with the frequent occurrence of EADs in DSC2$^{c.2147G>C}$–CMs.

In the context of arrhythmia detection, the root mean square of successive differences (RMSSD) was calculated to assess heart rate variability and regularity in a shorter time frame. The RMSSD was increased in DSC2 knockdown embryos, indicating a greater variability or irregularity in successive RR-intervals. This corresponds to the measured beat period irregularity in DSC2$^{c.2147G>C}$–CMs, which was significantly increased.

Comparable data was difficult to obtain since hardly any mutations of desmosomal compounds causing ARVC have been analyzed via ECG recordings of zebrafish embryos. It would be interesting to perform ECG recordings on adult zebrafish, since ARVC is a progressive disease and characteristic electrophysiological features may only be observed at later stages of the disease. Additionally, our findings might be influenced by the not yet fully mature conduction system of 48 hpf zebrafish embryos [25]. To obtain more consistent data, a transgenic zebrafish line could be established, in order to investigate the specific mutation across all developmental stages and in adulthood.

Since zebrafish embryos have a higher heart rate (approximately 120-180/min) the comparison to human ECG data of ARVC patients is limited [32]. Nonetheless, an attempt was made to compare *in vitro* and *in vivo* electrophysiological data, taking into account the methodologically different measurements and the resulting limitations when comparing MEAs with ECG recordings.

In summary, knockdown of DSC2 in zebrafish embryos results in a very similar cardiac phenotype to that previously described in literature and leads to an electrophysiological cardiac impairment. Particularly noteworthy are the frequently recorded extrasystoles in knockdown embryos, regularly found in ARVC patients. Taken together, our results show that the *in vitro* data aligns with the *in vivo* data, indicating a clear correspondence.

4.6 Drawing a conclusion from the *in vitro* and *in vivo* results

In conclusion, the results show that the DSC2$^{c.2147G>C}$ mutation induces significant electrophysiological alterations in ventricular cardiomyocytes under heterozygous conditions. Changes in electrophysiological behavior and Ca^{2+} handling in DSC2$^{c.2147G>C}$–CMs indicate increased cellular excitability. This in turn increases the susceptibility to the development of arrhythmias, and further elevates the occurrence of EADs, as observed *in vitro* in patient-derived DSC2$^{c.2147G>C}$–CMs and as extrasystoles *in vivo* in embryonic zebrafish with DSC2 knockdown. These observations highlight the mutation's direct contribution to arrhythmogenic susceptibility. While these results advance our understanding of the cellular mechanisms underlying ARVC, further investigation is required to clarify the precise pathways by which the DSC2$^{c.2147G>C}$ mutation drives arrhythmia development and to fully elaborate its role in disease pathogenesis.

5 Summary

Previous studies have shown that mutations in the desmocollin-2 (*DSC2)* gene can lead to desmosomal impairment, which contributes to the pathogenesis of Arrhythmogenic right ventricular cardiomyopathy (ARVC), an inherited heart muscle disease associated with life-threatening ventricular arrhythmias and high risk of sudden cardiac death.

The aim of this thesis is the evaluation of the role of the novel human DSC2$^{c.2147G>C}$ (DSC2$^{p.Cys716Ser}$) mutation *in vitro* by generating patient-specific human induced pluripotent stem cell-derived cardiomyocytes (hiPSC-CMs), and *in vivo* by performing a morpholino mediated knockdown of DSC2 in a zebrafish model.

Genetic testing of a 26-years-old female patient from the Ulm University Medical Center with ARVC revealed a missense mutation in the *DSC2* gene (DSC2$^{c.2147G>C}$, DSC2$^{p.Cys716Ser}$). The patient's family history indicated autosomal dominant heredity. To investigate the DSC2$^{c.2147G>C}$ mutation and clarify its pathogenicity *in vitro*, a patient-specific iPS cell-line was generated, differentiated into ventricular cardiomyocytes (DSC2$^{c.2147G>C}$–CMs) and analyzed. Characterization of DSC2$^{c.2147G>C}$–CMs was done by immunofluorescence staining to visualize desmosome organization, performing RT-PCR and Western-Blot to investigate DSC2 mRNA levels and protein expression, and by evaluating the lipid accumulation through Oil Red O staining. The DSC2$^{c.2147G>C}$ mutation led to slight structural impairments in cardiomyocytes, including reduced DSC2 protein levels and perinuclear accumulation of DSC2. Lipid accumulation tendency was noted.

For further analysis, a multielectrode-array (MEA) was performed to analyze spontaneous electrophysiological behavior of the DSC2$^{c.2147G>C}$–CMs compared to control. DSC2$^{c.2147G>C}$–CMs exhibited increased arrhythmogenic potential, including early after depolarizations (EADs) and altered electrophysiological behavior. MEA analysis revealed prolonged beat periods, increased beat period irregularities, spike amplitudes and conduction velocities, indicating an increased susceptibility to arrhythmias.

The DSC2$^{c.2147G>C}$ mutation affected Ca^{2+} handling in ventricular cardiomyocytes, as observed through Ca^{2+} imaging measurements. This impairment contributes to increased cellular excitability and arrhythmogenesis.

Additionally, to further support the pathogenicity of the DSC2$^{c.2147G>C}$ mutation, a DSC2 knockdown *in vivo*, using zebrafish as model organism, was established. The

knockdown in 48 hours post fertilization (hpf) zebrafish resulted in cardiac impairments consistent with ARVC, including abnormal electrophysiological parameters measured by ECG. Particularly noteworthy are frequently recorded extrasystoles in knockdown embryos.

Our results indicate that the DSC2$^{c.2147G>C}$ mutation not only leads to slight structural changes in ventricular cardiomyocytes, but primarily causes an electrophysiological remodeling and thus increases the susceptibility of cardiomyocytes to arrhythmias, further contributing to the development of ARVC. Further research is needed to understand the exact mechanisms involved in ARVC pathogenesis.

6 List of References

1. Adzhubei IA, Schmidt S, Peshkin L, Ramensky VE, Gerasimova A, Bork P, Kondrashov AS, and Sunyaev SR (2010) *A method and server for predicting damaging missense mutations.* Nat Methods 7:248-9. doi: 10.1038/nmeth0410-248
2. Asimaki A, Kapoor S, Plovie E, Karin Arndt A, Adams E, Liu Z, James CA, Judge DP, Calkins H, Churko J, Wu JC, MacRae CA, Kleber AG, and Saffitz JE (2014) *Identification of a new modulator of the intercalated disc in a zebrafish model of arrhythmogenic cardiomyopathy.* Sci Transl Med 6:240ra74. doi: 10.1126/scitranslmed.3008008
3. Asimaki A, Tandri H, Huang H, Halushka MK, Gautam S, Basso C, Thiene G, Tsatsopoulou A, Protonotarios N, McKenna WJ, Calkins H, and Saffitz JE (2009) *A new diagnostic test for arrhythmogenic right ventricular cardiomyopathy.* N Engl J Med 360:1075-84. doi: 10.1056/NEJMoa0808138
4. Austin KM, Trembley MA, Chandler SF, Sanders SP, Saffitz JE, Abrams DJ, and Pu WT (2019) *Molecular mechanisms of arrhythmogenic cardiomyopathy.* Nat Rev Cardiol 16:519-537. doi: 10.1038/s41569-019-0200-7
5. Bhuiyan ZA, Jongbloed JD, van der Smagt J, Lombardi PM, Wiesfeld AC, Nelen M, Schouten M, Jongbloed R, Cox MG, van Wolferen M, Rodriguez LM, van Gelder IC, Bikker H, Suurmeijer AJ, van den Berg MP, Mannens MM, Hauer RN, Wilde AA, and van Tintelen JP (2009) *Desmoglein-2 and desmocollin-2 mutations in dutch arrhythmogenic right ventricular dysplasia/cardiomypathy patients: results from a multicenter study.* Circ Cardiovasc Genet 2:418-27. doi: 10.1161/CIRCGENETICS.108.839829
6. Bogossian H, Linz D, Heijman J, Bimpong-Buta NY, Bandorski D, Frommeyer G, Erkapic D, Seyfarth M, Zarse M, and Crijns HJ (2020) *QTc evaluation in patients with bundle branch block.* Int J Cardiol Heart Vasc 30:100636. doi: 10.1016/j.ijcha.2020.100636
7. Brodehl A, Belke DD, Garnett L, Martens K, Abdelfatah N, Rodriguez M, Diao C, Chen YX, Gordon PM, Nygren A, and Gerull B (2017) *Transgenic mice overexpressing desmocollin-2 (DSC2) develop cardiomyopathy associated with myocardial inflammation and fibrotic remodeling.* PLoS One 12:e0174019. doi: 10.1371/journal.pone.0174019
8. Brodehl A, Weiss J, Debus JD, Stanasiuk C, Klauke B, Deutsch MA, Fox H, Bax J, Ebbinghaus H, Gartner A, Tiesmeier J, Laser T, Peterschroder A, Gerull B, Gummert J, Paluszkiewicz L, and Milting H (2020) *A homozygous DSC2 deletion associated with arrhythmogenic cardiomyopathy is caused by uniparental isodisomy.* J Mol Cell Cardiol 141:17-29. doi: 10.1016/j.yjmcc.2020.03.006
9. Bruford EA, Braschi B, Denny P, Jones TEM, Seal RL, and Tweedie S (2020) *Guidelines for human gene nomenclature.* Nat Genet 52:754-758. doi: 10.1038/s41588-020-0669-3
10. Burridge PW, Keller G, Gold JD, and Wu JC (2012) *Production of de novo cardiomyocytes: human pluripotent stem cell differentiation and direct reprogramming.* Cell Stem Cell 10:16-28. doi: 10.1016/j.stem.2011.12.013

11. Calabrese F, Basso C, Carturan E, Valente M, and Thiene G (2006) *Arrhythmogenic right ventricular cardiomyopathy/dysplasia: is there a role for viruses?* Cardiovasc Pathol 15:11-7. doi: 10.1016/j.carpath.2005.10.004
12. Caspi O, Huber I, Gepstein A, Arbel G, Maizels L, Boulos M, and Gepstein L (2013) *Modeling of arrhythmogenic right ventricular cardiomyopathy with human induced pluripotent stem cells.* Circ Cardiovasc Genet 6:557-68. doi: 10.1161/CIRCGENETICS.113.000188
13. Ciarambino T, Menna G, Sansone G, and Giordano M (2021) *Cardiomyopathies: An Overview.* Int J Mol Sci 22:doi: 10.3390/ijms22147722
14. Consortium TU (2020) *UniProt: the universal protein knowledgebase in 2021.* Nucleic Acids Research 49:D480-D489. doi: 10.1093/nar/gkaa1100
15. Corrado D, Basso C, Thiene G, McKenna WJ, Davies MJ, Fontaliran F, Nava A, Silvestri F, Blomstrom-Lundqvist C, Wlodarska EK, Fontaine G, and Camerini F (1997) *Spectrum of clinicopathologic manifestations of arrhythmogenic right ventricular cardiomyopathy/dysplasia: a multicenter study.* J Am Coll Cardiol 30:1512-20. doi: 10.1016/s0735-1097(97)00332-x
16. Corrado D, Calkins H, Link MS, Leoni L, Favale S, Bevilacqua M, Basso C, Ward D, Boriani G, Ricci R, Piccini JP, Dalal D, Santini M, Buja G, Iliceto S, Estes NA, 3rd, Wichter T, McKenna WJ, Thiene G, and Marcus FI (2010) *Prophylactic implantable defibrillator in patients with arrhythmogenic right ventricular cardiomyopathy/dysplasia and no prior ventricular fibrillation or sustained ventricular tachycardia.* Circulation 122:1144-52. doi: 10.1161/circulationaha.109.913871
17. Corrado D, Leoni L, Link MS, Della Bella P, Gaita F, Curnis A, Salerno JU, Igidbashian D, Raviele A, Disertori M, Zanotto G, Verlato R, Vergara G, Delise P, Turrini P, Basso C, Naccarella F, Maddalena F, Estes NA, 3rd, Buja G, and Thiene G (2003) *Implantable cardioverter-defibrillator therapy for prevention of sudden death in patients with arrhythmogenic right ventricular cardiomyopathy/dysplasia.* Circulation 108:3084-91. doi: 10.1161/01.cir.0000103130.33451.d2
18. Corrado D, Link MS, and Calkins H (2017) *Arrhythmogenic Right Ventricular Cardiomyopathy.* N Engl J Med 376:61-72. doi: 10.1056/NEJMra1509267
19. Corrado D, van Tintelen PJ, McKenna WJ, Hauer RNW, Anastastakis A, Asimaki A, Basso C, Bauce B, Brunckhorst C, Bucciarelli-Ducci C, Duru F, Elliott P, Hamilton RM, Haugaa KH, James CA, Judge D, Link MS, Marchlinski FE, Mazzanti A, Mestroni L, Pantazis A, Pelliccia A, Marra MP, Pilichou K, Platonov PGA, Protonotarios A, Rampazzo A, Saffitz JE, Saguner AM, Schmied C, Sharma S, Tandri H, Te Riele A, Thiene G, Tsatsopoulou A, Zareba W, Zorzi A, Wichter T, Marcus FI, and Calkins H (2020) *Arrhythmogenic right ventricular cardiomyopathy: evaluation of the current diagnostic criteria and differential diagnosis.* Eur Heart J 41:1414-1429. doi: 10.1093/eurheartj/ehz669
20. Corrado D, Wichter T, Link MS, Hauer RN, Marchlinski FE, Anastasakis A, Bauce B, Basso C, Brunckhorst C, Tsatsopoulou A, Tandri H, Paul M, Schmied C, Pelliccia A, Duru F, Protonotarios N, Estes NM, McKenna WJ, Thiene G, Marcus FI, and Calkins H (2015) *Treatment of Arrhythmogenic Right Ventricular Cardiomyopathy/Dysplasia: An International Task Force Consensus Statement.* Circulation 132:441-53. doi: 10.1161/CIRCULATIONAHA.115.017944

21. Costa S, Cerrone M, Saguner AM, Brunckhorst C, Delmar M, and Duru F (2021) *Arrhythmogenic cardiomyopathy: An in-depth look at molecular mechanisms and clinical correlates.* Trends Cardiovasc Med 31:395-402. doi: 10.1016/j.tcm.2020.07.006
22. Daliento L, Turrini P, Nava A, Rizzoli G, Angelini A, Buja G, Scognamiglio R, and Thiene G (1995) *Arrhythmogenic right ventricular cardiomyopathy in young versus adult patients: similarities and differences.* J Am Coll Cardiol 25:655-64. doi: 10.1016/0735-1097(94)00433-Q
23. Delmar M and McKenna WJ (2010) *The cardiac desmosome and arrhythmogenic cardiomyopathies: from gene to disease.* Circ Res 107:700-14. doi: 10.1161/circresaha.110.223412
24. Duong T, Rose R, Blazeski A, Fine N, Woods CE, Thole JF, Sotoodehnia N, Soliman EZ, Tung L, McCallion AS, and Arking DE (2021) *Development and optimization of an in vivo electrocardiogram recording method and analysis program for adult zebrafish.* Dis Model Mech 14:doi: 10.1242/dmm.048827
25. Echeazarra L, Hortigon-Vinagre MP, Casis O, and Gallego M (2020) *Adult and Developing Zebrafish as Suitable Models for Cardiac Electrophysiology and Pathology in Research and Industry.* Front Physiol 11:607860. doi: 10.3389/fphys.2020.607860
26. Eisen JS and Smith JC (2008) *Controlling morpholino experiments: don't stop making antisense.* Development 135:1735-43. doi: 10.1242/dev.001115
27. El-Battrawy I, Zhao Z, Lan H, Cyganek L, Tombers C, Li X, Buljubasic F, Lang S, Tiburcy M, Zimmermann WH, Utikal J, Wieland T, Borggrefe M, Zhou XB, and Akin I (2018) *Electrical dysfunctions in human-induced pluripotent stem cell-derived cardiomyocytes from a patient with an arrhythmogenic right ventricular cardiomyopathy.* Europace 20:f46-f56. doi: 10.1093/europace/euy042
28. Fang WK, Liao LD, Zeng FM, Zhang PX, Wu JY, Shen J, Xu LY, and Li EM (2014) *Desmocollin-2 affects the adhesive strength and cytoskeletal arrangement in esophageal squamous cell carcinoma cells.* Mol Med Rep 10:2358-64. doi: 10.3892/mmr.2014.2485
29. Fujita S, Terasaki F, Otsuka K, Katashima T, Kanzaki Y, Kawamura K, Tanaka T, and Kitaura Y (2008) *Markedly increased intracellular lipid droplets and disruption of intercellular junctions in biopsied myocardium from a patient with arrhythmogenic right ventricular cardiomyopathy.* Heart Vessels 23:440-4. doi: 10.1007/s00380-008-1079-0
30. Gandjbakhch E, Redheuil A, Pousset F, Charron P, and Frank R (2018) *Clinical Diagnosis, Imaging, and Genetics of Arrhythmogenic Right Ventricular Cardiomyopathy/Dysplasia: JACC State-of-the-Art Review.* J Am Coll Cardiol 72:784-804. doi: 10.1016/j.jacc.2018.05.065
31. Garcia-Gras E, Lombardi R, Giocondo MJ, Willerson JT, Schneider MD, Khoury DS, and Marian AJ (2006) *Suppression of canonical Wnt/beta-catenin signaling by nuclear plakoglobin recapitulates phenotype of arrhythmogenic right ventricular cardiomyopathy.* J Clin Invest 116:2012-21. doi: 10.1172/JCI27751
32. Gauvrit S, Bossaer J, Lee J, and Collins MM (2022) *Modeling Human Cardiac Arrhythmias: Insights from Zebrafish.* J Cardiovasc Dev Dis 9:doi: 10.3390/jcdd9010013

33. Gehmlich K, Lambiase PD, Asimaki A, Ciaccio EJ, Ehler E, Syrris P, Saffitz JE, and McKenna WJ (2011) *A novel desmocollin-2 mutation reveals insights into the molecular link between desmosomes and gap junctions.* Heart Rhythm 8:711-8. doi: 10.1016/j.hrthm.2011.01.010
34. Gerull B, Kirchner F, Chong JX, Tagoe J, Chandrasekharan K, Strohm O, Waggoner D, Ober C, and Duff HJ (2013) *Homozygous founder mutation in desmocollin-2 (DSC2) causes arrhythmogenic cardiomyopathy in the Hutterite population.* Circ Cardiovasc Genet 6:327-36. doi: 10.1161/CIRCGENETICS.113.000097
35. Gilotra NA, Bhonsale A, James CA, Te Riele ASJ, Murray B, Tichnell C, Sawant A, Ong CS, Judge DP, Russell SD, Calkins H, and Tedford RJ (2017) *Heart Failure Is Common and Under-Recognized in Patients With Arrhythmogenic Right Ventricular Cardiomyopathy/Dysplasia.* Circ Heart Fail 10:doi: 10.1161/CIRCHEARTFAILURE.116.003819
36. Han B, Trew ML, and Zgierski-Johnston CM (2021) *Cardiac Conduction Velocity, Remodeling and Arrhythmogenesis.* Cells 10:doi: 10.3390/cells10112923
37. Hawthorne RN, Blazeski A, Lowenthal J, Kannan S, Teuben R, DiSilvestre D, Morrissette-McAlmon J, Saffitz JE, Boheler KR, James CA, Chelko SP, Tomaselli G, and Tung L (2021) *Altered Electrical, Biomolecular, and Immunologic Phenotypes in a Novel Patient-Derived Stem Cell Model of Desmoglein-2 Mutant ARVC.* J Clin Med 10:doi: 10.3390/jcm10143061
38. Heuser A, Plovie ER, Ellinor PT, Grossmann KS, Shin JT, Wichter T, Basson CT, Lerman BB, Sasse-Klaassen S, Thierfelder L, MacRae CA, and Gerull B (2006) *Mutant desmocollin-2 causes arrhythmogenic right ventricular cardiomyopathy.* Am J Hum Genet 79:1081-8. doi: 10.1086/509044
39. Hoorntje ET, te Rijdt WP, James CA, Pilichou K, Basso C, Judge DP, Bezzina CR, and van Tintelen JP (2017) *Arrhythmogenic cardiomyopathy: pathology, genetics, and concepts in pathogenesis.* Cardiovascular Research 113:1521-1531. doi: 10.1093/cvr/cvx150
40. Howe K, Clark MD, Torroja CF, Torrance J, Berthelot C, Muffato M, Collins JE, Humphray S, McLaren K, Matthews L, McLaren S, Sealy I, Caccamo M, Churcher C, Scott C, Barrett JC, Koch R, Rauch GJ, White S, Chow W, Kilian B, Quintais LT, Guerra-Assuncao JA, Zhou Y, Gu Y, Yen J, Vogel JH, Eyre T, Redmond S, Banerjee R, Chi J, Fu B, Langley E, Maguire SF, Laird GK, Lloyd D, Kenyon E, Donaldson S, Sehra H, Almeida-King J, Loveland J, Trevanion S, Jones M, Quail M, Willey D, Hunt A, Burton J, Sims S, McLay K, Plumb B, Davis J, Clee C, Oliver K, Clark R, Riddle C, Elliot D, Threadgold G, Harden G, Ware D, Begum S, Mortimore B, Kerry G, Heath P, Phillimore B, Tracey A, Corby N, Dunn M, Johnson C, Wood J, Clark S, Pelan S, Griffiths G, Smith M, Glithero R, Howden P, Barker N, Lloyd C, Stevens C, Harley J, Holt K, Panagiotidis G, Lovell J, Beasley H, Henderson C, Gordon D, Auger K, Wright D, Collins J, Raisen C, Dyer L, Leung K, Robertson L, Ambridge K, Leongamornlert D, McGuire S, Gilderthorp R, Griffiths C, Manthravadi D, Nichol S, Barker G, Whitehead S, Kay M, Brown J, Murnane C, Gray E, Humphries M, Sycamore N, Barker D, Saunders D, Wallis J, Babbage A, Hammond S, Mashreghi-Mohammadi M, Barr L, Martin S, Wray P, Ellington A, Matthews N, Ellwood M, Woodmansey R, Clark G, Cooper J, Tromans A, Grafham D, Skuce C, Pandian R, Andrews R, Harrison E, Kimberley A, Garnett J, Fosker N, Hall

R, Garner P, Kelly D, Bird C, Palmer S, Gehring I, Berger A, Dooley CM, Ersan-Urun Z, Eser C, Geiger H, Geisler M, Karotki L, Kirn A, Konantz J, Konantz M, Oberlander M, Rudolph-Geiger S, Teucke M, Lanz C, Raddatz G, Osoegawa K, Zhu B, Rapp A, Widaa S, Langford C, Yang F, Schuster SC, Carter NP, Harrow J, Ning Z, Herrero J, Searle SM, Enright A, Geisler R, Plasterk RH, Lee C, Westerfield M, de Jong PJ, Zon LI, Postlethwait JH, Nusslein-Volhard C, Hubbard TJ, Roest Crollius H, Rogers J and Stemple DL (2013) *The zebrafish reference genome sequence and its relationship to the human genome.* Nature 496:498-503. doi: 10.1038/nature12111

41. Kawaguchi N and Nakanishi T (2023) *Animal Disease Models and Patient-iPS-Cell-Derived In Vitro Disease Models for Cardiovascular Biology-How Close to Disease?* Biology (Basel) 12:doi: 10.3390/biology12030468
42. Kim C, Wong J, Wen J, Wang S, Wang C, Spiering S, Kan NG, Forcales S, Puri PL, Leone TC, Marine JE, Calkins H, Kelly DP, Judge DP, and Chen HS (2013) *Studying arrhythmogenic right ventricular dysplasia with patient-specific iPSCs.* Nature 494:105-10. doi: 10.1038/nature11799
43. Kleinsorge M and Cyganek L (2020) *Subtype-Directed Differentiation of Human iPSCs into Atrial and Ventricular Cardiomyocytes.* STAR Protoc 1:100026. doi: 10.1016/j.xpro.2020.100026
44. Kowalczyk AP and Green KJ (2013) *Structure, function, and regulation of desmosomes.* Prog Mol Biol Transl Sci 116:95-118. doi: 10.1016/b978-0-12-394311-8.00005-4
45. Lehnart SE, Terrenoire C, Reiken S, Wehrens XH, Song LS, Tillman EJ, Mancarella S, Coromilas J, Lederer WJ, Kass RS, and Marks AR (2006) *Stabilization of cardiac ryanodine receptor prevents intracellular calcium leak and arrhythmias.* Proc Natl Acad Sci U S A 103:7906-10. doi: 10.1073/pnas.0602133103
46. Li Y, Nguyen HV, and Tsang SH (2016) *Skin Biopsy and Patient-Specific Stem Cell Lines.* Methods Mol Biol 1353:77-88. doi: 10.1007/7651_2015_225
47. Lien CL, Wu C, Mercer B, Webb R, Richardson JA, and Olson EN (1999) *Control of early cardiac-specific transcription of Nkx2-5 by a GATA-dependent enhancer.* Development 126:75-84. doi: 10.1242/dev.126.1.75
48. Lin CY, Chung FP, Lin YJ, Chang SL, Lo LW, Hu YF, Tuan TC, Chao TF, Liao JN, Chang TY, Kuo L, Wu CI, Liu CM, Liu SH, Huang JL, Hsieh YC, and Chen SA (2022) *Clinical significance of structural remodeling concerning substrate characteristics and outcomes in arrhythmogenic right ventricular cardiomyopathy.* Heart Rhythm O2 3:422-429. doi: 10.1016/j.hroo.2022.04.007
49. Ma D, Wei H, Lu J, Ho S, Zhang G, Sun X, Oh Y, Tan SH, Ng ML, Shim W, Wong P, and Liew R (2013) *Generation of patient-specific induced pluripotent stem cell-derived cardiomyocytes as a cellular model of arrhythmogenic right ventricular cardiomyopathy.* Eur Heart J 34:1122-33. doi: 10.1093/eurheartj/ehs226
50. Maron BJ, Towbin JA, Thiene G, Antzelevitch C, Corrado D, Arnett D, Moss AJ, Seidman CE, and Young JB (2006) *Contemporary definitions and classification of the cardiomyopathies: an American Heart Association Scientific Statement from the Council on Clinical Cardiology, Heart Failure and Transplantation Committee; Quality of Care and Outcomes Research and Functional Genomics and Translational Biology Interdisciplinary*

Working Groups; and Council on Epidemiology and Prevention. Circulation 113:1807-16. doi: 10.1161/circulationaha.106.174287
51. McKenna WJ, Judge, D.P. (2021) *Epidemiology of the inherited cardiomyopathies.* 18:22-36. doi: https://doi.org/10.1038/s41569-020-0428-2
52. Moccia F, Lodola F, Stadiotti I, Pilato CA, Bellin M, Carugo S, Pompilio G, Sommariva E, and Maione AS (2019) *Calcium as a Key Player in Arrhythmogenic Cardiomyopathy: Adhesion Disorder or Intracellular Alteration?* Int J Mol Sci 20:doi: 10.3390/ijms20163986
53. Mohammed F and Chidgey M (2021) *Desmosomal protein structure and function and the impact of disease-causing mutations.* J Struct Biol 213:107749. doi: 10.1016/j.jsb.2021.107749
54. Moreau A, Reisqs JB, Delanoe-Ayari H, Pierre M, Janin A, Deliniere A, Bessiere F, Meli AC, Charrabi A, Lafont E, Valla C, Bauer D, Morel E, Gache V, Millat G, Nissan X, Faucherre A, Jopling C, Richard S, Mejat A, and Chevalier P (2021) *Deciphering DSC2 arrhythmogenic cardiomyopathy electrical instability: From ion channels to ECG and tailored drug therapy.* Clin Transl Med 11:e319. doi: 10.1002/ctm2.319
55. Nemtsas P, Wettwer E, Christ T, Weidinger G, and Ravens U (2010) *Adult zebrafish heart as a model for human heart? An electrophysiological study.* J Mol Cell Cardiol 48:161-71. doi: 10.1016/j.yjmcc.2009.08.034
56. Nielsen JB, Graff C, Rasmussen PV, Pietersen A, Lind B, Olesen MS, Struijk JJ, Haunso S, Svendsen JH, Kober L, Gerds TA, and Holst AG (2014) *Risk prediction of cardiovascular death based on the QTc interval: evaluating age and gender differences in a large primary care population.* Eur Heart J 35:1335-44. doi: 10.1093/eurheartj/ehu081
57. Nuber UA, Schafer S, Schmidt A, Koch PJ, and Franke WW (1995) *The widespread human desmocollin Dsc2 and tissue-specific patterns of synthesis of various desmocollin subtypes.* Eur J Cell Biol 66:69-74. doi:
58. Pan Z, Ebert A, and Liang P (2021) *Human-induced pluripotent stem cells as models for rare cardiovascular diseases: from evidence-based medicine to precision medicine.* Pflugers Arch 473:1151-1165. doi: 10.1007/s00424-020-02486-y
59. Paul M and Schulze-Bahr E (2020) *Arrhythmogenic right ventricular cardiomyopathy : Evolving from unique clinical features to a complex pathophysiological concept.* Herz 45:243-251. doi: 10.1007/s00059-020-04907-1
60. Pires DEV, Rodrigues CHM, and Ascher DB (2020) *mCSM-membrane: predicting the effects of mutations on transmembrane proteins.* Nucleic Acids Res 48:W147-W153. doi: 10.1093/nar/gkaa416
61. Poon KL and Brand T (2013) *The zebrafish model system in cardiovascular research: A tiny fish with mighty prospects.* Glob Cardiol Sci Pract 2013:9-28. doi: 10.5339/gcsp.2013.4
62. Priori SG, Blomström-Lundqvist C, Mazzanti A, Blom N, Borggrefe M, Camm J, Elliott PM, Fitzsimons D, Hatala R, Hindricks G, Kirchhof P, Kjeldsen K, Kuck K-H, Hernandez-Madrid A, Nikolaou N, Norekvål TM, Spaulding C, Van Veldhuisen DJ, and Group ESD (2015) *2015 ESC Guidelines for the management of patients with ventricular arrhythmias and the prevention of sudden cardiac death: The Task Force for the Management of Patients with Ventricular Arrhythmias and the Prevention of Sudden Cardiac Death of the European Society of Cardiology*

(ESC)Endorsed by: Association for European Paediatric and Congenital Cardiology (AEPC). European Heart Journal 36:2793-2867. doi: 10.1093/eurheartj/ehv316

63. Rapezzi C, Aimo A, Barison A, Emdin M, Porcari A, Linhart A, Keren A, Merlo M, and Sinagra G (2022) *Restrictive cardiomyopathy: definition and diagnosis.* Eur Heart J 43:4679-4693. doi: 10.1093/eurheartj/ehac543
64. Reichart D, Magnussen C, Zeller T, and Blankenberg S (2019) *Dilated cardiomyopathy: from epidemiologic to genetic phenotypes: A translational review of current literature.* J Intern Med 286:362-372. doi: 10.1111/joim.12944
65. Reisqs JB, Moreau A, Charrabi A, Sleiman Y, Meli AC, Millat G, Briand V, Beauverger P, Richard S, and Chevalier P (2022) *The PPARgamma pathway determines electrophysiological remodelling and arrhythmia risks in DSC2 arrhythmogenic cardiomyopathy.* Clin Transl Med 12:e748. doi: 10.1002/ctm2.748
66. Reisqs JB, Moreau A, Sleiman Y, Boutjdir M, Richard S, and Chevalier P (2023) *Arrhythmogenic cardiomyopathy as a myogenic disease: highlights from cardiomyocytes derived from human induced pluripotent stem cells.* Front Physiol 14:1191965. doi: 10.3389/fphys.2023.1191965
67. Reisqs JB, Moreau A, Sleiman Y, Charrabi A, Deliniere A, Bessiere F, Gardey K, Richard S, and Chevalier P (2023) *Spironolactone as a Potential New Treatment to Prevent Arrhythmias in Arrhythmogenic Cardiomyopathy Cell Model.* J Pers Med 13:doi: 10.3390/jpm13020335
68. Roux-Buisson N, Gandjbakhch E, Donal E, Probst V, Deharo JC, Chevalier P, Klug D, Mansencal N, Delacretaz E, Cosnay P, Scanu P, Extramiana F, Keller D, Hidden-Lucet F, Trapani J, Fouret P, Frank R, Fressart V, Faure J, Lunardi J, and Charron P (2014) *Prevalence and significance of rare RYR2 variants in arrhythmogenic right ventricular cardiomyopathy/dysplasia: results of a systematic screening.* Heart Rhythm 11:1999-2009. doi: 10.1016/j.hrthm.2014.07.020
69. Sayers EW, Bolton EE, Brister JR, Canese K, Chan J, Comeau DC, Connor R, Funk K, Kelly C, Kim S, Madej T, Marchler-Bauer A, Lanczycki C, Lathrop S, Lu Z, Thibaud-Nissen F, Murphy T, Phan L, Skripchenko Y, Tse T, Wang J, Williams R, Trawick BW, Pruitt KD, and Sherry ST (2022) *Database resources of the national center for biotechnology information.* Nucleic Acids Res 50:D20-D26. doi: 10.1093/nar/gkab1112
70. Schinner C, Erber BM, Yeruva S, and Waschke J (2019) *Regulation of cardiac myocyte cohesion and gap junctions via desmosomal adhesion.* Acta Physiol (Oxf) 226:e13242. doi: 10.1111/apha.13242
71. Sedmera D, Reckova M, deAlmeida A, Sedmerova M, Biermann M, Volejnik J, Sarre A, Raddatz E, McCarthy RA, Gourdie RG, and Thompson RP (2003) *Functional and morphological evidence for a ventricular conduction system in zebrafish and Xenopus hearts.* Am J Physiol Heart Circ Physiol 284:H1152-60. doi: 10.1152/ajpheart.00870.2002
72. Shafraz O, Rubsam M, Stahley SN, Caldara AL, Kowalczyk AP, Niessen CM, and Sivasankar S (2018) *E-cadherin binds to desmoglein to facilitate desmosome assembly.* Elife 7:doi: 10.7554/eLife.37629
73. Shah D, Virtanen L, Prajapati C, Kiamehr M, Gullmets J, West G, Kreutzer J, Pekkanen-Mattila M, Helio T, Kallio P, Taimen P, and Aalto-Setala K (2019) *Modeling of LMNA-Related Dilated Cardiomyopathy Using Human Induced Pluripotent Stem Cells.* Cells 8:doi: 10.3390/cells8060594

74. Sommariva E, Brambilla S, Carbucicchio C, Gambini E, Meraviglia V, Dello Russo A, Farina FM, Casella M, Catto V, Pontone G, Chiesa M, Stadiotti I, Cogliati E, Paolin A, Ouali Alami N, Preziuso C, d'Amati G, Colombo GI, Rossini A, Capogrossi MC, Tondo C, and Pompilio G (2016) *Cardiac mesenchymal stromal cells are a source of adipocytes in arrhythmogenic cardiomyopathy.* Eur Heart J 37:1835-46. doi: 10.1093/eurheartj/ehv579
75. Syrris P, Ward D, Evans A, Asimaki A, Gandjbakhch E, Sen-Chowdhry S, and McKenna WJ (2006) *Arrhythmogenic right ventricular dysplasia/cardiomyopathy associated with mutations in the desmosomal gene desmocollin-2.* Am J Hum Genet 79:978-84. doi: 10.1086/509122
76. Takahashi K, Tanabe K, Ohnuki M, Narita M, Ichisaka T, Tomoda K, and Yamanaka S (2007) *Induction of pluripotent stem cells from adult human fibroblasts by defined factors.* Cell 131:861-72. doi: 10.1016/j.cell.2007.11.019
77. Tessadori F, van Weerd JH, Burkhard SB, Verkerk AO, de Pater E, Boukens BJ, Vink A, Christoffels VM, and Bakkers J (2012) *Identification and functional characterization of cardiac pacemaker cells in zebrafish.* PLoS One 7:e47644. doi: 10.1371/journal.pone.0047644
78. Vallverdu-Prats M, Carreras D, Perez GJ, Campuzano O, Brugada R, and Alcalde M (2023) *Alterations in Calcium Handling Are a Common Feature in an Arrhythmogenic Cardiomyopathy Cell Model Triggered by Desmosome Genes Loss.* Int J Mol Sci 24:doi: 10.3390/ijms24032109
79. Weintraub RG, Semsarian C, and Macdonald P (2017) *Dilated cardiomyopathy.* Lancet 390:400-414. doi: 10.1016/s0140-6736(16)31713-5
80. Wichter T, Paul M, Wollmann C, Acil T, Gerdes P, Ashraf O, Tjan TD, Soeparwata R, Block M, Borggrefe M, Scheld HH, Breithardt G, and Böcker D (2004) *Implantable cardioverter/defibrillator therapy in arrhythmogenic right ventricular cardiomyopathy: single-center experience of long-term follow-up and complications in 60 patients.* Circulation 109:1503-8. doi: 10.1161/01.cir.0000121738.88273.43
81. Yoshida Y and Yamanaka S (2017) *Induced Pluripotent Stem Cells 10 Years Later: For Cardiac Applications.* Circ Res 120:1958-1968. doi: 10.1161/CIRCRESAHA.117.311080

7 Acknowledgements

First of all, I would like to express my sincere appreciation to Prof. Dr. Steffen Just and Dr. Federica Diofano for their guidance in defining the research question for this thesis. Their expertise and direction, as well as the assistance of the whole laboratory team, were instrumental in shaping this work. I express my special thanks to Dr. Federica Diofano for her consistent support and supervision throughout my time in the laboratory and the writing process.

I am also deeply grateful to my parents for their unwavering support.

Last but not least, I would like to thank my siblings, Stefan and Maximilian, and my partner, Jakob, for their steady encouragement and confidence in me.

8 Curriculum vitae

Removed for privacy reasons.